ADVANCED COATING TECHNOLOGIES WITH SPECTRAL ALTERATION FOR SOLAR APPLICATIONS

By
Refet Ali Yalçın
B.S., Mechanical Engineering, Middle East Technical University, 2009
M.S., Mechanical Engineering, Boğaziçi University, 2012

Submitted to the Institute for Graduate Studies in
Science and Engineering in partial fulfillment
of the requirements for the degree of
Doctor of Philosophy

Graduate Program in Mechanical Engineering
Boğaziçi University
2018

ADVANCED COATING TECHNOLOGIES WITH SPECTRAL ALTERATION FOR SOLAR APPLICATIONS

APPROVED BY:

Assoc. Prof. Hakan Ertürk (Thesis Supervisor)	……
Assist. Prof. Altuğ Melik Başol	……
Assoc. Prof. Hasan Bedir	……
Assoc. Prof. Albert Güveniş	……
Prof. Kurşat Şendur	……

DATE OF APPROVAL: 02.03.2018

ACKNOWLEDGEMENTS

Firstly, I would like to express my gratitude to my supervisor Dr. Hakan Ertürk, who has been a role model to me. He has taught me how an academic ought to think and behave. I shall never forget how he has been like a father to me. I would also like to thank my committee members Dr. Hasan Bedir and Dr. Albert Güveniş, who have most kindly helped me with their wisdom and guidance.

I would also like to express my gratitude to my family. My mother Zozan has been a devoted, loving mother, who, I remember, was heating our car, while I was having breakfast waiting to be driven to school at an early age. I would also like to thank my brother Ömer, who has always been generous towards me with his mature ideas. I would like to thank my wife Fulya, with whom I share my life and my two cats, Pisinaz and Safiş. They altogether make the world a better place for me.

I would also like to thank TES-LAB colleagues with whom we shared both knowledge and fun memories.

Finally, I would like to thank Boğaziçi University for giving me the opportunity to study in such an academic environment with strong social, cultural and educational foundations.

ABSTRACT

ADVANCED COATING TECHNOLOGIES WITH SPECTRAL ALTERATION FOR SOLAR APPLICATIONS

Spectrally selective coatings are used to maximize the efficiency of solar thermal systems and they are designed based on the application. This study focuses on two solar applications; solar thermal energy systems and greenhouses. For solar thermal energy systems, the coating should have high absorptance at solar wavelengths and low emittance at the infrared wavelengths, where absorber emits heat to maximize the heat transfer to the working fluid. For greenhouse applications, coating should provide high radiation at the photosynthetic spectrum and distribute light uniformly and diffusely. This study focuses on fluorescent and non-fluorescent pigmented coatings that consist of a binder and well dispersed nanometer or micrometer sized particles that are known as pigments, selected to achieve the desired spectrally selective behavior based on application. Radiative behavior of coatings depends on coating thickness, pigment size, concentration, and the optical properties of the binder and pigment materials that can be identified by modeling the radiative transfer across these coatings. Models are developed for the problems considered to solve the radiative transfer equation based on the governing physics to predict the spectral reflectance, transmittance and light distributions in conjunction with Lorenz-Mie theory and T-matrix methods that are used for predicting radiative transfer properties. These models are used to design coatings to achieve optimal behavior for considered applications. It is found that the model used for designing pigmented coatings of solar thermal systems can be very critical, and coatings must be designed using a unified model considering the effective medium theory and four flux method together with Lorentz-Mie theory. Besides, it is found that while fluorescent coatings can improve spectral distribution of irradiation for photosynthetic production, they also lead to a significant decrease in the transmittance, decreasing the irradiance when used for traditional greenhouses. However, for vertical farms it is found that using fluorescent particles in coatings both improve distribution of light and effective PAR, resulting around 35% increase in yearly crop production for lettuce.

ÖZET

GÜNEŞ UYGULAMARI İÇİN DALGABOYUNA HASSAS ÖZELLİKLİ GELİŞMİŞ KAPLAMA TEKNOLOJİLERİ

Tayfsal seçici kaplamalar, ısıl güneş sistemlerinin verimini azami miktara çıkartmak için kullanılmış ve uygulama tipine göre tasarlanmıştır. Bu çalışma; ısıl güneş enerjisi sistemleri ve sera uygulamaları olarak iki tip güneş uygulamasına odaklanmaktadır. Isıl güneş enerjisi sistemleri için kaplamanın; solar ışınım dalgaboylarında yüksek emilim, kızılötesi dalgaboylarında düşük ışınım yaparak sistemde dönen sıvıya taşınan ısıyı azami miktara çekmesi beklenir. Sera uygulamaları için ise kaplamanın fotosenteze faydalı olan tayfta yüksek ışınım sağlaması, ışığı eşit yayması ve dağıtması gerekmektedir. Bu çalışma; uygulamaya göre arzulanan şekilde tayfsal seçici davranış gösteren, bağlayıcı madde içerisine iyi şekilde dağıtılmış floresanlı ve floresansız pigmentli kaplamalara odaklanmaktadır. Kaplamaların ışınım transferi modellenerek saptanabilen ışınımsal davranışı; kaplama kalınlığı, pigment boyutu, pigment derişimi ve pigment ile bağlayıcı maddenin optik özelliklerine bağlıdır. Işının geçişini, yansımasını ve dağılımını öngörebilmek için effective medium teorisi, four flux metodu ile Monte Carlo metodlarına dayanan modeller geliştirilip ışınım transfer denklemi çözülmüştür. Bu denklemin çözümü için gerekli ışınım transferi özellikleri ise Lorenz-Mie teorisi ve T-matrix metodu ile bulunmuştur. Bu modeller, kaplamaların tasarımında optimal davranışı elde etmek için kullanılmaktadır. Isıl güneş sistemleri için tasarlanan pigmentli kaplamalarda kullanılan modelin çok kritik önemde olduğu ve kaplamanın effective medium teorisi ile four flux metodunun kullanıldığı bütünleşik metodun kullanılarak tasarlanması gerektiği görülmüştür. Ayrıca, floresan kaplamaların, geleneksel seralardaki fotosentez artışı için tayf dağılımını daha iyi hale getirse de, ışık geçişinde kayda değer bir düşüşe neden olduğu görülmüştür. Ancak dikey sera uygulamalarında floresan parçacıkların kullanılması; ışığın hem uzaysal hem de tayfsal dağılımını iyileştirerek marul bitkisi için yıllık üretimde %35'e varan artış sağlamaktadır.

TABLE OF CONTENTS

LIST OF FIGURES

LIST OF TABLES

LIST OF SYMBOLS

A_1,..,A_5	Constants for four flux method
a_n, b_n	Lorenz-Mie coefficients
C	Fresh weight per pot of lettuce plant
C_0,..,C_2	Constants for four flux method
C_f	Concentration factor of the concentrating solar collector
$C_{ext,\lambda}$	Spectral extinction cross section [m^2]
$C_{sca,\lambda}$	Spectral scattering cross section [m^2]
D	Normalized light density function,
$E_{b,\lambda}$	Spectral blackbody emissive power [W/m^2-μm]
$G_{s,\lambda}$	Spectral solar irradiance [W/m^2-μm]
$I_{c,\lambda}$	Collimated spectral intensity in +z direction [W/m^2-μm-sr]
$I_{d,\lambda}$	Diffuse spectral intensity in +z direction [W/m^2-μm-sr]
$J_{c,\lambda}$	Collimated spectral intensity in -z direction [W/m^2-μm-sr]
$J_{d,\lambda}$	Diffuse spectral intensity in -z direction [W/m^2-μm-sr]
$F(\chi)$	Objective function to be minimized
f_v	Pigment volume fraction
h	Hour of the day
H	Haze
k	Extinction index of material
m	Relative complex refractive index of material
n	Refractive index of material
N_s	Number of shelves

$p(\mu)$	Scattering phase function
r_p	Pigment radius [nm]
R_λ	Spectral reflectance
S	Source
q''	Absorber net radiant flux [W/m^2]
t	Thickness of the coating [μm]
T_a	Absorber temperature [K]
x	Size parameter
V	Volume [m^3]
Y	Photosynthetic quantum efficiency
α_λ	Spectral absorptance
β_λ	Spectral extinction coefficient [1/m]
χ	Unknown vector
ε	Dielectric constant
ϵ_λ	Spectral emittance
η	Efficiency
μ	Cosine of theta [cos(θ)]
σ_c	Forward scattering ratio for the collimated intensity
σ_d	Forward scattering ratio for the diffuse intensity
$\sigma_{s,\lambda}$	Spectral scattering coefficient [1/m]
θ	Polar angle
ϕ	Latitude
ρ_c	Boundary reflectivity for the collimated intensity from outside to coating

ρ_c'	Boundary reflectivity for the collimated intensity from substrate to coating
ρ_d	Boundary reflectivity for the diffuse intensity from coating to outside
ρ_d'	Boundary reflectivity for the diffuse intensity from coating to substrate
ξ	Average pathlength parameter

1. INTRODUCTION

1.1. Motivation

Food and energy are driving forces of civilizations, and production of these has been one of the major interests of engineers and scientists throughout history. Energy and food consumption has been increasing with increasing prosperity and population. Major resource of food and energy source is the solar energy. The fossil fuel is derived from old life forms, which is thrived using solar energy millions of years ago. Similarly, major renewable energy sources either depend on the sun directly (e.g. solar energy) or indirectly (e.g. wind and hydroelectric energy). Food production and natural food chain are also depended on solar energy; since most of the primary producer organisms such as plants and algae are photosynthetic, and use solar energy to produce biomass from inorganic materials. These producer organisms are basis for food chain, which composed of herbivores, omnivores and carnivores.

In order to increase efficiency of food and energy productions, their utilization mechanisms should be understood and modeled. Radiative energy emitted from the sun has a spectral variation, global solar radiation is incident upon earth depending on latitude, and reaches to surface of the Earth after atmospheric absorption and scattering. Modeling energy and crop productions, under incoming spectral solar energy and then creating the mathematical model are essential steps to estimate the efficiencies. Then proper parametric studies and/or optimizations method can be performed to maximize the outcome.

1.1.1. Energy Production

Major energy sources can be classified as fossil, nuclear, renewable and biofuels, and utilization of each source has its advantages and disadvantages. Fossil fuels such as oil, coal and natural gas have been the most widely used energy source since the industrial revolution. Although use of other resources have been increasing in the recent decades, the ratio of the energy produced by fossil fuels to the total energy produced is about 78% as shown in Figure 1.1. The portion of wind, solar and geothermal energy in the total energy

consumption is only 1.6% [1]. It is relatively easier to utilize and transport fossil fuels and their low cost per kilowatt hour as presented in Figure 1.2. is the major reason behind their popularity.

Increasing demand on a limited resource leads to an increase in energy prices that is a major concern for global economy. Moreover, many political problems and conflicts have been arising as controlling energy resources is an important concern for all states. Besides all these, utilizing fossil fuels causes serious environmental problems. Solar energy is considered as one of the leading alternatives as life on earth relies on sun as it is fundamental energy source. Although mankind has been using solar energy extensively throughout history, solar energy has not been utilized for production of useful work directly until recently. Solar energy can be utilized for heating, electricity generation, lighting and some other minor purposes, such as desalination.

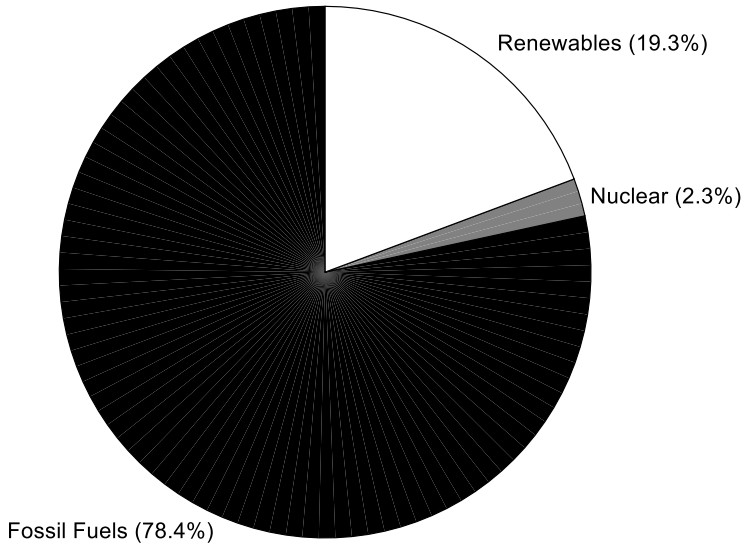

Figure 1.1. Total final energy consumption in 2015. [1]

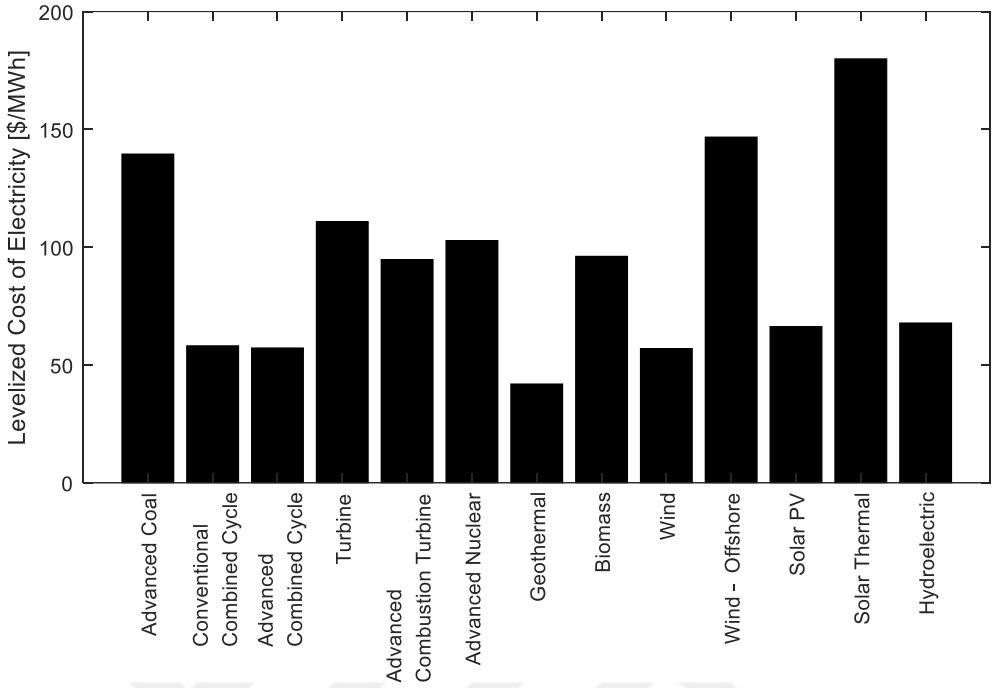

Figure 1.2. Variation in levelized cost of resources. [2]

The available solar energy depends on time, geographical location, and the economic feasibility of a solar system depends highly on available solar energy per collection area. Concentrating systems and solar tracking systems that follow direct sunlight are used to maximize solar flux. Although south of Turkey's annual average sum of global irradiation is about 2000 kWh/m^2 that is suitable for electricity generation, flat-plate collectors for domestic hot water systems are main solar energy utilization in Turkey and there is only negligible energy production. Whereas, Germany's annual average solar irradiation is half of that of Turkey's, but 3% of electricity consumed in Germany is generated by solar power.

One of the most important roadblocks for utilization of solar energy is its relatively high cost per power as it could be seen from Figure 1.2. Although fossil fuel costs are expected to increase due to limited resources, their costs are still expected to be lower in the near future. Therefore, cost of energy produced from solar systems must be decreased so that it could become a competitive alternative. Reducing manufacturing costs and improving the performance of systems are required to reduce the cost per power for solar

technologies and any means of improving the performance of the solar energy systems is critical.

There are two main approaches to produce useful work in the form of electricity using solar energy. The first one is by using photovoltaic systems, and the other is through solar thermal systems. While solar energy is directly converted to electricity by photovoltaic systems, it is transferred to a fluid using collectors and the heated fluid is used by a thermodynamic power cycle to generate electricity in solar thermal systems. While solar thermal systems used for domestic hot water applications and PVs used for domestic electric generations are most widely adopted technologies; both PV farms and concentrated solar thermal systems can be operated for large scale power production with comparable levelized cost of electricity ($/kWh).

There are three common types of collectors that are used in solar thermal applications: Parabolic-trough reflectors focus light to heat a vacuum tube where working fluid flows. The mirrors surrounding the tower that are also known as heliostats focus light to the absorber located in the tower heating the working fluid in central tower receiver. Lastly, parabolic dish receiver, which collect incoming radiation above the center of the dish. These dishes have independent engines or PVs on its focal point, which eliminates use of working fluid.

Parabolic through systems are the most widely adopted concentrated solar power system. The absorber of a parabolic through system is usually comprised of a pipe that has an absorbing coating, surrounded by a transparent evacuated tube in order to minimize convective losses as shown in Figure 1.3. Radiative emission becomes the major heat loss mechanism in the absence of convective losses. Therefore, an ideal absorber must absorb as much solar energy as possible, whereas it must emit as low heat as possible to the environment. Considering the high temperatures achieved in the absorbers due to concentration effect, the radiative heat lost can be significant; therefore, special coatings should be used to maximize absorbed solar energy and minimize energy loss by emission of the absorber surface.

Solar radiation can be approximated as a blackbody heat source at 5777 K and is predominantly in the visible light wavelength range, 0.4-0.7 μm. Whereas, the radiation emitted by absorber is at infrared wavelengths, larger than 1μm, considering the typical absorber temperatures, as it is shown on Figure 1.4. Therefore, the ideal coating must have high absorptivity in shorter wavelengths, whereas it must have low emmisivity in longer wavelengths.

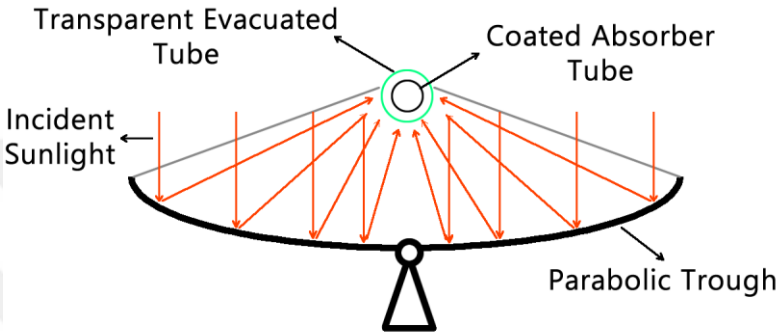

Figure 1.3. Parabolic through collector and its absorber tube

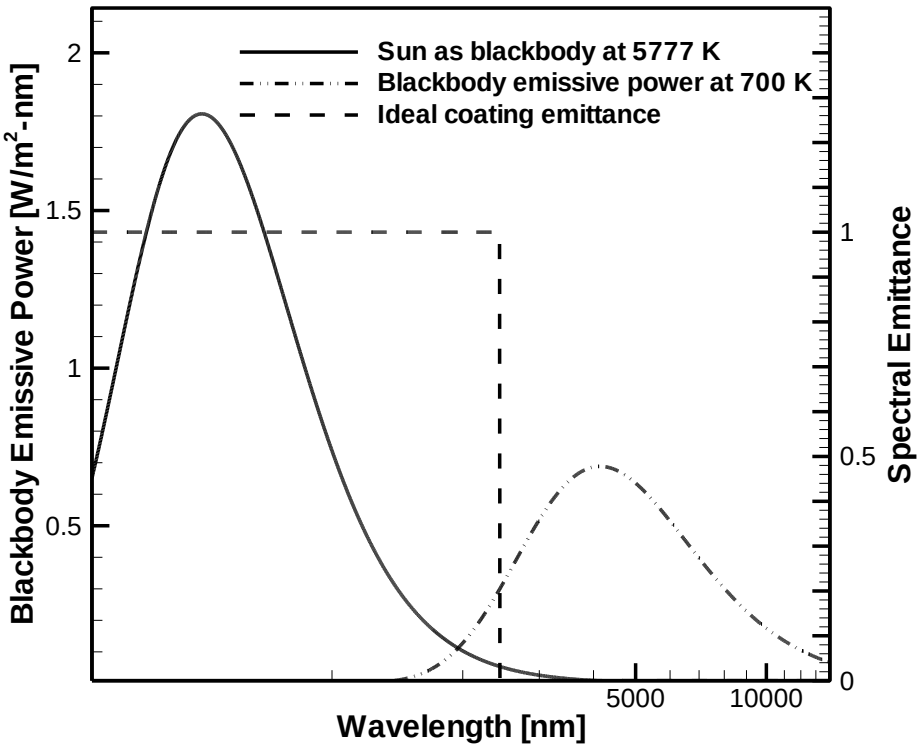

Figure 1.4. Distribution of solar irradiation and absorber emission, and ideal emissivity at various wavelengths.

1.1.2. Food Production

Population increase rate of Turkey was reported to be 1.6%, which is over global population increase that is reported as 1.1% in 2016. These increases result a proportional increase on food demand. Unfortunately, the land is restricted and, agricultural lands are decreasing with historically agricultural lands are converted to industrial and residential areas. The change of agricultural land area in Turkey for last 20 years is presented in Figure 1.5. If increase of food demand and decrease of agricultural area cannot be compensated by crop efficiency increase, which is total crop per land, food should be imported and food prices will increase due to increasing costs and demands.

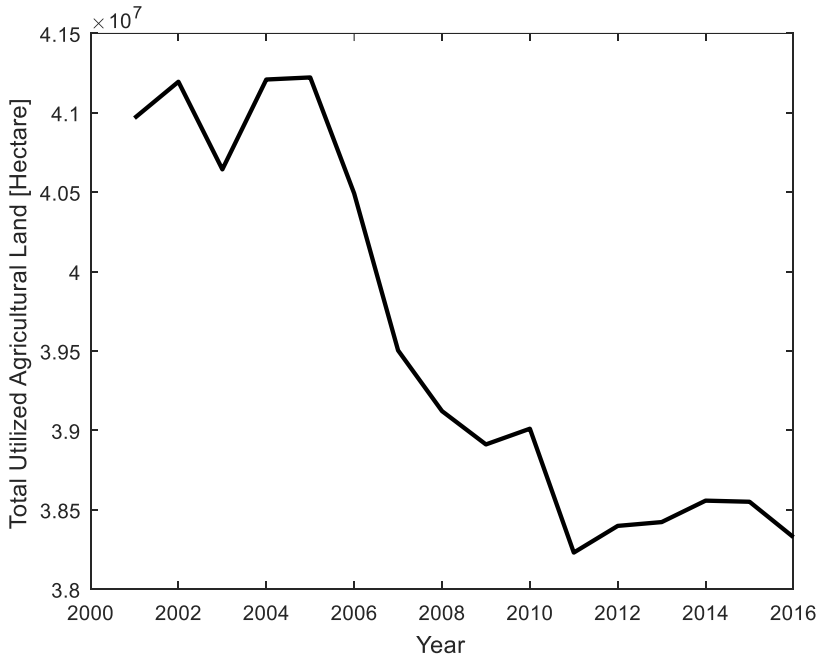

Figure 1.5. Change of total agricultural land in Turkey by years. [3]

Greenhouse farming has many advantages over traditional agriculture. Crops are not effected from climate in a greenhouse; therefore, more crops can be harvested throughout the year. Farming in a closed area also help farmers to prevent from diseases and bugs more easily. Moreover, agriculture in a controlled environment uses far less water (70–80%) [4]. Total area of greenhouses in the world was 1.2 million hectare, where Turkey holds 70,000 hectare as of 2016 [3]. Increase in the greenhouse farming can be observed from Figure 1.6. There are 4 greenhouse types that are widely used; glass, plastic,

high tunnel and low tunnel. Variation of their number is also presented in Figure 1.6. As of 2014, 6.6 million tons of crops were grown in greenhouses, which had a corresponding income of 16 billion Turkish Lira. While most of the crops were consumed within Turkey, only 15% is exported [5]. Ratio of greenhouse area to total vegetable growing agricultural area was about 8% in 2016 and the ratio is increasing both by increasing greenhouse area and decreasing total vegetable growing agricultural area as it could been observed from Figure 1.7. [3]

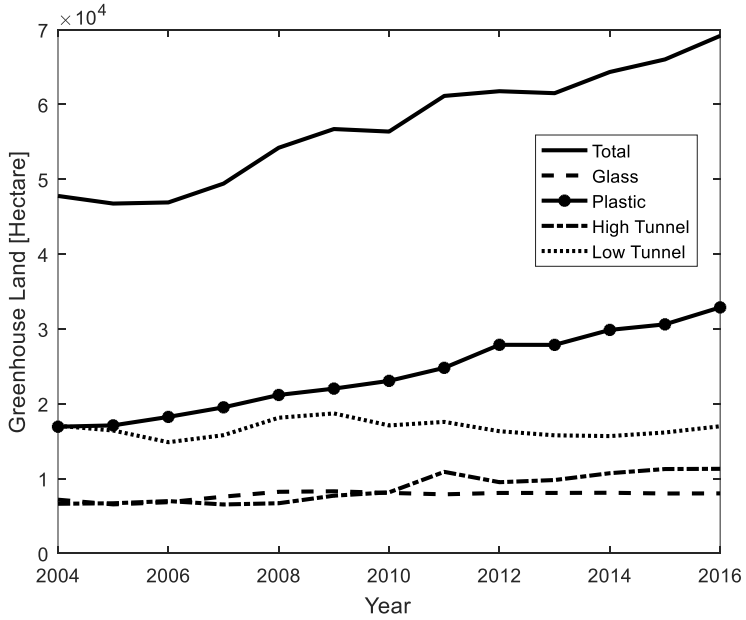

Figure 1.6. Change of total greenhouse land in Turkey by years. [3]

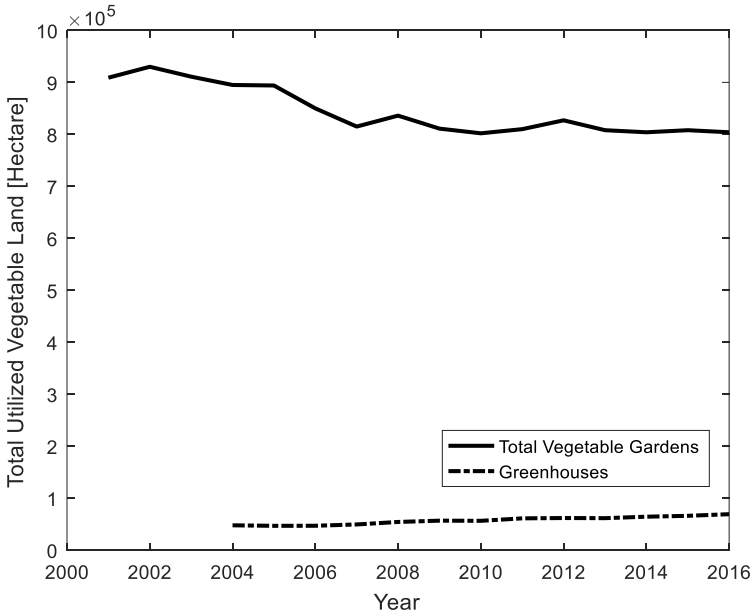

Figure 1.7. Change of total utilized vegetable land. [3]

1.2. Literature Survey

1.2.1. Spectrally Selective Thickness Sensitive Pigmented Coatings for Solar Thermal Applications

There has been growing concern on global climate change, availability of existing sources and environmental safety for the current energy infrastructure that predominantly rely on fossil fuel and nuclear technologies. These concerns have increased interest on utilization of renewable energy sources, and solar energy systems are considered as one of the leading alternatives. However, the most important roadblock for wide adoption of solar energy is considered as its relatively high cost per power. Reducing manufacturing costs and improving the performance of the systems are required to reduce the cost per power for solar technologies.

Solar thermal systems rely on transferring solar energy to a working fluid that is either used directly or in a thermodynamic cycle such as Rankine cycle for producing useful work. A brief review of solar thermal systems and their applications is presented in [6]. Concentrating systems such as parabolic-trough collectors are used to produce high temperature working fluids that is required for power cycles. The concentrator and absorber design must be optimized to maximize the amount of energy transferred to the working fluid and the performance of concentrating solar-thermal systems accordingly. However, majority of the installed solar thermal systems are for domestic water heating.

Special coatings are used for receivers to maximize absorption of incident solar energy. Depending on receiver temperature, energy loss by emission must also be minimized to maximize the net radiative transfer to the receiver and the working fluid. Therefore, spectrally selective coatings must have high absorptance at shorter solar wavelengths and low emittance at longer IR wavelengths. A detailed review of spectrally selective coatings for medium to high temperature concentrating solar systems is presented in [7].

Pigmented coatings comprise of a binder or a resin material and micro to nanometer sized particles known as pigments, and they are widely used as solar coatings due to their low cost [8]. The pigmented coating’s radiative properties depend on pigment and resin materials’ optical properties, pigment size and concentration, and the thickness of the

coating. Therefore, optimizing a solar coating for maximizing the performance of the solar system necessitates the estimation of these parameters.

Radiative properties of solar coatings produced through different manufacturing processes were characterized experimentally in earlier studies such as [9], and thickness, volume fraction and radius are altered in various experimental and theoretical studies such as [10–12]. A summary of the earlier works on pigmented coatings with comparisons of effective medium theory (EMT) based predictions and experimental results are presented in [13]. While use of EMT is practical, it does not yield accurate predictions unless small pigments or infrared (IR) radiation is considered [14]. A more accurate prediction of the radiative behavior of pigmented coatings can be achieved using Lorenz-Mie theory (LMT) and Kubelka-Munk theory (KMT) considering independent single scattering. Kubelka-Munk theory is based on two-flux model and describes radiative behavior of thin translucent films subject to diffuse irradiation. Extended KMT considers collimated irradiation rather than diffuse [15] and therefore, it is more appropriate to use it for modeling solar coatings. The multiple scattering effects can be incorporated by extended Hartel theory (EHT) [16]. Using four-flux method (FFM) improves accuracy further considering both collimated and diffuse components of radiation [17], in conjunction with LMT and EHT [18]. When pigments are densely spaced with respect to the wavelength, the effects of dependent scattering must be considered in IR wavelengths [19]. T-matrix method can be used in conjunction four flux method is used to estimate the spectral behavior of the coating [20].

The models proposed in [15–18] are applied to predict the spectral behavior of solar coatings [21], and their validation for polymer based TiO_2 or SiO_2 pigmented coatings for radiative cooling applications are presented in [22]. Effects of particle size and volume fraction is also presented through a parametric study [23]. More recently, LMT and radiation element method by ray emission model (REM^2) has been employed for optimizing TiO_2 based coatings for thermal and aesthetic effects, where radiative cooling is desired while minimizing the glare for buildings [24]. A comparison of CuO and TiO_2 pigmented coatings for radiative cooling are presented in [25], and a black-color coating with high reflectance in the NIR region is established by altering CuO particles' size in [26]. The optimal pigment size and concentration is identified through Nelder-Mead Simplex method and Quasi-Newton Opmization for various solar thermal applications to

closely match ideal coating behavior relying on inverse design, where the system is modeled using LMT with EHT and FFM, considering a fixed coating thickness [27].

However, coating thickness also effects spectral coating's behavior and should also be optimized [28]. Thickness sensitive, spectrally selective solar coatings are investigated using LMT and FFM, estimating the solar absorptance and total emittance and a range where the optimal values of coating thickness, pigment radius and concentration for commonly used pigments are suggested based on a parametric study [29]. Optimizing pigmented coatings to obtain high transmission in visible wavelengths and low transmission in UV wavelengths by altering thickness, volume fraction and radius are considered in [30], where numerical calculations are compared with experimental measurements.

1.2.2. Greenhouse Coatings with Scattering and Fluorescent Pigments

Greenhouse farming has many advantages over traditional agriculture and it enables production of higher number of crops per year. Agriculture in a controlled environment uses far less water (70–80%), and the crops are subjected to more limited microbes and pests [4]. There are various numerical and experimental studies about solar concentrators, passive coatings, desalination roofs, anti-condensation materials that target improving greenhouse conditions such as humidity, temperature and light. Of these, studies incorporating solar radiation manipulations have received significant attention [31]. It is well known that solar radiation that reaches the surface of the earth has a wide spectrum from ultraviolet (UV) to infrared (IR). However; only the visible light, between 400 nm - 700 nm is usable by plants, which is defined as Photosynthetic Active Radiation (PAR) [32]. Photosynthetic efficiency also varies within PAR and reduces within 450-550 nm spectrum, as the green plants tend to reflect these wavelengths. The possibility of converting the less photosynthetically efficient photons and transmitting them to photovoltaic devices (PVs) that are attached to both sides of the coating is described by [33]. Converting the photons from less efficient bands of spectrum to more efficient bands by using fluorescence to increase photosynthesis was also considered and applied in experimental studies [34–37]. These studies compared the photosynthetic growth under fluorescent pigmented coatings with bare coatings and report better growth under

fluorescent pigmented coatings. El-bashir *et.al.* [37] showed that under solar radiation, soybeans under fluorescent and scatterer pigment doped film grow better than those grow under bare film. Spectral measurements of this study also showed the effects of fluorescent particles in the coating on broadband diffuse reflectance and transmittance. While fluorescent pigments can convert photons with low photosynthetic efficiency to photons with higher efficiency, some portion of these converted photons will be diffusely reflected due to isotropic fluorescence emission [31], as experimentally measured by [37, 38]. It is widely known that plant growth increases with increasing light intensity. However, recent studies showed that growth of plants being subjected to high intensity light is reduced due to stressing of plants [39, 40]. Wakachaure and Minhas [39] performed experiments with 3 types of soybean genotypes and found that photosynthesis rate starts to decrease after exceeding a certain irradiance. Moreover, it is also reported that the diffuse irradiation that can be achieved by increasing the haze of the coatings also increases the photosynthetic rate [41, 42]. Therefore, a rigorous radiative transfer analysis of fluorescence coatings is necessary to be able to explain the observed increase in the growth rates under fluorescent coatings in the experimental studies. Radiative transport equation (RTE) must be solved to identify the radiation transfer in a scattering, absorbing and fluorescence medium for lighting [43] and bio-medical [44] applications. There are various methods to solve RTE in a fluorescent medium such as diffusion approximation [45], Monte Carlo method [45] and Kubelka-Munk theory [46]. While the validity of diffusion approximation and Kubelka-Munk theory are relatively limited, Monte Carlo method (MCM) has been considered as one of the standard approaches for solving radiative heat transfer [47]. The first application of MCM for biomedical systems was by Wilson and Adam [48], Keijzer *et. al.* [49] introduced generation, reflection and transmission of tissue auto-fluorescence. Wang *et.al.* [50] presented a fluorescence MCM that is capable of solving the RTE for monochromatic excitation and emission wavelengths. Neuman *et.al.* [51] introduced fluorescent term to RTE for a broadband system and solved it by using mathematical particle method.

Scattering particles are also used in fluorescent medium in some biomedical [52], lighting [53] and greenhouse [37] applications. Effective scattering coefficient, absorption coefficient and quantum yields are calculated to estimate optical behavior of these hybrid coatings as suggested by [44]. Excitation and emission bands of some fluorescent

materials can overlap as presented by [54]. Both path length based MCM and Kubelka-Munk theory is found to estimate that region poorly, whereas a collision based MCM can successfully handle overlapped excitation and emission bands with emission spectrum at desired pigment concentration.[55].

1.2.3. Concentrated Optical Fiber Lighting with Fluorescence Reflectors for Vertical Farming

Food scarcity and rising food prices are common problems of humanity. Although setup and upkeep costs of greenhouses are higher, their use increases due to the negative effects of climate change and spreading of pesticide resistant microorganisms on the traditional open farm agriculture. Indoor farming is referred as Controlled Environment Agriculture (CEA), where farming conditions controlled to achieve optimal survival and growth conditions [4]. The agricultural production is mostly carried out in rural areas, away from both consumption and labor due to high land costs in densely populated urban areas. Vertical farms, where plants are kept in stacked shelves, can be used in rural areas to overcome these issues by increasing yield per land. There are increasing use of commercial vertical farms in different geographies, from Asia to North America, but further technological developments are necessary to increase the feasibility of the concept [4].

The electricity consumption in buildings constitutes approximately 40% of the total electricity consumption [2], and about 40-50% of that consumption is due to lighting [3]. Therefore, utilization of optical fibers to carry sunlight inside the buildings has been attracting attention. The availability and feasibility of solar lightning systems is studied by Ghisi and Tinker [56] and the potential for energy savings on lighting is found to be ranging from 56 % to 89 % in the UK. Ullah and Shin [57] outlined a detailed model to concentrate sunlight into optical fibers using collectors and then to transmit it to multiple floors. A similar system can be implemented to vertical farms in order to reduce cost of electricity [58].

Solar radiation that reaches the surface of the earth ranges from ultraviolet (UV) to infrared (IR). However, only visible light that is between 400 nm - 700 nm is usable by

plants, which is referred as Photosynthetic Active Radiation (PAR) [32]. Photosynthetic efficiency also varies within PAR wavelengths and it is reduced within 450-550 nm, as the green plants tend to reflect within this band. Corrado *et al.* [33] proposed converting less photosynthetically efficient photons to more efficient ones via fluorescent coatings for photovoltaic devices (PVs). Converting photons from less efficient bands of spectrum to more efficient bands by using fluorescent coatings to increase photosynthesis was also considered for greenhouses in numerous experimental studies [34–37]. These studies compared the photosynthetic growth under fluorescent pigmented coatings with bare coatings, and observed improved growth under fluorescent pigmented coatings.

While fluorescent pigments can convert photons with low photosynthetic efficiency to photons with higher efficiency, more than half of these converted photons will be diffusely reflected out from the greenhouse once they are introduced to semitransparent coatings due to isotropic fluorescence emission [31, 32]. This is experimentally observed in [37, 38], and limits the increase in the photosynthetic growth rate. A rigorous radiative transfer analysis of fluorescent coatings is necessary to understand the experimentally observed increase in the growth rates under fluorescent coatings. For that, Radiative Transport Equation (RTE) must be solved for absorbing, emitting, scattering, and fluorescent medium, as in the case of lighting [43] and bio-medical [44] applications. There are various methods to solve RTE in a fluorescent medium such as diffusion approximation [45], Monte Carlo method [45] and Kubelka-Munk theory [46]. While the validity of diffusion approximation and Kubelka-Munk theory are relatively limited, Monte Carlo method (MCM) has been considered as one of the standard approaches for solving radiative heat transfer [47].

1.3. Objective

This study aims to increase the performance of solar energy systems by implementing suitable pigmented coatings to alter spectral solar flux. The proper pigment and binder types are chosen along with the optimal pigment size, concentration and coating thickness to achieve the desired coating behavior for the considered problems, using the proper models and theories. Three applications are considered in this study:

The first study presents a unified model for predicting the spectral reflectance of the pigmented coatings considering EMT, independent, and dependent scattering regimes combining models developed in the earlier studies [15–18]. The unified model is then used for design of the spectrally selective coatings for solar thermal applications. Two different collector types; flat plate and parabolic trough collectors are considered to find optimum pigmented coating types at different conditions such as absorber temperature and solar irradiation. An ideal coating behavior, in terms of spectral emittance, is defined to maximize the net radiant energy transferred to the working fluid in solar thermal systems. The design problem is considered as predicting the pigment size, volume fraction and coating thickness that best approximates the ideal coating's net heat flux, and it is formulated as an inverse problem, where the cause of a known or desired effect is sought. This design is usually referred as inverse design was applied for radiative transfer problems earlier. Solution of non-linear inverse design problems is possible by optimization methods [59, 60], and a global search algorithm, simulated annealing method (SAM), is used in this study as the introduction of thickness to the unknowns results in a topology with multiple local extrema.

In the next study, the effect of fluorescent and scattering coatings to net photosynthesis is identified through rigorous numerical analysis. Growth of soybean, which is a widely used and investigated agricultural plant with available experimental data in the literature, is considered. While the reasons behind observed improved growth rates under fluorescent pigmented coatings are investigated, the effect of concentration to haze and net photosynthesis is further discussed. A collision based MCM based model is developed to solve the fluorescence embedded broadband RTE and validated with experimental data from literature [44].

A solar illuminated vertical greenhouse, capturing solar slight using parabolic through collectors, and using a light distribution system, is considered in the final study. The collected solar irradiation is brought to each shelf layer by optical fibers, and is distributed over the crops with the help of optical lenses. Use of fluorescent reflectors is proposed in this study, to improve the growth rate by altering the irradiation spectrum for crops, and the improvement in the growth rate is investigated through rigorous numerical analysis. A collision based MCM model is developed to predict the irradiation distribution over the shelves for both cases. The developed model is capable of solving the broadband

RTE in the fluorescent medium that is validated with experimental data from the literature [44]. Vertical greenhouses with different number of shelves, illuminated by a solar collector and optical fiber light distribution system are considered at three different latitudes. The effects of using fluorescent reflectors and distribution of irradiation over the shelf on the growth rates are analyzed. Moreover, optimal reflector design, optimal number of shelves and the corresponding increase in the growth rate are identified for a fixed collector size.

1.4. Organization of the Thesis

This dissertation is divided into five chapters. Chapter 2 presents inverse design of spectrally selective thickness sensitive pigmented coatings for solar thermal applications. The problem, formulation and results presented here are from [61]. Improving photosynthetic efficiency using greenhouse coatings with scattering and fluorescent pigments is presented in Chapter 3. Whereas, the formulation and results presented in this Chapter are also presented in [62]. The improving concentrated optical fiber lighting with fluorescence reflectors for vertical farming constitutes Chapter 4. The study and its outcomes are also presented in [63]. The conclusions and the recommendations for future work are included in Chapter 5.

2. PIGMENTED COATINGS FOR SOLAR THERMAL APPLICATIONS

2.1. Radiative Transfer Properties of Pigmented Coatings

The scattering behavior of particles can be classified according to their particle volume fraction and size parameter, $x=2\pi nr_p/\lambda$, using the regime map introduced by Tien and Brewster [30]. Three regions of interest for pigmented coatings are those where EMT, independent multiple scattering and dependent scattering approximations are valid.

2.1.1. Effective medium theory

The optical properties of small particles in a medium ($x<0.3$) can be represented based on EMT that approximates the particles and the medium as a single homogeneous medium [10]. The effective behavior of coating while interacting with other media such as substrate and air can then be estimated based on the effective properties [19]. The effective complex dielectric function can be defined by the Maxwell Garnett approximation as

$$\bar{\varepsilon}_{e,\lambda} = \bar{\varepsilon}_{r,\lambda} \frac{\bar{\varepsilon}_{p,\lambda} + 2\varepsilon_{r,\lambda} + 2 f_v(\bar{\varepsilon}_{p,\lambda} - \bar{\varepsilon}_{r,\lambda})}{\bar{\varepsilon}_{p,\lambda} + 2\bar{\varepsilon}_{r,\lambda} - f_v(\bar{\varepsilon}_{p,\lambda} - \bar{\varepsilon}_{r,\lambda})} \tag{2.1}$$

The resin materials are non-magnetic; therefore, the refractive and extinction indices of the coating can be represented in terms of complex dielectric function, [64] as,

$$n_{e,\lambda}{}^2 = \frac{1}{2}\left(\varepsilon'_{e,\lambda} + \sqrt{\varepsilon'_{e,\lambda}{}^2 + \varepsilon''_{e,\lambda}{}^2}\right) \tag{2.2}$$

$$k_{e,\lambda}{}^2 = \frac{1}{2}\left(-\varepsilon'_{e,\lambda} + \sqrt{\varepsilon'_{e,\lambda}{}^2 + \varepsilon''_{e,\lambda}{}^2}\right) \tag{2.3}$$

If thickness of absorbing thin film coating on a metal substrate is larger than wavelength [15], the spectral reflectance for normal incidence can be estimated as;

$$R_\lambda = \frac{\rho_{c,\lambda} + \rho'_{c,\lambda}(1-2\rho_{c,\lambda})\exp(-8\pi \cdot t \cdot k_{e,\lambda}/\lambda)}{1-\rho_{c,\lambda}\rho'_{c,\lambda}\exp(-8\pi \cdot t \cdot k_{e,\lambda}/\lambda)} \tag{2.4a}$$

otherwise, interference effects occur and spectral reflectance for normal incidence can be estimated as;

$$R_\lambda = \left| \frac{r_{c,\lambda} + r'_{c,\lambda}\exp(-4i\pi \cdot t \cdot n_{e,\lambda}/\lambda)}{1+r_{c,\lambda}r'_{c,\lambda}\exp(-4i\pi \cdot t \cdot n_{e,\lambda}/\lambda)} \right|^2 \tag{2.4b}$$

where spectral reflection coefficient at air to coating boundary is

$$r_{c,\lambda} = \frac{1-(n_{e,\lambda} - ik_{e,\lambda})}{1+(n_{e,\lambda} - ik_{e,\lambda})} \tag{2.5}$$

and spectral reflection coefficient at coating to substrate boundary is

$$r'_{c,\lambda} = \frac{(n_{e,\lambda} - ik_{e,\lambda}) - (n_{s,\lambda} - ik_{s,\lambda})}{(n_{e,\lambda} - ik_{e,\lambda}) + (n_{s,\lambda} - ik_{s,\lambda})} \tag{2.6}$$

where n_e, n_s, are effective coating refractive index and substrate refractive index, k_e and k_s are effective coating absorption and substrate absorption index respectively.

2.1.2. Independent scattering: Lorenz-Mie theory

When the particles are larger, and they are distinctive, EMT is no longer valid and the radiative transfer equation must be solved. LMT defines scattering and absorption behavior of a single scattering medium consisting of spherical particles based on analytical solution of Maxwell equations [19] and it can be used to model the radiative behavior of the pigmented coatings approximating pigments as uniformly sized spheres, considering

the resin material as dielectric. Formulation of the theory is described in [27–29] with details, and it is not repeated here.

2.1.3. Dependent Scattering: T-matrix method

When clearance to wavelength ratio is small ($c/\lambda \leq 0.5$), effect of neighboring particles becomes significant. This effect arises from two reasons: Radiation scattered from a particle can interfere with scattered radiation from another particle (far field effect), and the internal electromagnetic field of a particle can be affected by scattering by neighboring particles (near field effect). In such a case, the radiative transfer properties must be predicted through the solution of Maxwell equations considering the neighboring particles. T-matrix method (TMM), also known as extended boundary condition method or null-field method, is a general solution method to electromagnetic field equations that is applicable to dependent or independent scattering problems of spherical or non-spherical particles. Detailed information in regards to TMM is not presented here as it is already presented elsewhere [65]. In this study, open source implementation developed by Mackowski and

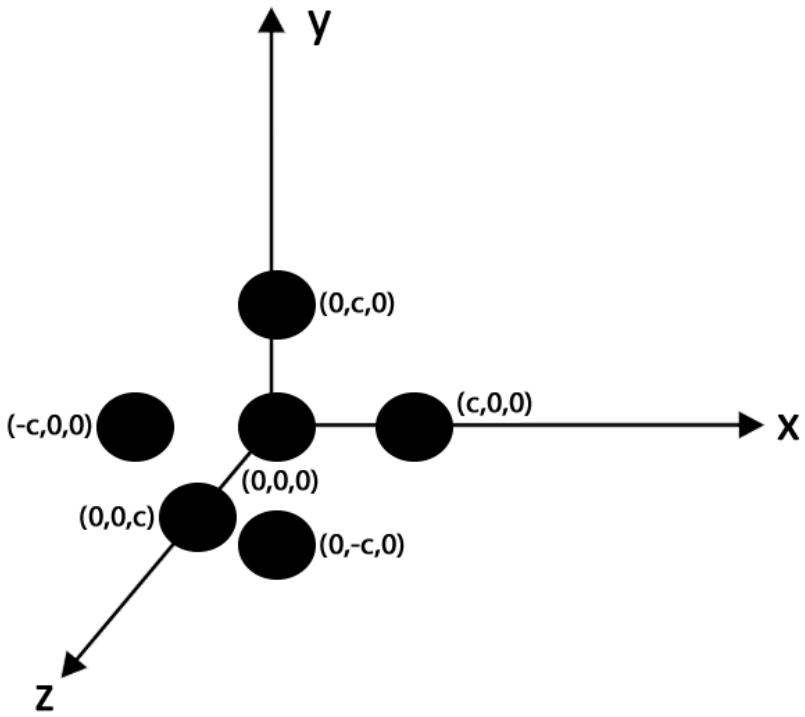

Figure 2.1. Pigment distribution [16] that is used to model dependent scattering.

Mishchenko [65] is used to estimate orientation averaged scattering and absorption cross sections and the phase function of particles in the cluster. The predictions using different number of particles and orientations were presented in [20] and the recommended configuration that is shown in Figure 2.1 is adopted in this study.

2.1.4. Radiative Transfer Model of Pigmented Coatings with Four Flux Method

The pigmented coating applied on a metal substrate can be considered as a thin slab as shown in Figure 2.2 that is illuminated from one side. For small particles with respect to wavelength, where effective medium approximation is valid, the absorption behavior of the coating can be estimated through Fresnel formalism (Equation 2.4). For larger particles, the radiative transfer equation must be solved considering the radiative transport properties based on independent or dependent scattering. There are different methods that can be used for solution of radiative transfer equation for the one dimensional thin slab problems shown in Figure 2.2. For solar collectors, the incident light have diffuse and collimated component; therefore, using four flux method is more appropriate. The FFM considers four intensities traveling through the slab as shown in Figure 2.2 [17, 18], where I_d is the diffuse forward, J_d is the diffuse backward, I_c is the collimated forward, and J_c is the collimated backward intensity. Through the solution of coupled differential equations written for each intensity component, the diffuse, $R_{d,\lambda}$, and collimated reflectances, $R_{c,\lambda}$, can be estimated, yielding spectral reflectance, R_λ, as:

$$R_\lambda = R_{d,\lambda} + R_{c,\lambda} \tag{2.7}$$

The four coupled differential equations and their solution are presented in detail in [17, 18, 26]. Once the spectral reflectance is calculated, spectral emittance and absorptance can be defined as:

$$\alpha_\lambda = 1 - R_\lambda \tag{2.8}$$

$$\epsilon_\lambda = \alpha_\lambda \tag{2.9}$$

Therefore, through the solution of FFM, for radiative transport properties defined by LMT or TMM, the spectral emittance of the coating can be defined based on pigment radius, volume fraction, thickness, optical properties and resin thickness.

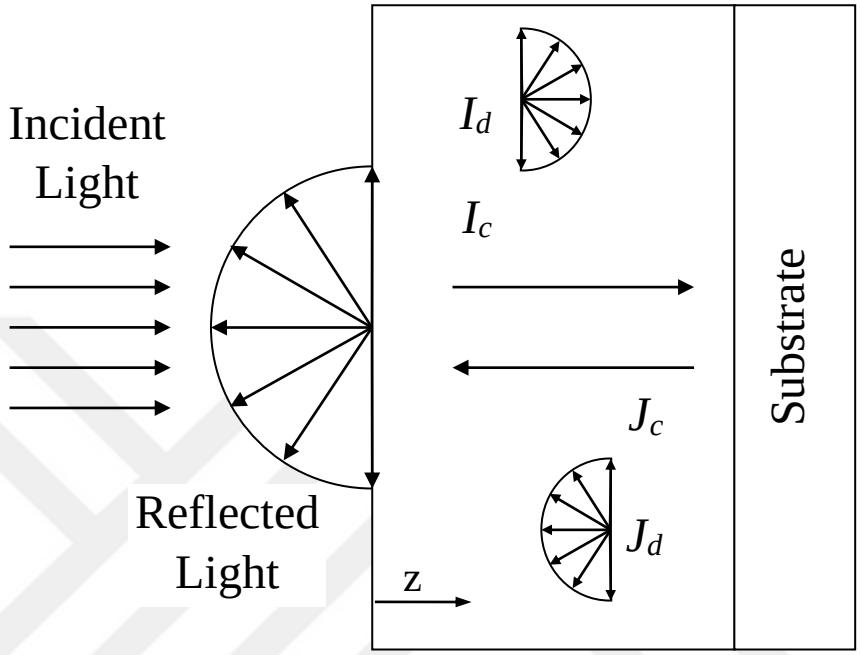

Figure 2.2. Sketch of the spectrally selective coating on a substrate.

A global search algorithm is to be used in this study, and a unified model (UM) is developed so that for a given set of parameters, the proper method (EMT or FFM with LMT-EHT or FFM with TMM) can be used according to the scattering regime map, as discussed earlier. Moreover, a simplified version of unified model (SUM) is developed, where only EMT and independent scattering regimes (FFM with LMT) are considered, whereas dependent scattering is ignored and LMT-EHT is used within this region instead of TMM. Coatings optimized with UM will be compared to those optimized by SUM in order to observe the effect of considering dependent scattering in optimization. A list of the models, their validity ranges and limitations are provided in Table 2.1.

The spectral reflectance of a coating with 400 nm PbS pigment 40% by volume in 2 μm thick polybinder is presented in Figure 2.3. It can be observed that prediction of UM is identical to that of LMT-EHT in the first region ($\lambda<0.8$ μm), TMM in the second region ($0.8<\lambda<8.2$ μm) and EMT in the last region ($\lambda>8.2$ μm). Whereas, prediction of SUM is

identical to that of LMT-EHT in the first two regions (λ<8.2 μm), and EMT in the last region (λ>8.2 μm). Prediction of UM and SUM are presented along with the estimations of all models for the entire spectrum and it was observed that there is a good agreement at model transitions. It can also be observed that estimation of different models at each region differs. Therefore, it can clearly be observed that the estimates by using a single model along the whole spectrum will yield erroneous results.

Table 2.1. Validity ranges and limitations of different models used for solving radiative transfer equations and its parameters.

Methods to Estimate Scattering Phase Function, Absorption Coefficient and Scattering Coefficient			
Method name	**Validity**		**Handled Scattering Type**
Lorentz Mie Theory (LMT)	Single sphere		Single Scattering
T-Matrix Method (TMM)	Single / Cloud of spheres		Single / Multiple Scattering
Methods to Implement Multiple Scattering to LMT			
Method Name	**Validity**		
Hartel Theory	Optically thin medium		
Extended Hartel Theory (EHT)	Optically thick and thin medium		
Methods to Estimate Reflectance			
Method Name	**Scattering Type**	**Valid for Size Parameter**	**Valid for Particle Clearance Wavelength Ratio**
Four-Flux Method (FFM) with LMT - EHT	Independent Multiple	x>0.3	c/λ>0.5
Four-Flux Method (FFM) with TMM	Dependent Multiple	x>0.3	c/λ ≤0.5
Effective Medium Theory (EMT)	No scattering	x ≤0.3	Particles are indistinguishable

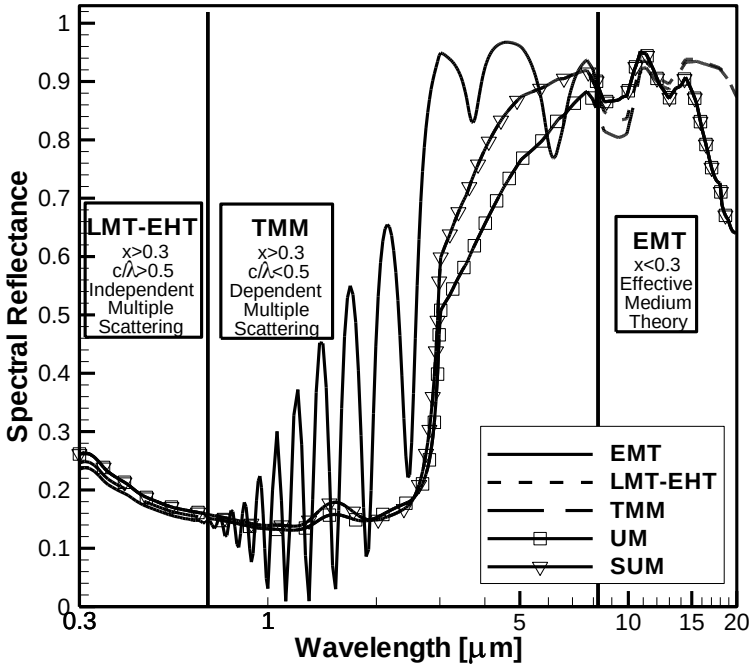

Figure 2.3. Spectral reflectance for different regimes of unified model.

2.2. Problem Statement and Formulation

The net heat transferred to the working fluid must be maximized in order to maximize the performance of a solar thermal system. The radiation incident to the absorber of a generic system can be defined in terms of solar irradiation and a concentration factor, C_f, which is 1 for flat plate collectors and larger than 1 for concentrating collectors. For a given absorber temperature, concentration factor, coating properties the net heat transfer can be formulated as:

$$q'' = \int_0^\infty \left[\alpha_\lambda G_{s,\lambda} C_f - \epsilon_\lambda E_{b,\lambda}\left(T_a\right) \right] d\lambda \tag{2.10}$$

Considering that, and dominant emission wavelengths of sun and absorber, the spectral emittance of an ideal solar coating that maximizes the net heat flux can be represented as:

$$\epsilon_{ideal,\lambda} = \begin{cases} 1 & \lambda \le \lambda_c \\ 0 & \lambda > \lambda_c \end{cases} \tag{2.11}$$

where λ_c represents a cut-off wavelength that depends on the absorber temperature, T_a, concentration factor, C_f, and solar irradiation $G_{s,\lambda}$. For a given set of T_a, C_f and $G_{s,\lambda}$,λ_c can be identified by maximizing net heat flux as explained in [27]. In this study, standard solar radiation based on ASTM-G-173-3 [66] is considered and corresponding λ_c values for given set of T_a, C_f are presented in Table 2.2.

The design problem is considered as an inverse problem of predicting the cause of a desired behavior. Since ideal coating yields the maximum net absorber radiant heat flux, the objective function to be minimized can be formulated so that the parameters yielding similar or identical performances with that of the ideal coating

$$F(\boldsymbol{\chi}) = \int_0^\infty \{[G_{s,\lambda} C_f - E_{b,\lambda}(T_a)][\epsilon_{ideal,\lambda} - \epsilon_\lambda(\boldsymbol{\chi})]\} d\lambda \tag{2.12}$$

where χ represents the set of parameters to be identified, $[r_p\ f_v\ t]^T$.

Considering the non-linearity of spectral emittance of the pigmented coating, a direct solution for minimization of Equation 2.12 is not possible. Optimization is used for solution non-linear inverse design problem similar to [59, 60].

There are various pigments used in spectrally selective solar coatings such as, nickel, germanium, carbon, silicon, copper dioxide, lead sulfide which are tabulated in [26]. Achieving high solar absorptance is possible by using dark colored or black pigments with relatively higher extinction index such as nickel (Ni), lead sulfide (PbS) and carbon (C). Therefore, these three pigments are considered for the optimization study along with the polybinder. Refractive index for these pigments and binder are available in [29] respectively, and is not presented here.

A maximum volume fraction of 0.52 is experimentally observed in [67]. Thus, upper limit for volume fraction is selected as 0.5, which is also the upper limit for Maxwell-Garnett Effective Medium theory. Gunde and Orel defines minimum clearance between particles as:

$$c = \frac{x\lambda}{\pi}\left(\frac{0.905 - f^{1/3}}{f^{1/3}}\right) \tag{2.13}$$

Etherden *et al.* [29] suggested that pigment size should be substantially smaller than the film thickness. A constraint is introduced to ensure that coating thickness is greater than 5 radii, As a result, single layer pigment structure is avoided and FFM is applicable at all cases. Pigments with radii as low as 20 nm is reported in [67], which is considered as the lower limit for radius in this study. Similarly, 0.3 μm coating thickness is reported in [11] for pigmented coatings, and this thickness is considered as the lower limit for thickness.

Carbon element is stable up to 1023 K, whereas PbS particles are stable up to 400 K [68] and 100% silicone binder can be stable up to 800 K [37]. Considering the material properties, medium temperature and high-temperature absorber cases are considered as 373K and 773 K, respectively. For concentrating collector cases, C_f is considered as 30 and 60, which are within the practical range suggested by literature [38].

2.3. Optimization Method

The minimization of the objective function described by Equation 2.12 is a non-linear optimization problem and the system has a complex topology with multiple local extrema. Therefore, use of gradient based methods could yield solutions dependent on the initial guess and global search algorithms must be used to overcome this problem. Simulated annealing (SA) is one of the most widely used global search algorithms due to its high performance and wide applicability [39].

The method mimics the physical process of annealing of solids [69]. It starts with an initial guess, $\chi_0=[r_{p,0}\ f_{v,0}\ t_0]^T$, that is considered as the current point and an initial temperature, $T_o=100$. At every step, temperature is decreased based on, $T=0.95^k*T_o$, where k is the iteration number. A random candidate point $\chi_{cp}=[r_{p,cp}\ f_{v,cp}\ t_{cp}]^T$ is created in a random direction, with a step length T from the current point. If the value of the objective function at the candidate point, $F(\chi_{cp})$ is smaller than that of the current point, $F(\chi_k)$, the candidate point replaces the current point as $\chi_{k+1}=\chi_{cp}$. Otherwise the acceptance of the candidate point is randomly evaluated based on a probability distribution function representing the annealing process as:

$$P = \frac{2}{1+\exp\left(\frac{\Delta F}{T}\right)} \tag{2.14}$$

Here P is the probability of acceptance, ΔF is difference between current value of the objective function and previous one. If P is smaller than a generated pseudo random number, then candidate point is accepted although the current solution is better, which resembles the candidate point proceeding through a local minimum. If P is not smaller than the generated pseudo number, then a new random candidate point χ_{cp} is created. At first iterations, where the temperature is high, possibility of selecting worse candidate point is high; therefore, method can check values from different local minimums. As temperature decreases, method converges near the global minimum.

Metaheuristic methods such as SA execute more objective function evaluations than gradient based optimization methods such as Newton or Quasi Newton method. However, SA is capable of handling discontinuous and multiple extremum systems. While Genetic Algorithm is another widely used global optimization method, it was reported in [70] that SA has higher convergence than genetic algorithm. Thus, SA is used in this study due to its robustness and ease of applicability [70]. More detailed information about SA is available in literature [71].

2.4. Results and Discussion

This study considers inverse design of spectrally selective pigmented coatings to maximize the energy harvesting from sun for solar-thermal applications. Integrated form of Equation 2.12, represents net heat flux when all convection loses are ignored and can be presented

$$q'' = \alpha_s C_f G_s - \varepsilon \sigma T_a^4 \tag{2.15}$$

where α_s is the solar absorptance, ϵ is the total emittance of the coating, and G_s is the total solar irradiance. In order to maximize the net heat flux received by absorber, high solar absorptance is desired along with low total emittance.

2.4.1. Model Validation and Verification

Verification and validation studies are performed to understand the predictive accuracy of the UM before using it for design of pigmented coatings. The verification of the UM for dependent and independent scattering regime is performed by comparing predicted results with those in [20] and represented in Figure 2.4. Predictions show good agreement with data from literature for both LMT-EHT and TMM. Besides, significant difference is observed between estimations of spectral reflectance considering dependent and independent scattering approximations from 1μm to 2 μm, which implies that predictions by LMT-EHT are not accurate within this band. The model is further validated for small size parameters where EMT is valid and the predictions are presented in Figure 2.4 together with experimental data from literature [28]. The comparisons presented indicate that the UM is in good agreement with measured and calculated values, thus validating the model. However, predictions of SUM that ignores dependent scattering, diverge from those of UM within this regime as expected.

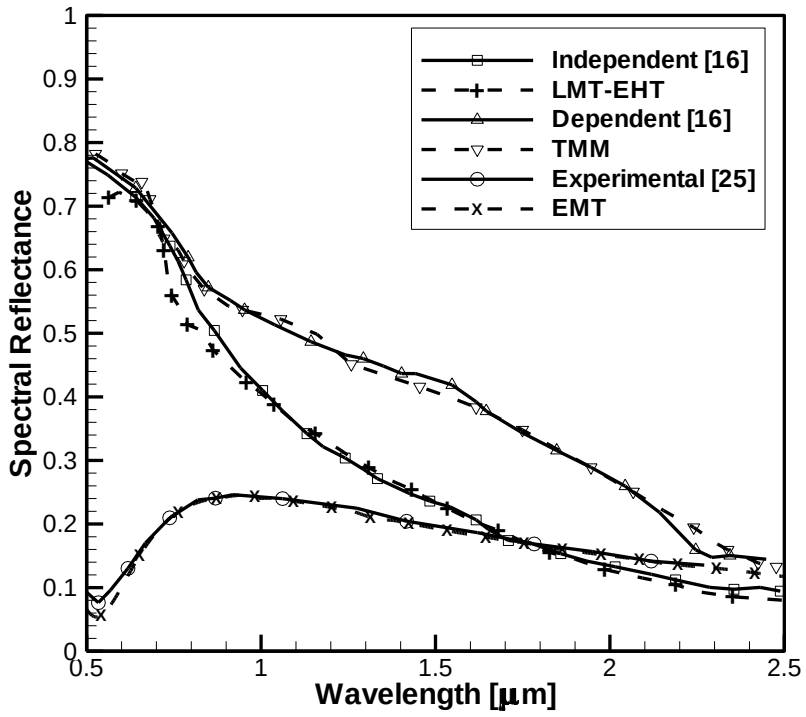

Figure 2.4. Spectral reflectance vs wavelength for validation and verification studies.

2.4.2. Demonstration of SA

The optimal coating leading to maximum net heat transfer is identified by inverse design by minimizing the objective function presented in Equation 2.12. In order to demonstrate inverse design's capability of finding optimum coating leading to maximum heat flux, a design problem is considered with PbS pigment in polybinder, for an absorber at 373 K and C_f=1. The contour plots of net heat flux change with r_p and t, for three discrete f_v values (f_v = 0.1, 0.2 and 0.3) are presented in Figures 2.5a-d, respectively. It can be

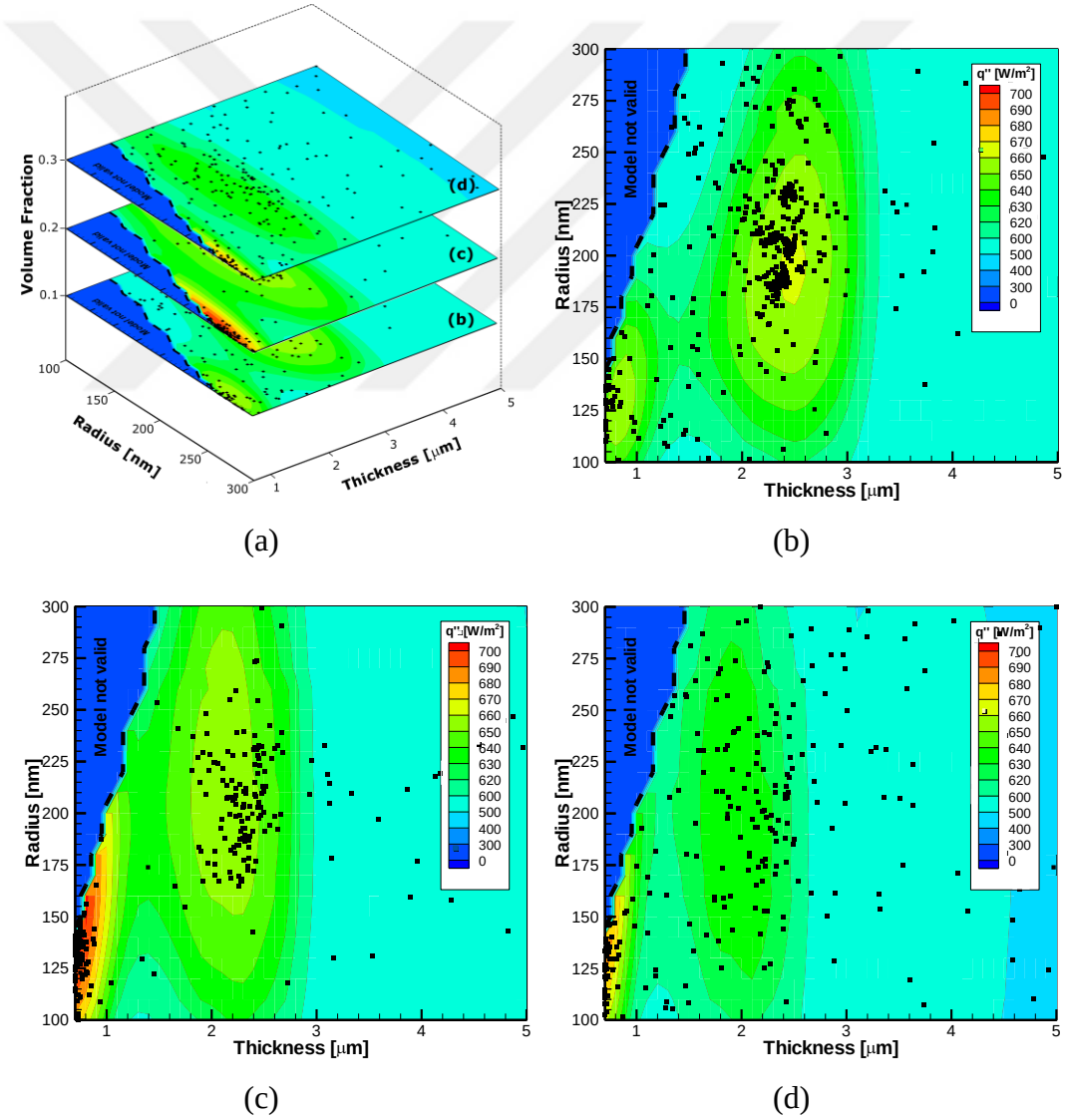

Figure 2.5. SA iterations and variation of net heat flux for (a) f_v=0.1,0.2,0.3 together, (b) f_v=0.1, (c) f_v=0.2, and (d) f_v=0.3.

observed that the system has multiple local extrema and SA is capable of identifying the global maximum, by minimizing the objective function presented in Equation 2.12. The iteration points initially populating around the local minima, populates to global maximum more densely as iterations proceed and at the end the algorithm converge to global maximum.

2.4.3. Evaluation of Different Pigments

Solution of the design problem using objective function defined by Equation 2.12, for three different pigments, C, Ni and PbS, are carried out for different concentration factors and absorber temperatures by using UM and SA algorithm. A summary of the results are presented in Table 2.2, where it can be observed that the total solar absorptance of PbS and carbon pigmented coatings are similar, whereas Ni pigmented coatings has a lower absorptance for an absorber temperature of 373 K. Moreover, total emittance of carbon pigmented coating is larger than that of PbS and nickel pigmented coatings. Besides, the coating with PbS pigments follows the behavior of the ideal coating more closely than carbon and nickel (Figure 2.6). Therefore, PbS appears to be a more suitable pigment material for the flat plate problem, with carbon pigmented coating has excessive heat loss due to higher emission, and nickel pigmented coating results has lower absorption.

Although pigmented coatings are mostly preferred for low cost applications, where temperatures are relatively low, the study also considers high temperature cases to further identify the behavior of pigmented coatings. Using PbS pigmented coatings for high temperature applications is not possible due to their instability at higher temperatures. Moreover, as carbon pigmented coatings has higher absorptance than nickel pigmented ones, and their relatively high emissivity has less significant effect as concentration factor increases, only carbon pigmented coatings are considered for high temperature applications. The total and spectral emittance of the carbon pigmented coatings for C_f of 1, 30 and 60 are presented in Table 2.2 and Figure 2.7, respectively. It can be observed hat, as concentration factor increases, the optimal coating's total emittance and solar absorptance both increase. However, emittance becomes less significant and increasing absorptance dominates with increasing concentration factor. Etherden *et al.* [29] suggested

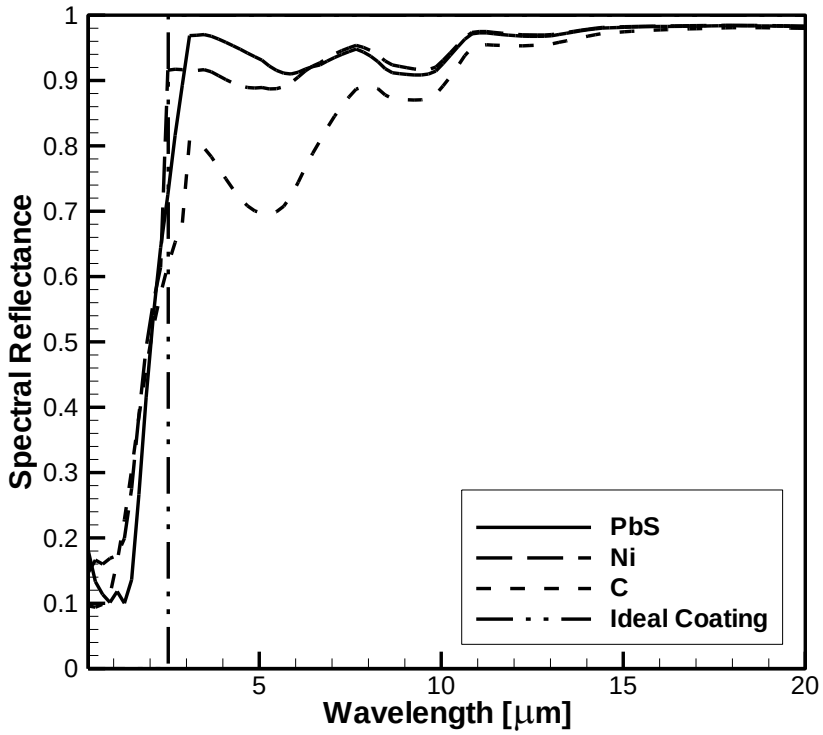

Figure 2.6. Optimal spectral emittance of different materials at T_a=373 K, C_f=1

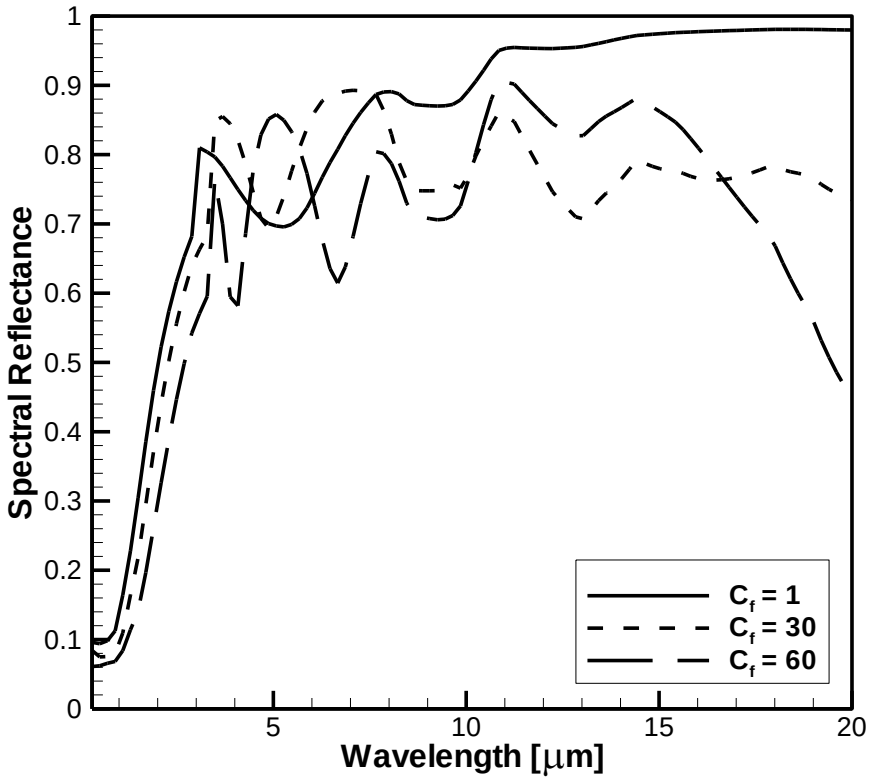

Figure 2.7. Comparison of spectral reflectance of the optimal pigmented coatings with carbon pigments for flat plate, and two concentrating solar collectors.

Table 2.2. Summary of optimal parameters for spectrally selective coatings for solar thermal systems.

T_a [K]	Pigment Material	r_p [nm]	f_v	t [μm]	α_s	ϵ	q'' [kW/m^2]	λ_c [μm]
373	PbS (C_f=1)	142	0.21	0.7	0.85	0.05	0.72	2.5
	Ni (C_f=1)	110	0.18	0.6	0.80	0.05	0.67	2.5
	C (C_f=1)	130	0.3	0.7	0.84	0.10	0.65	2.5
773	C (C_f=30)	163	0.11	2.1	0.89	0.23	19.48	2.3
	C (C_f=60)	163	0.11	2.9	0.91	0.27	43.96	2.4

that optimal radii for pigmented coatings are around 100 nm and they also claimed if further optimization study is carried out the exact optimum radii could be found between 100 and 200 nm, for Ni, C and PbS pigmented coatings and different absorber temperatures. The optimal radii estimated in this study are in agreement with their suggested range as presented in Table 2.2.

2.4.4. Parametric Analysis

Parametric analysis is carried out next to identify the effect of each design variable on collection efficiency. Here the collection efficiency is defined as;

$$\eta_c = \frac{q''_{net}}{G_s \cdot C_f} \tag{2.16}$$

and it represents the ratio of net absorber radiant heat flux to solar irradiation. The parametric analysis considers the optimal coating parameters presented in Table 2.2, varying one parameter at a time, keeping the other two constant. The effect of coating thickness on collection efficiency is presented in Figure 2.8. Absorptance and emittance increases with increasing thickness. Increase of emittance dominates increase of absorptance after optimum point, thus efficiency starts to decrease. Oscillatory behavior of the decrease is due to interference effect modeled by EMT, which is discussed in detail by

Laaksonen *et.al.* [72]. A number of local extrema can be observed aside from the global extremum that justifies the use of global search algorithms. Oscillation effect in emittance due to interference is more noticeable than reflectance as longer wavelengths results a lower coating thickness to wavelength ratio. Therefore the oscillation is more prevailing for flat plate collectors than concentrated collectors.

FFM with LMT - EHT and FFM with TMM use scattering and absorption coefficients to estimate reflectance. Etherden *et.al.* [29] states particle size is crucial for scattering and absorption coefficients and an optimization study that considers radii between 100 and 500 nm will reveal exact optimal particle for different pigments. Figure 2.9 shows that pigments has optimum radius values that meets with predictions of Etherden *et.al.* [29]. From Figure 2.9, it can be observed that the particle size have a limited effect on collection efficiency for carbon. However, it appears to be critical for nickel pigments. Considering that the pigments have a size distribution, ignoring the size distribution will not have any significant effect on carbon pigments, whereas a narrow distribution is desired for nickel.

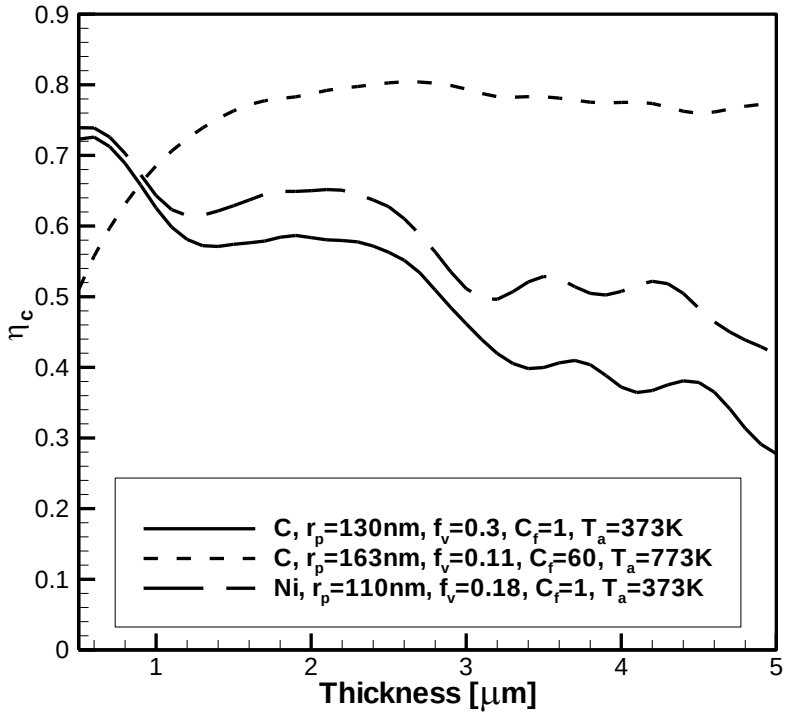

Figure 2.8. Variation of collection efficiency with thickness.

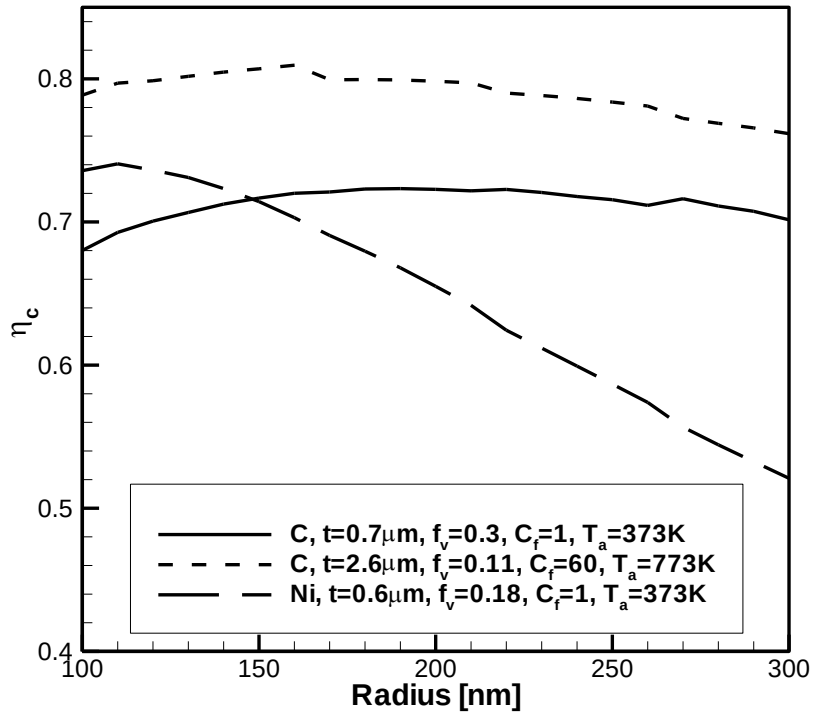

Figure 2.9. Variation of collection efficiency with radius.

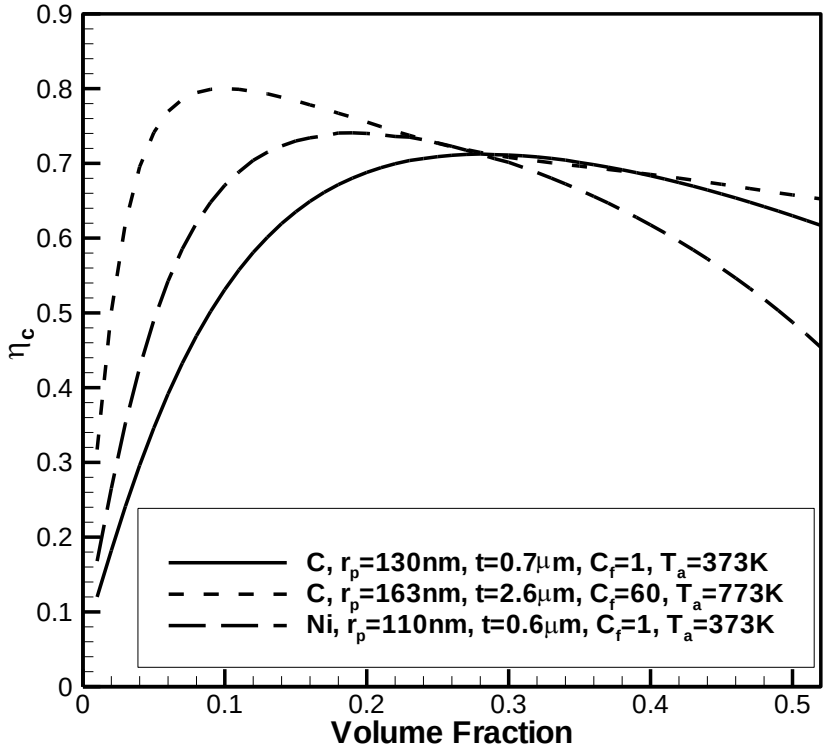

Figure 2.10. Variation of collection efficiency with volume fraction.

The effect of pigment volume fraction is presented in Figure 2.10, where a significant variation in collection efficiency is observed with changing pigment volume fraction. Absorptance and emittance increases with increasing volume fraction, after optimum volume fraction; increase of emittance dominates increase of absorptance and efficiency starts to decrease. This effect is more pronounced at higher concentration ratios, where the optimal particle volume fraction is lower.

2.4.5. Evaluation of Different Models

Most of the prior studies rely on a single model such as EMT or LMT over entire variable domain [25, 26]. In this study, unified models are developed and verified for designing pigmented coatings to overcome the limitations in regards to each model. In an additional study, use of EMT, LMT-EHT, UM and its simplified version SUM is evaluated for such an optimization by considering resulting collector efficiency and required computation time. This is accomplished by designing 4 coatings using EMT, LMT-EHT, SUM and UM for a prescribed case, and predicting the performance of the 4 identified coating parameters using UM that is the most accurate model.

Design of PbS and carbon pigmented coatings are performed for flat a plate collector at 373K, and for a parabolic collector at 773 K, respectively. Optimized design variables (r_p, f_v, t) and the corresponding performance parameters (α_s, ϵ, q'', η_c) predicted by each model compared to the expected values predicted by UM are presented in Tables 2.3 and 2.4. For flat plate, the coating designed by using EMT is 11% less efficient than the one that is optimized by using UM as seen in Table 2.3. The coating designed by EMT has a higher emittance than the coating designed by UM, which is more critical for a flat plate collector. However, the predicted emittances are similar for EMT and UM, as the absorber emits mostly in longer wavelengths where the size parameter is low and UM uses EMT. Although using LMT-EHT yields a coating design with relatively higher solar absorptance (α_s=0.92), the resulting efficiency is 19% lower due to the high emittance (ϵ=0.25) of the coating. LMT-EHT is not capable of accurately predicting the emittance at these wavelengths, predicting emittance as 0.04 that is significantly different from the prediction by UM leading to a poorly performing design. However, using SUM and UM yield almost identical designs and performances (α_s=0.85 and ϵ=0.05).

As it can be seen in Table 2.4, the coating designed by using EMT is 4.2% less efficient than the one that is designed by using UM, for concentrating collector. Considering the high concentration factor, the maximizing the absorptance is more critical than minimizing the emittance for this case. Therefore, using carbon pigments leads to a coating with relatively higher solar absorptance and emittance (α_s=0.90 and ϵ=0.35). Using LMT-EHT yields a slightly better coating design than that by using EMT in this particular case where emittance is less significant. Similar to the previous case, using SUM and UM yield identical designs and performances (α_s=0.91 and ϵ=0.27).

Results indicate that SUM can be used to optimize pigmented solar coatings. Coating designed by LMT-EHT performs weakly for flat plate applications due to high total emittance as presented in Table 2.3. Effect of total emittance becomes less significant for concentrating collectors; therefore, using LMT-EHT results in more accurate predictions for concentrating collector applications as presented in Table 2.4.

Table 2.3. Optimized design variables (r_p, f_v, t) and the corresponding performance parameters (α_s, ϵ, q'', η_c) predicted by each model compared to the expected values predicted by UM for PbS pigmented coating at T=373K

Model	r_p [nm]	f_v	t [μm]	*Model* α_s	ϵ	q'' [W/m^2]	η_c [%]	*UM* α_s	ϵ	q'' [W/m^2]	η_c [%]
EMT	20	0.32	2.4	0.86	0.15	619	68.4	0.87	0.15	619	68.4
LMT-EHT	192	0.05	4.9	0.92	0.04	777	86.0	0.92	0.25	550	60.8
SUM	140	0.20	0.7	0.85	0.05	709	78.4	0.85	0.05	717	79.3
UM	142	0.21	0.7	-	-	-	-	0.85	0.05	718	79.4

Computation time required for estimation of total reflectance using each model is presented in Table 2.5. While TMM is the most expensive method due to increased matrix size based on number of spheres considered in the estimation of extinction and scattering efficiencies, UM reduces computation time by 95% with respect to solely using TMM. Considering that the optimization algorithm performs about 1500-2500 total reflectance

estimations depending on initial guess and coating properties. For TMM, the optimization takes about 50 days, and UM requires approximately two and a half days of computation. However, using SUM provides further significant improvement and design can be completed within minutes. Therefore, SUM is suggested as a good compromise between accuracy and computational efficiency.

Table 2.4. Optimized design variables (r_p, f_v, t) and the corresponding performance parameters (α_s, ϵ, q'', η_c) predicted by each model compared to the expected values predicted by UM for C pigmented coating for C_f=60 at T=773K

Model	r_p [nm]	f_v	t [μm]	*Model* α_s	ϵ	q'' [kW/m^2]	η_c *(%)*	*UM* α_s	ϵ	q'' [kW/m^2]	η_c *(%)*
EMT	20	0.26	1.7	0.90	0.35	41.9	77.0	0.90	0.35	41.7	76.9
LMT-EHT	180	0.03	9.9	0.91	0.25	44.3	81.7	0.92	0.34	42.1	77.6
SUM	163	0.11	2.9	0.91	0.26	43.9	80.9	0.91	0.27	43.9	80.9
UM	163	0.11	2.9	-	-	-	-	0.91	0.27	44.0	81.1

Table 2.5. Computation time of calculating objective function with TMM, EMT, LMT-EHT and unified models separately for PbS pigment. r_p=170 nm, f_v=0.2, t=1 μm on single core of 3.40 GHz CPU.

Method	CPU Time (seconds)
EMT	0.2
LMT-EHT	0.5
TMM	2437
SUM	0.4
UM	123

3. FLUORESCENT GREENHOUSE COATINGS

3.1. Problem Statement

The horizontal roof of a greenhouse coating made of 40 μm thickness polyethylene terephthalate (PET) is considered as a plane parallel layer under diffuse and beam solar irradiation as presented in Figure 3.1. The coating is embedded with fluorescent ($K_2SiF_6:Mn^{4+}$) or scattering (TiO_2) pigments to alter coating's optical properties.

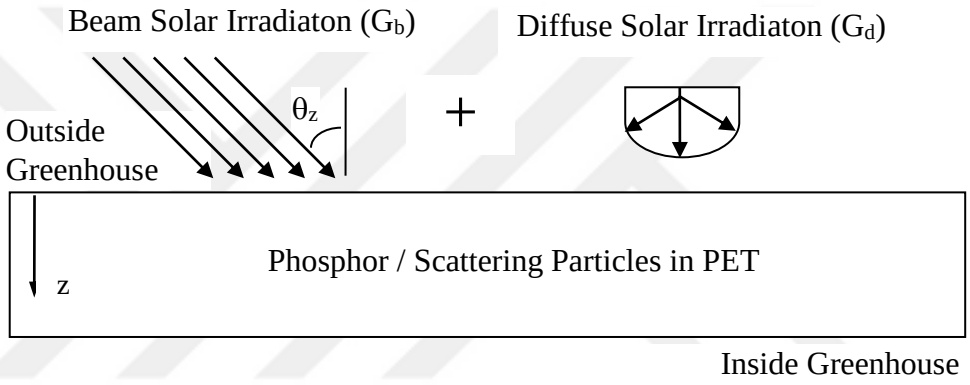

Figure 3.1. Sketch of the greenhouse coating for total solar irradiation.

McCree [73] showed the spectral variation of photosynthetic quantum efficiency of crop plants as represented in Figure 3.2. Pearson *et al.* [32] defined and suggested to use effective quantum transmission (τ_{eff}) to calculate effective transmissivity for photosynthesis by considering the effect of photosynthetic quantum efficiency suggested by McCree [73]. The effective quantum transmission for beam (direct) and diffuse irradiation is defined as:

$$\tau_{eff,b}(\theta_z) = \frac{\int_0^\infty G_{b,\lambda}(\theta_z)\lambda\tau_\lambda(\theta_z)Y(\lambda)d\lambda}{\int_0^\infty G_{b,\lambda}(\theta_z)\lambda Y(\lambda)d\lambda} \tag{3.1}$$

$$\tau_{eff,d} = \frac{\int_0^{\pi/2}\int_0^\infty G_{d,\lambda}\lambda\tau_\lambda(\theta)Y(\lambda)\cos(\theta)d\lambda d\theta}{\int_0^{\pi/2}\int_0^\infty G_{d,\lambda}\lambda Y(\lambda)\cos(\theta)d\lambda d\theta} \tag{3.2}$$

where $G_{b,\lambda}$ and $G_{d,\lambda}$ are the spectral beam and diffuse incident clear sky solar radiation, τ_λ is the spectral transmissivity of coating, Y is photosynthetic weighting factor that can be determined from quantum yield relationship represented in Figure 3.2. The angle of incidence (θ_z), diffuse and direct components of clear sky solar irradiation on a horizontal plane changes with respect to latitude (φ), day of year (n_d) and time of the day (h) [8]. The effective transmitted, photosynthetically active radiation (PAR) can be defined as

$$G_{eff}(\varphi, n_d, h) = \tau_{eff,d} \int_{400\,nm}^{700\,nm} G_{d,\lambda}(\varphi, n_d, h) d\lambda + \tau_{eff,b}(\theta_z) \int_{400\,nm}^{700\,nm} G_{b,\lambda}(\varphi, n_d, h) d\lambda \tag{3.3}$$

Three different latitudes (φ = 24.77^o for Riyadh, 41.02^o for Istanbul, and 52.38^o for Amsterdam) are considered in this study to identify the coating effect on plant growth under different solar conditions. The diffuse and direct components of clear sky solar spectral irradiation for these latitudes are calculated using SMARTS developed by NREL [74].

Photosynthetic growth is represented in terms of net photosynthesis that describes the difference between gross photosynthesis and rate of respiration and it is calculated by measuring CO_2 gas exchange and leaf area. Wakchaure and Minhas [39], Hu *et al.* [40] showed that while net photosynthesis increases with increasing PAR incident upon plant up to a light saturation point, and it starts to decrease due to stress with further increase. The net photosynthesis of soybean culture with varying incident PAR reported by [39] that is presented in Figure 3.3 is used in this study.

For a given latitude, φ, the net daily photosynthesis is estimated by

$$NP_{day}(\varphi, n_d) = \int_0^{24} NP\left[G_{eff}(\varphi, n_d, h)\right] dh \tag{3.4}$$

Estimation of the daily net photosynthesis (NP_{day}) under different greenhouse coatings necessitates the prediction of effective transmissivity. RTE must be solved for different coating configurations for predicting the corresponding effective transmissivity.

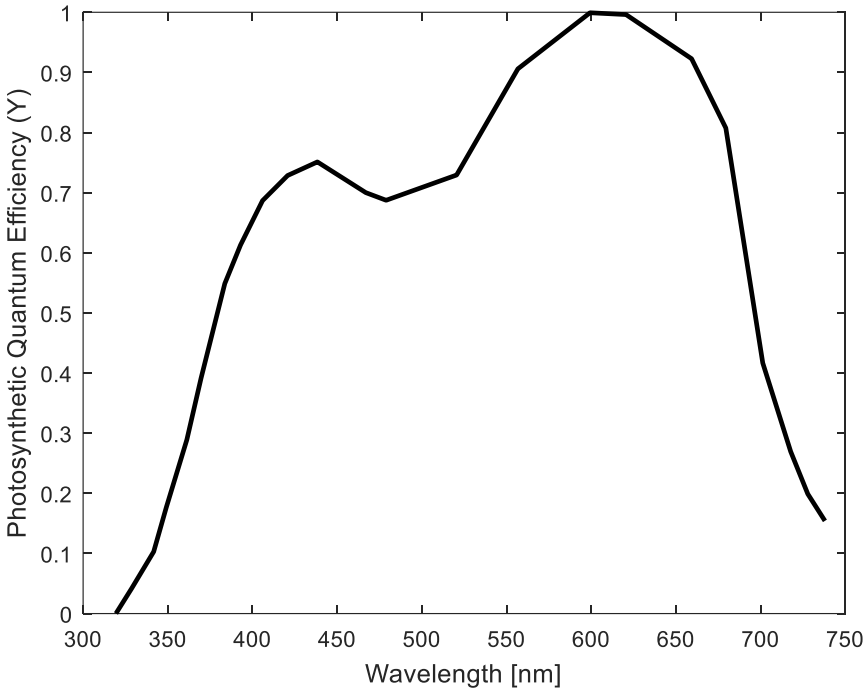

Figure 3.2. Relationship between photosynthetic quantum efficiency and wavelength of crop plants. [73]

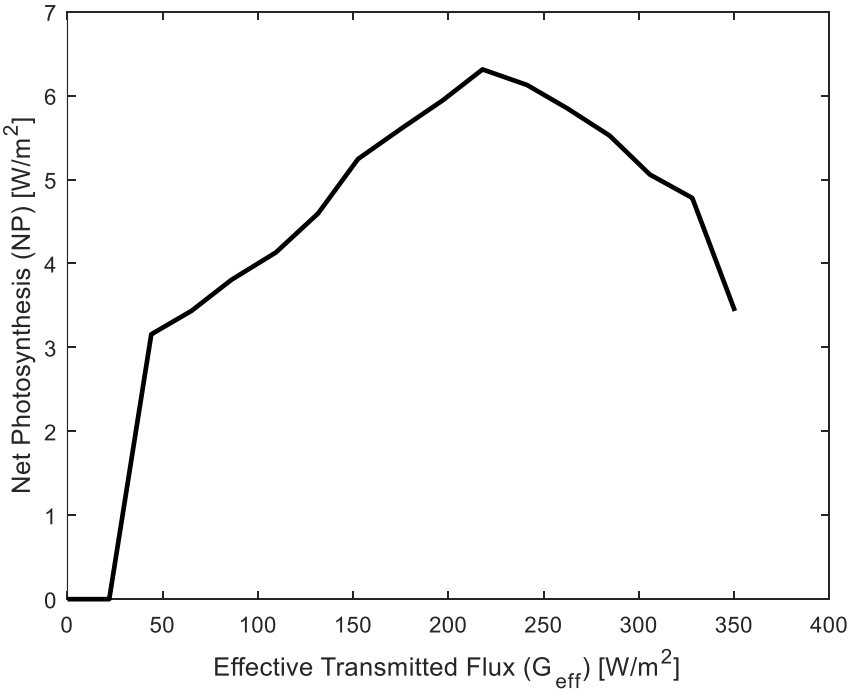

Figure 3.3. Net photosynthesis with changing vs. G_{eff} for soybean culture. [75]

For fluorescent medium, RTE is defined [45] as:

$$\frac{dI_\lambda}{ds} = \kappa_\lambda I_{b\lambda} - \kappa_\lambda I_\lambda - \sigma_{s,\lambda} I_\lambda + \frac{\sigma_{s,\lambda}}{4\pi}\int I_\lambda \Phi_\lambda(\Omega', \Omega) d\Omega' + S_\lambda \tag{3.5}$$

where I_λ is spectral intensity, $\sigma_{s\lambda}$ is spectral scattering coefficient and S_λ is the fluorescent source term representing the emitted fluorescent intensity at wavelength λ due to absorbed intensity in the fluorescent medium at λ'. In presence of fluorescent medium, the absorption in the medium is due to both fluorescent and non-fluorescent components of the medium, and the absorption coefficient, κ_λ, can be defined as:

$$\kappa_\lambda = \kappa_{f,\lambda} + \kappa_{nf,\lambda} \tag{3.6}$$

where $\kappa_{f,\lambda}$ and $\kappa_{nf,\lambda}$ are absorption coefficients of fluorescent and non-fluorescent components of the medium, respectively. Considering isotropic fluorescent emission, the fluorescent source term can be defined as;

$$S_\lambda = \frac{1}{4\pi}\int_0^\infty \kappa_{f,\lambda'} I_{\lambda'} QY(\lambda') \frac{\lambda'}{\lambda} P_f(\lambda) d\lambda' \tag{3.7}$$

The emitted energy due to fluorescent excitation follows a distribution that is usually identified in terms of normalized fluorescent intensity, $f_{fl}(\lambda)$ that represents the fluorescent emission at a wavelength with respect to its maximum value. The ratio of energy emitted at a particular wavelength λ to the total energy emitted is defined as

$$P_f(\lambda) = \frac{f_{fl}(\lambda)}{\int_0^\infty f_{fl}(\lambda) d\lambda} \tag{3.8}$$

Equation 3.7 can be further simplified by using the spectral power yield from λ' to λ, $Y(\lambda', \lambda)$.

$$Y(\lambda',\lambda) = QY(\lambda')\frac{\lambda'}{\lambda}P_f(\lambda) \tag{3.9}$$

The RTE with fluorescent source term defined in terms of spectral power yield then becomes

$$\frac{dI_\lambda}{dS} = \kappa_\lambda I_{b\lambda} - \kappa_\lambda I_\lambda - \sigma_{s,\lambda} I_\lambda + \frac{\sigma_{s,\lambda}}{4\pi}\int_{4\pi} I_\lambda \Phi_\lambda(\Omega',\Omega)d\Omega' + \frac{1}{4\pi}\int_0^\infty \kappa_{f,\lambda'} I_{\lambda'} Y(\lambda',\lambda)d\lambda' \tag{3.10}$$

Here the last term introduced represents the increase in intensity due to fluorescent emission due to excitations from all incident directions and wavelengths. Equation 3.10 can be used to predict the divergence of radiative heat flux for broadband fluorescence and considers energy transfer from one wavelength to another. While a spectral energy balance might not be satisfied for all wavelengths, the total energy balance must be satisfied.

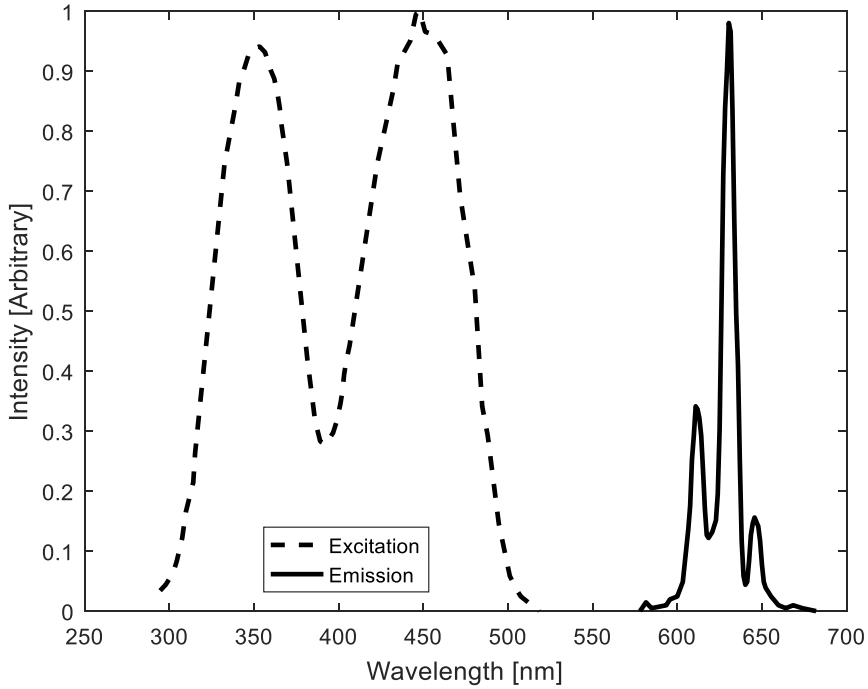

Figure 3.4. Excitation and emission properties of $K_2SiF_6:Mn^{4+}$ phosphor. [76]

The spectral reflectance and transmittance is calculated through the solution of the RTE for the system presented in Figure 3.1. Surface reflectivities required for the solution of Equation 3.10 are calculated by Fresnel formalism [19]. The optical properties for PET

and TiO_2 used in model are presented by [78, 79] respectively. Excitation and emission spectra of phosphor $K_2SiF_6:Mn^{4+}$ is from Pust *et.al.* [80] that is presented in Figure 3.4. Emission intensity of $K_2SiF_6:Mn^{4+}$ is stable up to 100 ºC [81], it is compatible to use in PET [82] and it is an effective material that is used in greenhouse led based lighting research for red spectrum [83]. Finally, quantum yield of the phosphor is 0.74 [85]. The calculation of total reflectance and transmittance, transmission haze and its daily average from spectral transmittance and reflectance are then straightforward.

3.2. Solution Method

The MCM is used in this study for solution of RTE through a 1D layer with fluorescent and scattering pigments subject to broadband solar radiation. A detailed description of the method is not presented here as the details of the collision based algorithm adopted is presented by Howell *et.al.* [47]. Wang *et.al.* [50] presents the details of handling the fluorescence. The highlights of the fluorescent MCM can be summarized as follows:

The PAR spectrum is approximated by N_λ=301 discrete wavelength bands, and $N_p=10^5$ photons are simulated for every wavelength. Each incident photon bundle at a particular wavelength has energy based on total spectral irradiation that is defined by, $w_{\lambda'}=G_{\lambda'}/N_p$. Once a photon bundle is absorbed within the medium, it is either absorbed by the binder or the fluorescent pigments. The probability of a bundle being absorbed due to fluorescent pigments is $\kappa_{f,\lambda}/\kappa_\lambda$, and as quantum yield represents the probability of re-emission once the photons are absorbed by fluorescent pigments, overall probability of re-emission once a bundle is absorbed by layer is $QY(\lambda)$ $(\kappa_{f,\lambda}/\kappa_\lambda)$. Therefore, once a photon bundle is absorbed by the layer, a pseudorandom number is generated and compared to $QY(\lambda)(\kappa_{f,\lambda}/\kappa_\lambda)$; a photon at a different wavelength will be re-emitted if the random number is smaller, otherwise no re-emission takes place. In the case of re-emission, the re-emitted photon's wavelength must be identified based on the probability density function (PDF) presented by Equation 3.8. The corresponding cumulative distribution function (CDF) can be defined as

$$R_{fl}(\lambda) = \frac{\int_0^{\lambda} f_{fl}(\lambda^*)d\lambda^*}{\int_0^{\infty} f_{fl}(\lambda^*)d\lambda^*} \tag{3.11}$$

The CDF is calculated numerically using trapezoidal rule for N_λ discrete wavelengths considered, and the wavelength of re-emission is determined by linear interpolation based on a generated pseudorandom number as an analytical random number relation (RNR) cannot be derived. The PDF and CDF for the fluorescent re-emission are presented in Figure 3.5. Once the re-emitted photon's wavelength is identified, its energy is calculated as $w_\lambda = w_{\lambda'}(\lambda'/\lambda)$, and the difference, $w_\lambda - w_{\lambda'}$, is absorbed by the medium.

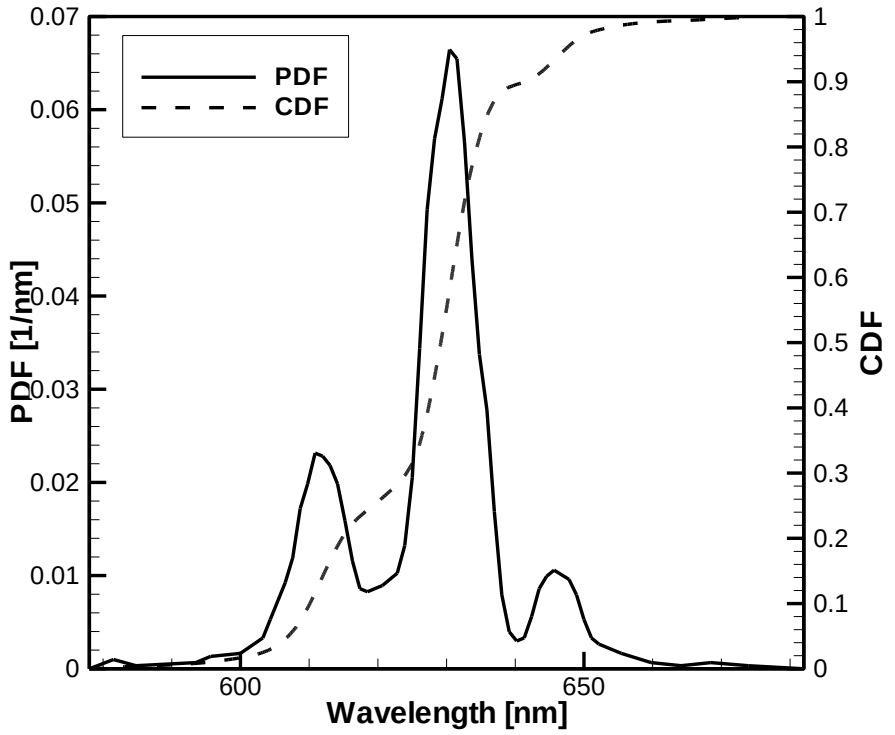

Figure 3.5. PDF and CDF for re-emission wavelength of the fluorescent layer.

The re-emitted photon is traced considering the radiative properties of the re-emission wavelength until it is absorbed, or it leaves the medium from either side. Once tracing of all photon samples is completed, spectral radiative properties; reflectance, absorptance and transmittance, can be estimated. While discretized spectral absorptance for N_λ wavelength bands would suffice for the analysis, discretized spectral reflectance and transmittance must be defined as a N_λ x N_λ tensor so that the spectral distribution of reflected and transmitted energy can be defined for an incident wavelength. Flow chart of

the Monte Carlo method that is introduced for broadband solution of RTE is presented in Appendix.

3.3. Results and Discussion

3.3.1. Model Validation

Solving RTE in a scattering and fluorescent medium by Monte Carlo method is validated by comparing estimated reflectance and fluorescence with experimental data presented by Liu *et.al.* [44]. Problem definition is well defined in the study and is not represented here. The presented results of fluorescent medium for diffuse reflectance and fluorescence in Figure 3.6 are in the same error margins with literature and there is a good agreement between the estimated and measured results. Each experimental and simulation data point have been normalized by the sum of all experimental and simulation data points respectively, as suggested by Liu *et.al.* [44].

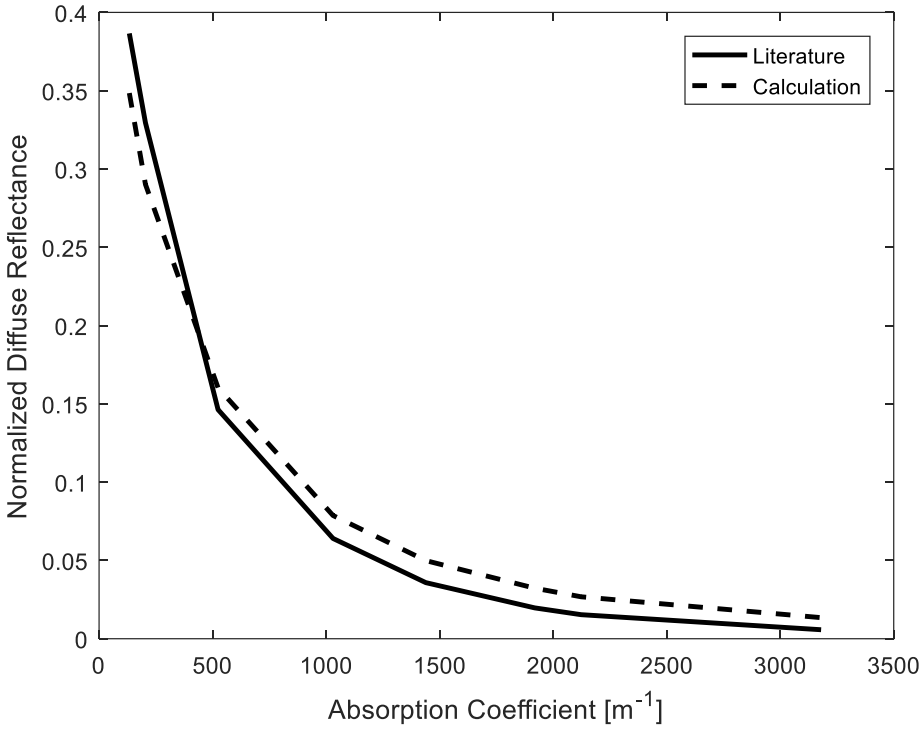

(a)

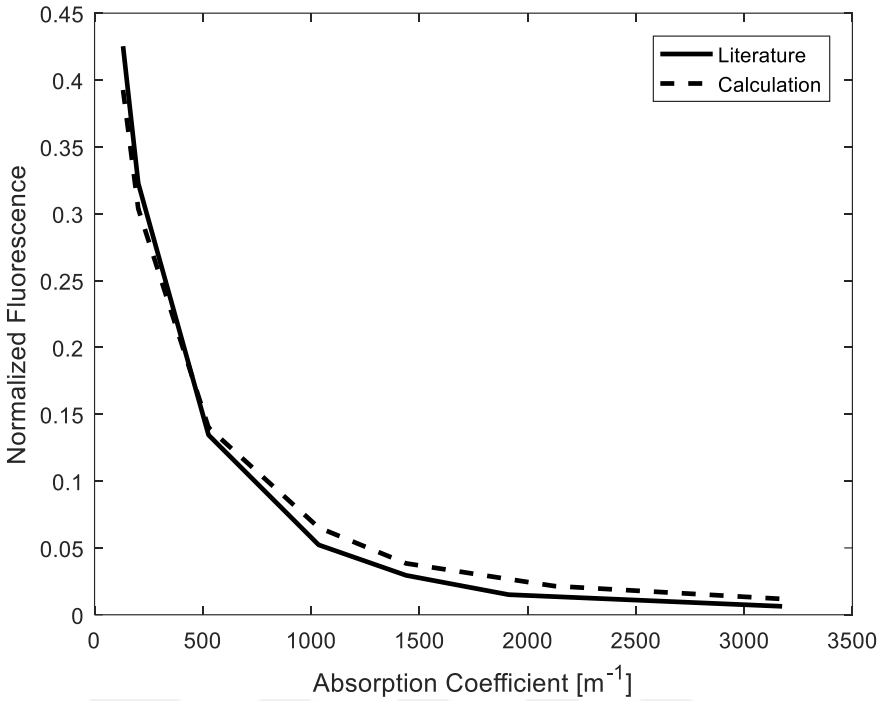

(b)

Figure 3.6. (a) Normalized diffuse reflectance and (b) normalized fluorescence for different absorption coefficients.

3.3.2. Fluorescent Coating for Different Latitudes

A parametric study is performed in order to investigate the effect of fluorescent particles on net photosynthesis and effective transmitted energy for low, middle and high latitudes, considering $K_2SiF_6:Mn^{4+}$ pigments with volume fraction of 0 to 0.2. Although the fluorescent conversion of photons to higher photosynthetic efficiency increases G_{eff}, the combined effect of absorbed energy due to down-conversion and quantum yield, and reflected energy due to isotropic fluorescent re-emission is more effective, resulting in a reduction in G_{eff} with increasing fluorescent particle volume fraction for all latitudes considered (Figure 3.7a).

The change in net photosynthesis (*NP*) with changing fluorescent pigment particle concentration depends on latitude as observed in Figure 3.7b. While fluorescent pigment concentration has a weak effect on *NP* for Istanbul, it is more significant for Amsterdam and Riyadh. However, the trends are stronger and opposing for the other two latitudes

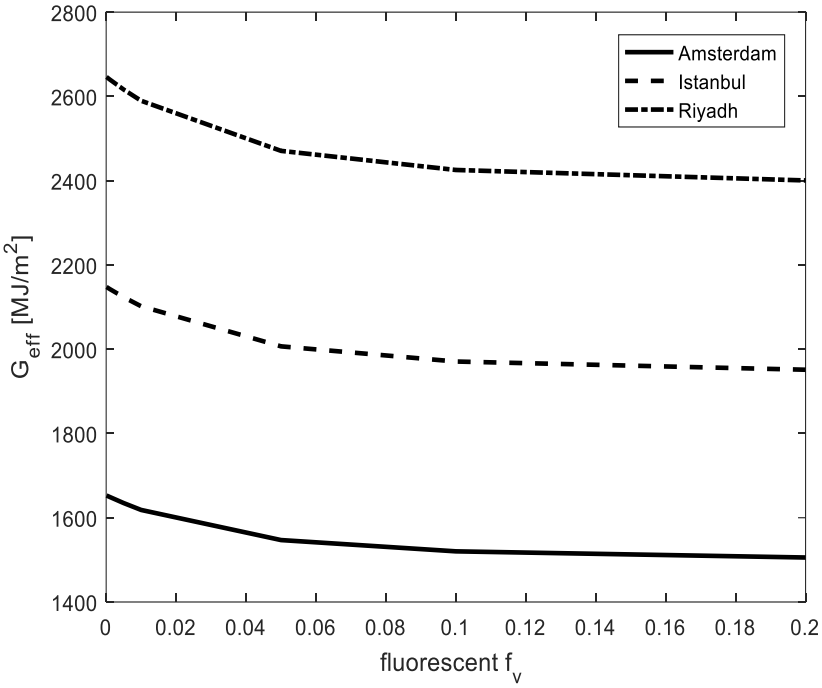

(a)

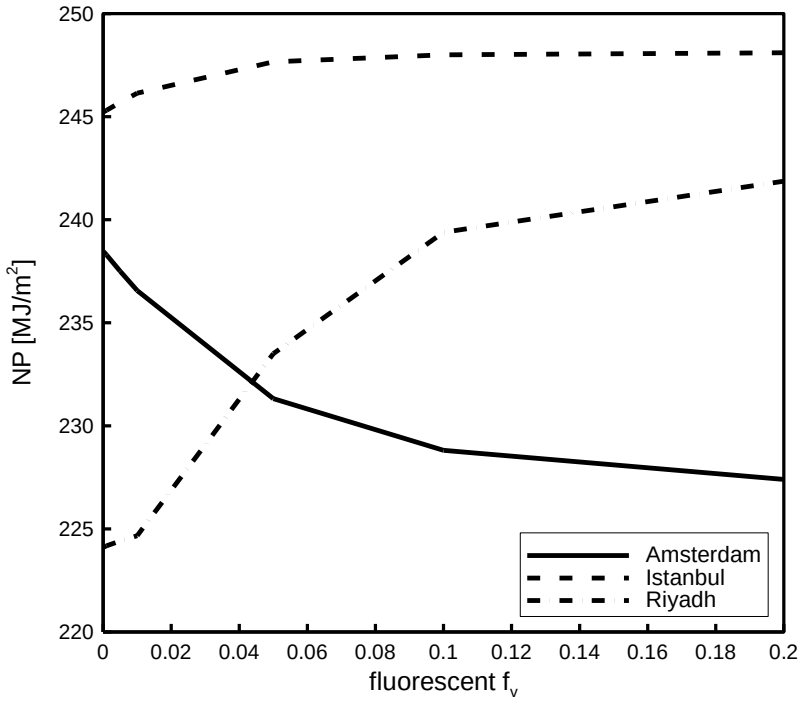

(b)

Figure 3.7. Effect of increasing fluorescent pigment concentration on (a) G_{eff} and (b) *NP*.

being investigated. While *NP* increases with fluorescent pigment concentration for Riyadh and it decreases with increasing concentration for Amsterdam. Solar irradiance of Amsterdam does not exceed the optimum irradiance presented in Figure 3.3, and increasing fluorescence pigments concentration decreases both effective solar energy and net photosynthesis. Therefore, using pigments at higher latitudes where solar irradiance is below optimal is not beneficial. Whereas, solar irradiance is higher than the optimal value in Figure 3.3 for Riyadh, and increasing fluorescent pigment concentration decreases effective solar irradiation that leads to an 8% increase in *NP*. Solar irradiance of Istanbul is slightly larger than the optimum irradiance thus using fluorescent can only achieve 1% improve in NP.

El-bashir *et. al.* [37] observed an increase in growth for soybean using PMMA coating doped with fluorescent and scattering particles with respect to non-pigmented PMMA coating in Riyadh in September. Their results also confirm the results being presented; the introduction of pigments leads to a reduction in effective solar irradiance that leads to an increase in growth in Riyadh.

3.3.3. Scattering Coating for Different Latitudes

Previous section showed that increase in net photosynthesis is a result of change in G_{eff}, where a decrease in low latitudes and increase in high latitudes might be desirable based on the plant of interest. Therefore, embedding scattering particles to the coating could also be an effective and cheaper way to reduce G_{eff}. TiO_2 particles are embedded to 40 μm PET coating to investigate the effect of scattering particles, and its effect at different volume fractions is estimated for 3 different latitudes. The particles are considered to be 300 nm as their scattering behavior is dominant at this size [88] .

The effective solar irradiation, G_{eff}, is almost halved for 0.02 particle concentration as presented in Figure 3.8a due to the back-scattering effects of TiO_2 particles. The observed G_{eff} decrease in Figure 3.8a is more significant than it is in Figure 3.7a, as there exist no physical means for increasing G_{eff}, unlike the case in fluorescent particles. Moreover, there exists an optimal particle concentration where *NP* is maximized for Istanbul and Riyadh, which is not the case for Amsterdam as observed in Figure 3.8b. The

optimal particle concentration for Istanbul is about 0.001, which does not introduce a significant growth rate increase with respect to using a coating without any scattering particles. Whereas optimal scattering particle concentration is about 0.004 for Riyadh that leads to a 10% increase in growth.

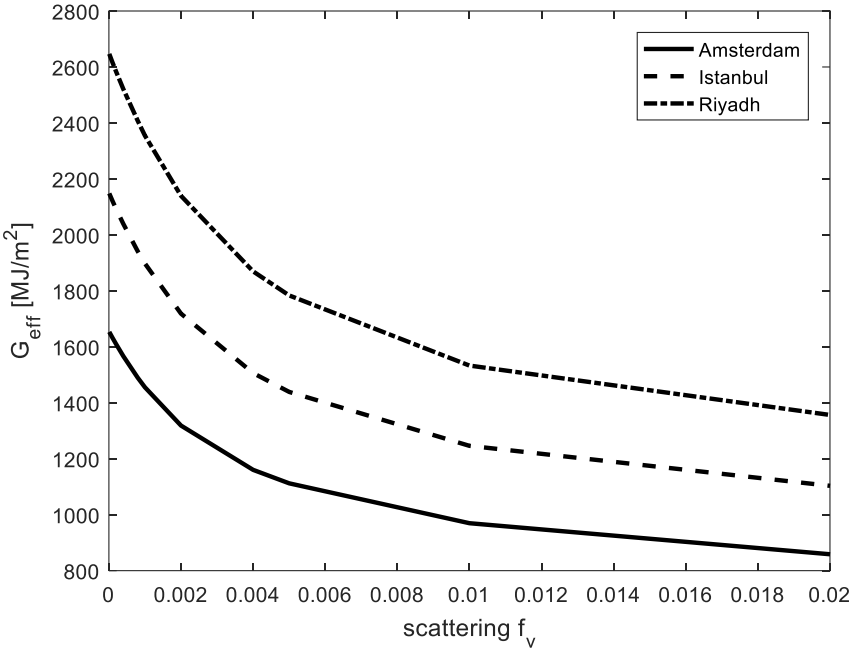

(a)

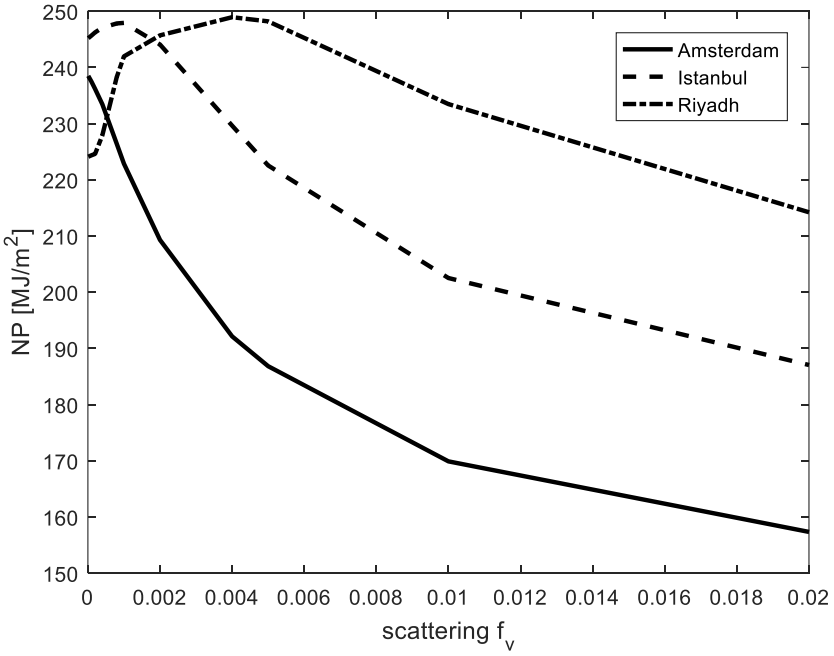

(b)

Figure 3.8. Effect of increasing scattering pigment concentration on (a) G_{eff} and (b)*NP*.

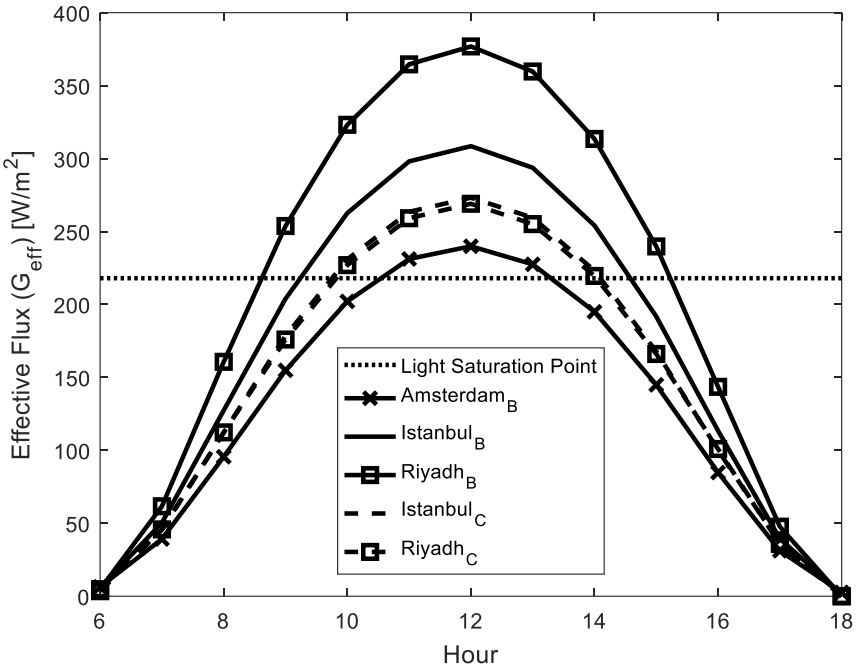

(a)

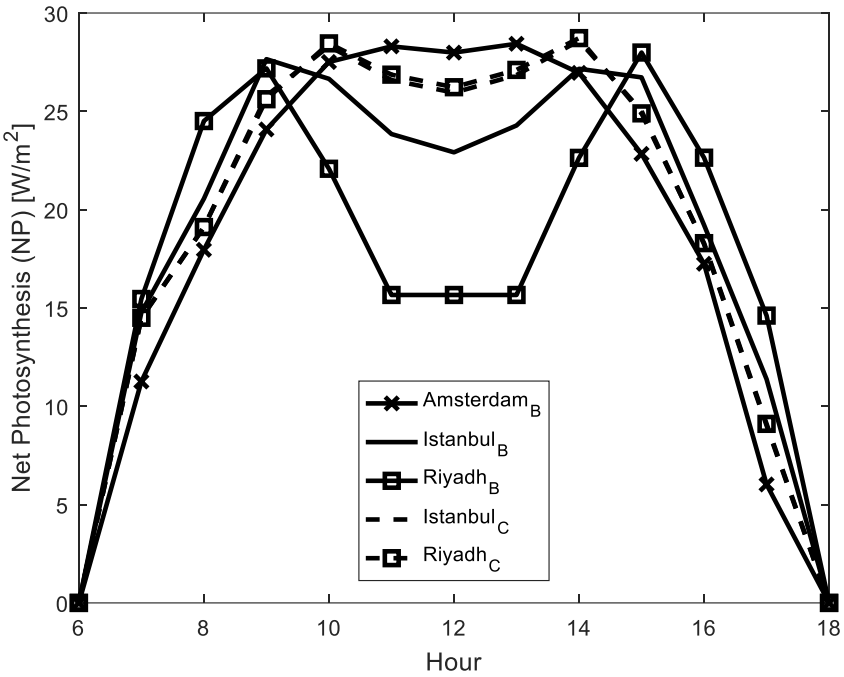

(b)

Figure 3.9. (a) G_{eff} (b) *NP* for different latitudes for bare (subscripted B) and optimal scattering coatings (subscripted C).

Hourly change of effective transmitted flux and net photosynthesis rates are also investigated, and presented in Figures 3.9a-b, respectively. Plants get stressed as G_{eff} level exceeds 218 W/m^2 as it can be seen in Figures 3.3. and 3.9a-b, which is the case for low and mid latitudes at midday. While the optimized coating for Riyadh and Istanbul is nearly coincident in Figure 3.9a, this coincident distribution is the optimum G_{eff} distribution. Although coating leads to a reduction in *NP* for earlier and later hours, it increases net photosynthesis at midday which contributes to overall daily *NP* for low latitudes such as Riyadh. The reduction in *NP* at earlier and later hours is compensated by the observed increase in midday for Istanbul. Use of pigments in the coating reduce net daily photosynthesis for high latitudes, where effective transmitted flux is always smaller than optimum flux levels.

3.3.4. Spectral Properties of Coatings

Spectral, effective solar irradiation of optimal scattering coating (f_v=0.004) and the fluorescent coating with highest particle concentration (f_v=0.2) under direct irradiation in Riyadh at September 15th, 1:00 pm is presented in Figures 3.10a and 3.10b, respectively. While spectral balance between incident, and sum of reflected, absorbed and transmitted radiation is satisfied through the entire spectrum for the scattering coating as presented in Figure 3.10a, similar balance is not satisfied for the fluorescent coating at all wavelengths as presented in Figure 3.10b. Spectral energy balance is satisfied for fluorescent coating between 520-575 nm and 675-700 nm, where excitation and emission effect does not exist. However, the sum of absorbed, reflected and transmitted flux is smaller than irradiation between 400-520 nm, as most of the incoming flux is down-converted to other bands with fluorescence excitation. However, total irradiation equals to sum of total reflected, absorbed and transmitted radiation, satisfying the radiative energy balance for the fluorescent coating.

The effect of using a fluorescent coating to spectral transmitted radiation can be observed in Figure 3.10b, where the increase in transmitted flux at certain wavelengths is not enough to increase G_{eff} as discussed earlier. Results show that due to isotropic nature of fluorescent emission, re-emitted portion, the shaded areas in Figure 3.10b, leaves the

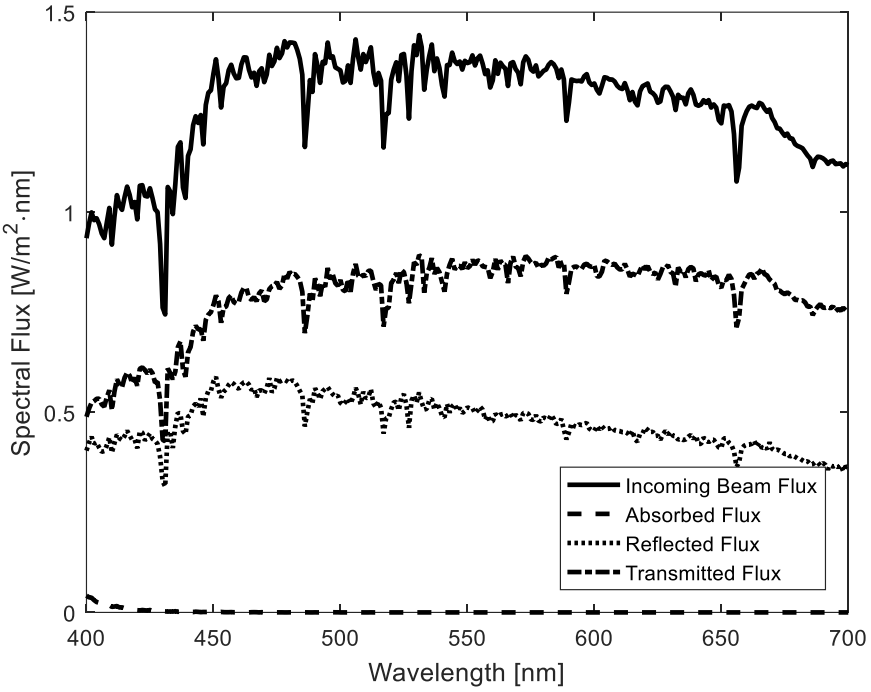

(a)

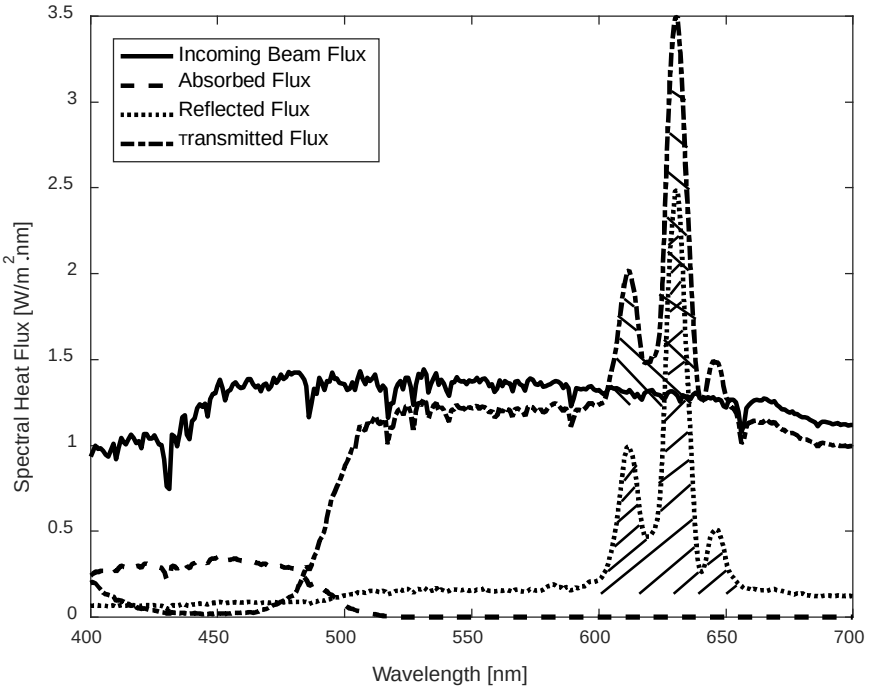

(b)

Figure 3.10. Spectral incident, reflected, transmitted and absorbed intensity of the (a) scattering (b) fluorescent coating.

system as reflected and transmitted flux. Since the diffuse reflected part is reflected back to the atmosphere, transmitted fluorescence cannot compensate diffuse reflectance and fluorescence absorption loss and as a result effective transmissivity reduces.

Although the growth model used in this study relates growth with total effective irradiance, diffuse irradiation improves plant growth as lower parts of the plant can receive more light under diffuse illumination (Aikman, 1989; Pieters and Deltour, 1999) as mentioned earlier. Scattering and fluorescent pigments in the coatings augment the diffuse irradiation by reducing beam irradiation. The optical behavior of transparent or semi-transparent layers and coatings should also be described by the directionality of the reflectance or transmittance besides their values. Transmission haze is defined as the ratio of diffuse transmittance (T_d) to hemispherical transmittance (T) and it can be used for describing directional characteristics according to ASTM-D 1003 Standard [89]. The diffuse transmittance can be described based on transmitted light that deviates 2.5° more than the direction of incidence, and the transmission haze can be defined as

$$H_T(\varphi, n_d, h) = \frac{G_{eff}(\varphi, n_d, h) - G_b(\varphi, n_d, h) \int_{\theta_z - 2.5^o}^{\theta_z + 2.5^o} \tau_{eff,b}(\theta) \cos(\theta) d\theta}{G_{eff}(\varphi, n_d, h)} \cdot 100 \tag{3.11}$$

and the daily weighted average of transmission haze, $H_{T,av}$ is defined as

$$H_{T,av}(\varphi, n_d) = \frac{\int_0^{24} H_T(\varphi, n_d, h) G_{eff}(\varphi, n_d, h) dh}{\int_0^{24} G_{eff}(\varphi, n_d, h) dh} \tag{3.12}$$

Haze calculations of both fluorescent and scatterer are carried out at the optimum concentrations for net photosynthesis. Use of fluorescent coating leads to a slightly increases haze from 14% to 16% in Istanbul, and 12% to 14% in Riyadh. Since fluorescence effect is only observed in excitation spectrum, its effect on haze is less significant than effect of scattering. Using TiO_2 doped coating increase transmission haze from 12% to 32% in Riyadh and 14% to 24% in Istanbul. An optimum concentration does

not exist as both fluorescent and scattering coating decrease net photosynthesis for Amsterdam; thus, haze is not estimated for there.

Considering the increase in haze, it is expected that estimated net photosynthesis increase would have been larger in an actual system as haze effects are not included in the growth model used in this study due to lack of reported experimental data that relates haze and intensity to net photosynthesis.

4. FLUORESCENCE REFLECTORS FOR VERTICAL FARMING

4.1. Problem Statement

The solar illuminated vertical farm introduced here comprised of parabolic collectors, a light distribution system and shelves as shown in Figure 4.1a. Beam or direct part of sunlight is collected by the parabolic trough collectors (Figure 4.2), and the collected light is distributed to the shelves of the vertical farm by a light distribution system, which consists of optical fibers, splitters and lenses. A solar tracking system is used with collectors to maximize collected radiation amount. In a typical system, referred as the "baseline system" in this study, the solar radiation transmitted through the optical fiber, passes through an optical lens to achieve a uniform irradiation distribution over the shelf, and it is directly exposed to crops as shown in Figure 4.1.

A modified system is proposed in this study, in which the optical fiber bundle is directed to the fluorescent reflector at ceiling of shelf that uniformly distributes the radiation over the crops as it is presented in Figure 4.3. The proposed reflector is comprised of a 4 mm BK7 optical glass embedded with fluorescent ($K_2SiF_6:Mn^{4+}$) pigments and have a Lambertian back reflector, as presented in Figure 4.4. Preparation of fluorescent glasses are described in the literature [90]. $K_2SiF_6:Mn^{4+}$ is chosen to convert blue-green light to red and the surface of the BK7 glass is coated with a 100 nm thick MgF_2 antireflection coating to reduce specular reflection.

The solar irradiation that can reach the shelves diminish due to losses from the absorption in parabolic trough collector, the reflection with angles of incidence larger than cable acceptance angle, and the attenuation of light through the distribution system. Liang *et al.* [91] measured 60% efficiency during collection and transmission of 60 W of radiative energy by 19 optical fibers. Jaramillo *et al.* [92] transmitted 26 W of radiative energy with 88% efficiency over one optical fiber with 10 meter length, and 5 mm diameter. The collection and transmission parts of the design in this study are adopted from Ullah and Shin [57], and 60% efficiency for the multiple optical fiber system is considered based on the study of Liang *et al.* [91].

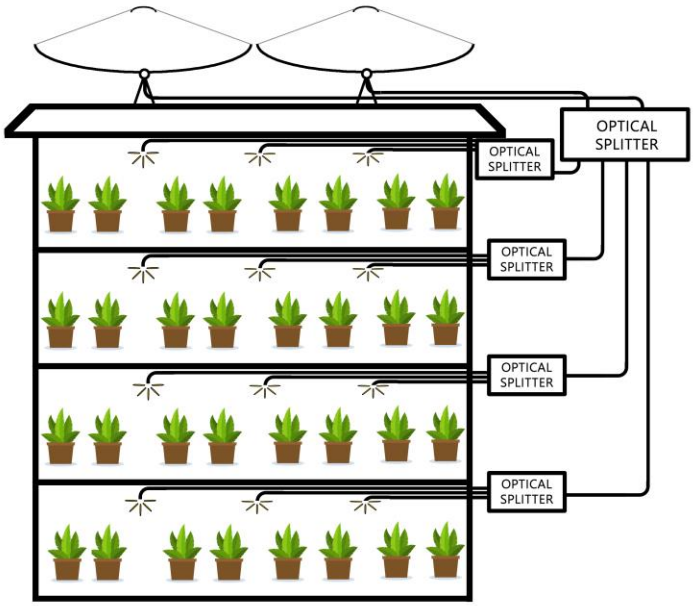

(a)

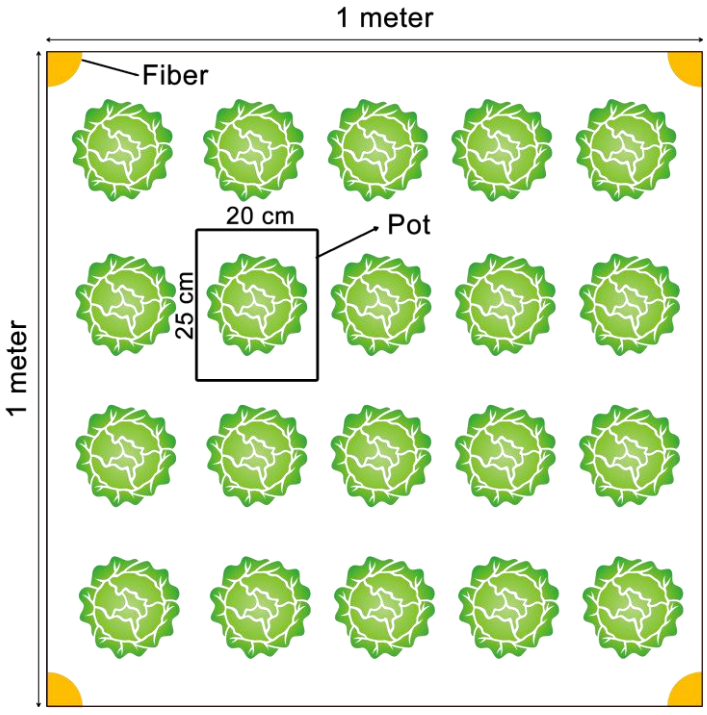

(b)

Figure 4.1. (a) Layout of the vertical greenhouse lighting system. (b) Top view of a shelf.

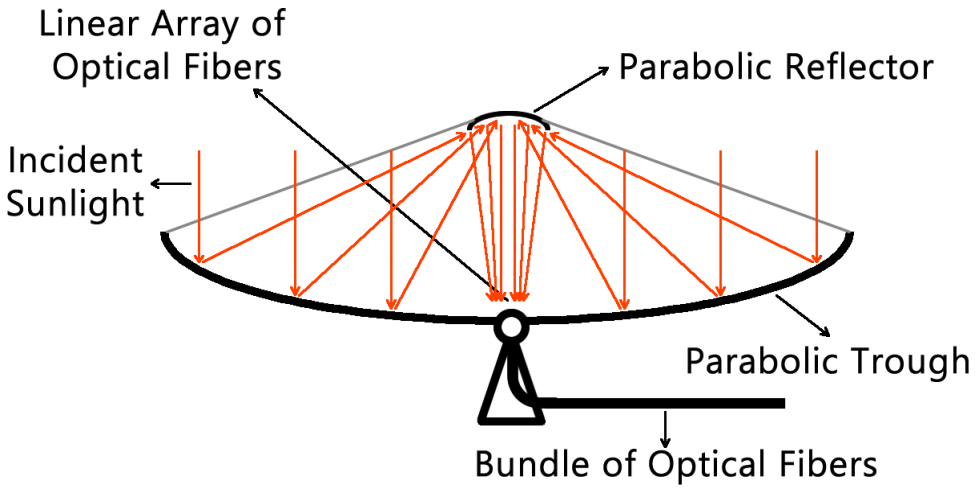

Figure 4.2. Detailed physical layout of collector system. [57]

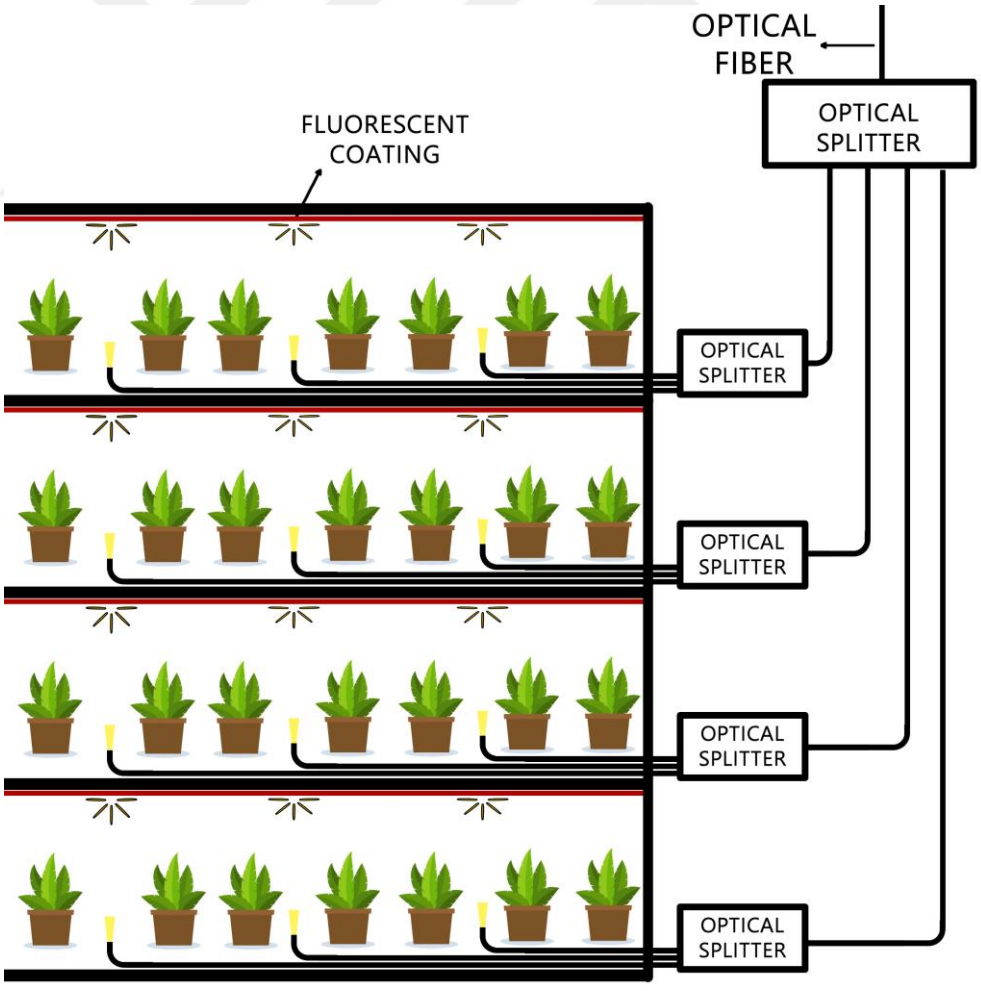

Figure 4.3. Layout of proposed vertical greenhouse with fluorescent reflector.

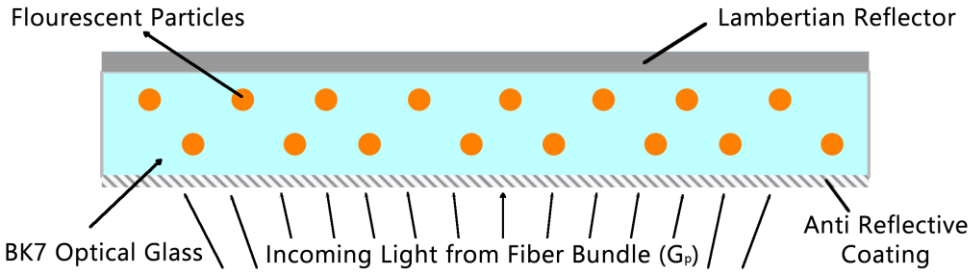

Figure 4.4. Detailed layout of fluorescent reflector.

The analysis is carried out per greenhouse cross-sectional area. Therefore, 1 m^2 collector and shelf area is considered for each unit, as shown in Figure 4.1b, and the number of shelves in a unit area is defined as N_s. Three different latitudes at northern hemisphere, ϕ_l = 20° for low, ϕ_m =40° for medium and ϕ_h =60° for high, are considered in this study to identify the feasibility of crop production using vertical farms at different latitudes. Growth of lettuce is considered as it is a widely grown crop with growth data available in the literature. Lettuces are placed within pots, with dimensions of 20 x 25 cm^2 as described in literature [93], and the pots are distributed to the shelves so that 1 m^2 of greenhouse shelf holds 20 pots as shown in Figure 4.1b. The shelves are separated apart by 50 cm and one optical fiber is dedicated to a unit area a single shelf. Therefore, total number of fiber output bundle for each m^2 cross-sectional area of vertical farms is N_s. The optical fibers are placed on top in the baseline system, and they are placed on the bottom in the modified system with the fluorescent reflectors placed on top as shown in Figures. 1a and 3, respectively. Biconcave lens [57] which have a focal length of 13.2 mm and a radius of 12 mm is used on fiber tips to distribute light output. Incoming light from the probe is directed to the reflector uniformly within 53° incidence angle, θ, by using the biconcave lenses.

4.2. Formulation

Beam component of solar irradiation is collected with a parabolic collector, distributed by optical fibers and transmitted to tips/probes of the cables with an overall collection and distribution efficiency, η_{cd}, of 60% [91]. The beam component of the clear sky solar spectral irradiation for corresponding latitudes is calculated using Simple Model

of the Atmospheric Radiative Transfer of the Sunshine (SMARTS) developed by NREL [74]. Considering the number of shelves, transmitted spectral solar radiation per probe, $G_{p,\lambda}$, is defined as;

$$G_{p,\lambda}(\varphi, n_d, h, \theta) = \frac{\eta_{cd} G_{\lambda}(\varphi, n_d, h)}{N_s} H(\frac{53\pi}{180} - \theta) \frac{2.511}{2\pi} \tag{4.1}$$

where spectral solar irradiation, G_{λ}, changes with respect to latitude (ϕ), day of the year (n_d) and time of the day (h) [94], η_{cd} is considered as 60%, H is heaviside step function. The PAR for a probe is then defined as;

$$\mathrm{PAR}(\varphi, n_d, h, \theta) = \int_{400nm}^{700nm} G_{p,\lambda}(\varphi, n_d, h, \theta) d\lambda \tag{4.2}$$

As it was mentioned earlier, lettuce is considered in this study due to the availability of experimental data relating PAR with lettuce growth. Fu *et al.* [93] reported the fresh weight of the above-ground parts of lettuce plants growing under different PAR. Seeded lettuce plants are exposed to different PAR for 14 hours per day, for 17 days [93]. The fresh weight of above-ground parts grown per pot within the specified period is defined as the crop function C (PAR) based on data reported by Fu *et al.* [93], and it represents the lettuce harvest for a specific PAR as presented in Figure 4.5.

The experiment in [93] is conducted at constant PAR during 14 hours for 17 days; therefore, growth per total lighting hour is defined as;

$$C_{n,h}(\mathrm{PAR}) = \frac{C(\mathrm{PAR})}{14 \cdot 17} \tag{4.3}$$

PAR can simply be multiplied with transmittance for a non-fluorescent coating between solar irradiation and plants. However for a fluorescent coating, Pearson *et al.* [95] defined and suggested using effective quantum transmission to calculate effective transmittance in order to implement photosynthetic quantum efficiency of the fluorescent particles in the coating to PAR. As the proposed system relies on reflection, the effective

quantum reflectance, ρ_{eff}, analogous to the effective transmittance used in the literature, is defined as;

$$\rho_{eff}(\varphi, n_d, h) = \frac{\int_0^{\pi/2}\int_{400nm}^{700nm} G_{p,\lambda}(\varphi, n_d, h, \theta)\rho_\lambda(\varphi, n_d, h, \theta)Y(\lambda)\lambda\cos(\theta)d\lambda d\theta}{\int_0^{\pi/2}\int_{400nm}^{700nm} G_{p,\lambda}(\varphi, n_d, h, \theta)Y(\lambda)\lambda\cos(\theta)d\lambda d\theta} \tag{4.4}$$

for the proposed design, where $\rho\lambda$ is the spectral reflectance of coating and Y is photosynthetic weighting factor known as photosynthetic quantum efficiency that identifies the effects of light at different wavelengths within PAR on crop growth.

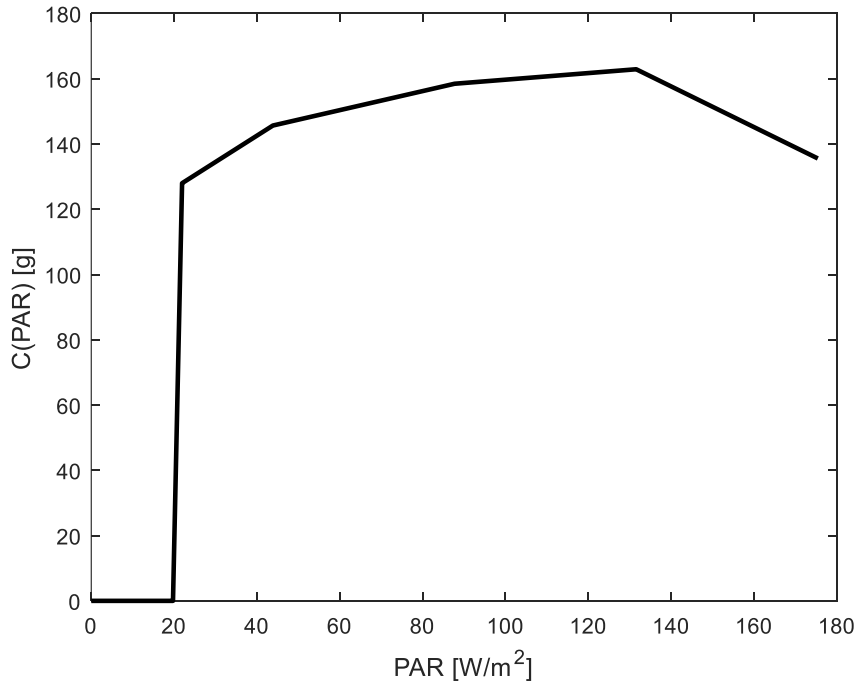

Figure 4.5. Fresh weight per pot of above-ground part of lettuce plant with changing PAR [93].

The photosynthetic quantum efficiency of crop plants as outlined by McCree [73] is presented in Figure 4.6. Here, the spectral reflectance of the coating is calculated by;

$$\rho_\lambda(\varphi, n_d, h, \theta) = \frac{\int_0^{\infty} G_{p,\lambda'}(\varphi, n_d, h, \theta)\rho_{\lambda'\to\lambda}(\varphi, n_d, h, \theta)d\lambda'}{\int_0^{\infty} G_{p,\lambda'}(\varphi, n_d, h, \theta)d\lambda'} \tag{4.5}$$

where the spectral reflectance of the fluorescent coating ρ_λ under irradiation $G_{p,\lambda}$ (ϕ,n_d,h,θ) is estimated from the bi-spectral reflectance, $\rho_{\lambda'\to\lambda}$, that is defined by a tensor and represents the fluorescent spectral conversion by the proposed coating. The effective PAR, PAR_{eff}, can then be defined as;

$$\mathrm{PAR}_{eff}\left(\varphi,n_d,h\right)=\rho_{eff}\left(\varphi,n_d,h\right)\int_0^{\pi/2}\mathrm{PAR}\left(\varphi,n_d,h,\theta\right)\cos\theta d\theta \tag{4.6}$$

There exists a spatial PAR distribution over the greenhouse shelf and it should be identified to estimate the lettuce growth at different regions of the shelf. Therefore, a normalized light density function, $D(x,y)$, is defined as;

$$D(x,y)=\frac{G(x,y)}{\int_0^1\int_0^1\left[G(x,y)\right]dxdy} \tag{4.7}$$

where $G(x,y)$ represents the spatial distribution of irradiation over a shelf.

The irradiation distribution is estimated with Monte Carlo method for both systems presented in Figures 4.1 and 4.3a. Diffusely and specularly reflected photon bundles from the coating are traced up to shelf floor, which is divided into a 100 x 100 grid. The energy of the photons that reaches a surface sub-element are summed to estimate the irradiation distribution $G(x,y)$. The distribution function, $D(x,y)$ is defined by normalizing $G(x,y)$ using the total irradiation over the shelf. Similar to spectral reflectance, $\rho_\lambda(\phi,n_d,h)$, D is implicitly dependent on λ,ϕ, n_d and h. However, it is found that these dependencies are negligible after performing calculations for different ϕ, n_d and h. Moreover, its dependence on λ is also weak due to the diffuse back reflector used and isotropic fluorescence emission. As a result, $D(x,y)$ is approximated to be independent of ϕ, n_d, h and spectral change, that holds for the fluorescent and non-fluorescent cases considered in the study.

The total crop depends on the light density distribution function that depends on how the PAR leaving the probe is distributed across the shelf by the reflectors. Therefore, estimation of irradiation field, $G(x,y)$, and $\rho_\lambda(\phi,n_d,h)$ necessitates the prediction of the

effective reflectance through solution of the RTE. RTE for the fluorescent medium is defined as [51]:

$$\frac{dI_\lambda}{dS} = \kappa_\lambda I_{b\lambda} - \kappa_\lambda I_\lambda - \sigma_{s,\lambda} I_\lambda + \frac{\sigma_{s,\lambda}}{4\pi}\int_{4\pi} I_\lambda \Phi_\lambda(\Omega',\Omega)d\Omega' + \frac{1}{4\pi}\int_0^\infty \kappa_{f,\lambda'} I_{\lambda'} QY(\lambda') \frac{\lambda'}{\lambda} P_f(\lambda)d\lambda' \quad (4.8)$$

where the last term represents the increase in intensity based on fluorescent emission due to excitations from all incident directions and wavelengths. In the presence of fluorescent medium, the absorption in the medium is due to both fluorescent and non-fluorescent components of the medium. Hence, the absorption coefficient can be defined as;

$$\kappa_\lambda = \kappa_{f,\lambda} + \kappa_{nf,\lambda} \quad (4.9)$$

where $\kappa_{f,\lambda}$ and $\kappa_{nf,\lambda}$ are absorption coefficients of fluorescent and non-fluorescent components of the medium, respectively.

The emitted energy due to fluorescent excitation follows a distribution that is identified in terms of normalized fluorescent intensity, $f_{fl}(\lambda)$, which represents the fluorescent emission at a wavelength with respect to its maximum value and represented in Figure 4.6. Then the probability of fluorescent emission at a specific wavelength, λ, is defined as:

$$P_f(\lambda) = \frac{f_{fl}(\lambda)}{\int_0^\infty f_{fl}(\lambda)d\lambda} \quad (4.10)$$

Scattering and absorption coefficients must be known to solve the RTE. These coefficients for the phosphor particle in the BK7 glass are calculated by Mie theory using the complex refractive index of the phosphor presented in [96]. The resulting scattering albedo and normalized absorbing coefficient, $f_{ex}(\lambda)$, based on its peak value of 4.6 cm^{-1} at 450 nm, is presented in Figure 4.6. The optical properties for BK7 Glass and MgF_2 used in the model are adopted from [97] and [98], respectively.

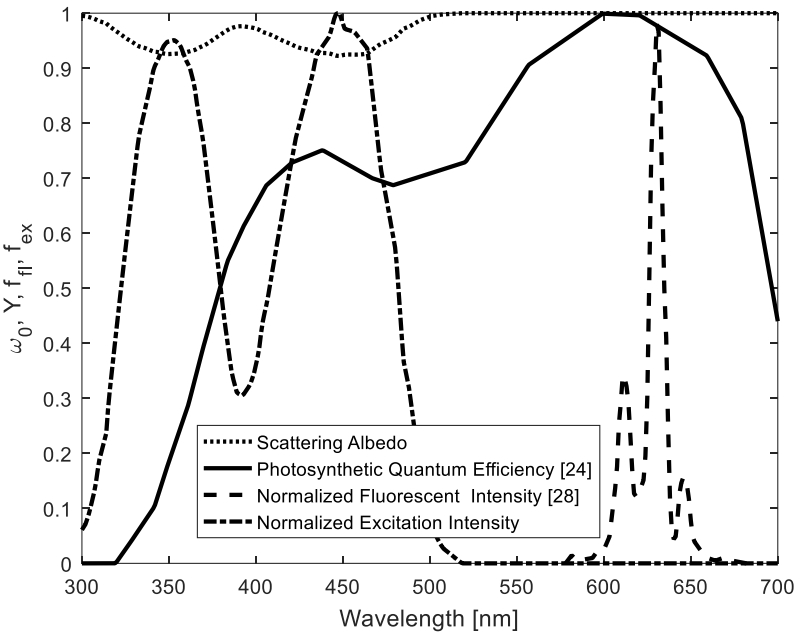

Figure 4.6. Excitation and emission [76] properties of $K_2SiF_6:Mn^{4+}$ phosphor, photosynthetic quantum efficiency change of crop plants with respect to incident wavelength [73] and scattering albedo.

Equation 4.7 is solved to predict the divergence of radiative heat flux for a broadband fluorescent system, considering energy transfer from one wavelength to another. While a spectral energy balance might not be satisfied for all wavelengths due to fluorescence, the total energy balance must be satisfied. The estimation of the directional spectral reflectance, ρ_λ, through the solution of RTE is well known and can be found in literature such as [77].

Once the directional spectral reflectance is calculated through the solution of the RTE for the system presented in Figure 4.4; $G(x,y)$ and ρ_{eff} can be evaluated from Equation 4.4, the PAR_{eff} can be calculated from Equation 4.5 from the estimated ρ_{eff}. The total crop per greenhouse unit area, *TC*, can then be calculated by considering the PAR distribution defined in terms of light density distribution function over the greenhouse shelf considered. Annual total crop growth for a latitude, $TC(\phi)$, can be calculated considering there are 20 pots per unit shelf area, and N_s shelves in the unit area of the vertical farm. The annual growth per unit area is defined as:

$$TC(\phi) = N_s 20 \sum_{n_d=1}^{365} \sum_{h=0}^{23} \int_0^{1m} \int_0^{1m} C_{n,h} \left[D(x,y) PAR_{eff}(\phi, n_d, h) \right] dxdy \quad (4.10)$$

A red emitting phosphor that is used in greenhouse lighting research [98] ($K_2SiF_6:Mn^{4+}$), with high quantum yield (QY=0.92), and emission peak that matches well with the peak of photosynthetic weighting factor is selected [99]. While the particle size of the phosphor can be reduced to 1 μm, it is reported that this also significantly reduces the quantum yield [100] and it is reported to have high quantum yield around 55 μm [100]. Therefore, phosphor pigment with 55 μm radius is considered in the study to have high quantum yield. The pigment volume fraction is defined based on a parametric study. The maximum effective reflectance, $\rho_{eff,max}$, is the maximum value of the ρ_{eff} (ϕ,n_d,h). The change of maximum effective reflectance, $\rho_{eff,max}$, with the pigment volume fraction up to 74% pigment volume fraction, which represents the maximum packaging limit for sphere pigments, is shown in Figure 4.7. The estimated $\rho_{eff,max}$ value 1.13 for the proposed design, is within the theoretical effective limit, 1.20, reported in the literature [32]. While the maximum effective reflectance is observed at the maximum packaging limit; it can be

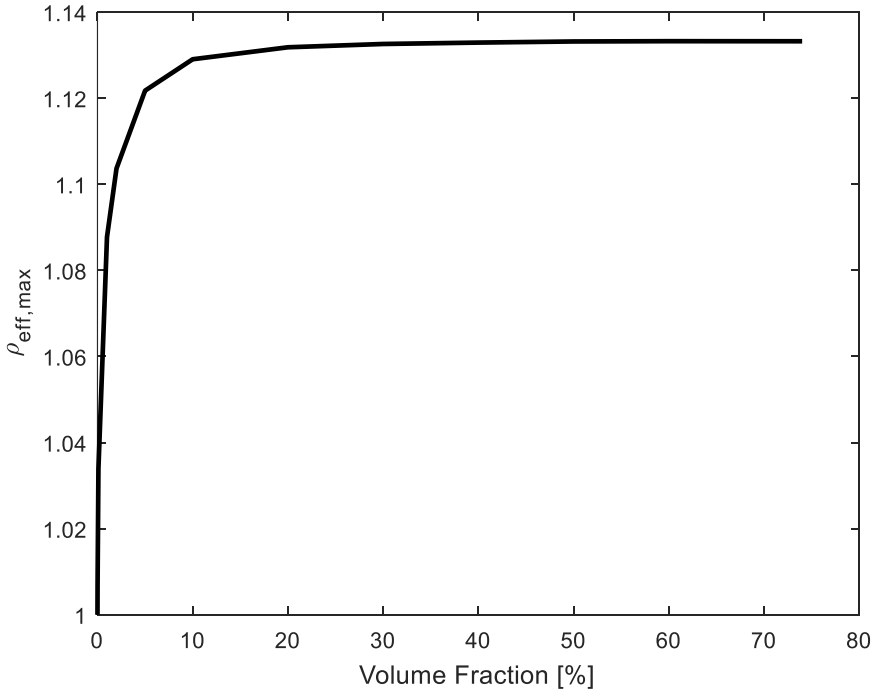

Figure 4.7. Change of effective reflectance with varying volume fraction.

observed in Figure 4.7 that effective reflectance with 30% pigment volume fraction leads to 99% of the maximum value, and it corresponds to a particle concentration of 430 particles/mm^3 that is within manufacturing limits [101]. Thus, volume fraction of fluorescent pigments for the reflector is chosen as 30%.

4.3. Results and Discussion

4.3.1 Model Validation

Validation of RTE solution for scattering and fluorescent medium by MCM is carried out through the comparison of estimated reflectance and fluorescence with the experimental data presented by Lie *et al.* [44]. Detailed definition of the experimental system is available in Lie *et al.* [44] and is not presented here. The diffuse reflectance and fluorescence presented in Figure 3.6 are in a good agreement with measurements within acceptable error margins.

4.3.1 Effective Quantum Reflectance

Effective quantum reflectance, ρ_{eff} (ϕ, n_d, h), is estimated from Equation 4.4 in order to implement fluorescence effect on PAR that is defined by Equation 4.5. As it relies on three independent variables, it should be estimated for all three latitudes, 365 days and 24 hours. Spectral incoming heat flux calculated for ϕ=40º, n_d=195 and h=12, is presented in Figure 4.8 along with its absorbed and reflected parts. For the particular set of parameters, ρ_{eff} is estimated as 1.12. The fluorescent pigment can also absorb light between 300-400 nm; therefore; wavelengths of interest is extended to 300-700 nm. Considering this wavelength interval, for the particular set of ϕ, n_d and h; total incoming solar flux is 441.1 W/m^2 (39.6 W/m^2 in 300-400 nm, and 401.6 W/m^2 in 400-700 nm), 60.0 W/m^2 of the incoming flux is absorbed (17.3 W/m^2 in 300-400 nm, and 42.7 W/m^2 in 400-700 nm), whereas 381.2 W/m^2 (2.7 W/m^2 in 300-400 nm, and 378.6 in 400-700 nm) is reflected. Although total heat flux is conserved, spectral heat flux is not due to fluorescence. Transfer of energy from 300-520 nm to 600-650 nm results in a spectral reflectance greater than unity between 600-650 nm as it could be seen from Figure 4.8. Energy is absorbed in excitation wavelengths due to conversion losses.

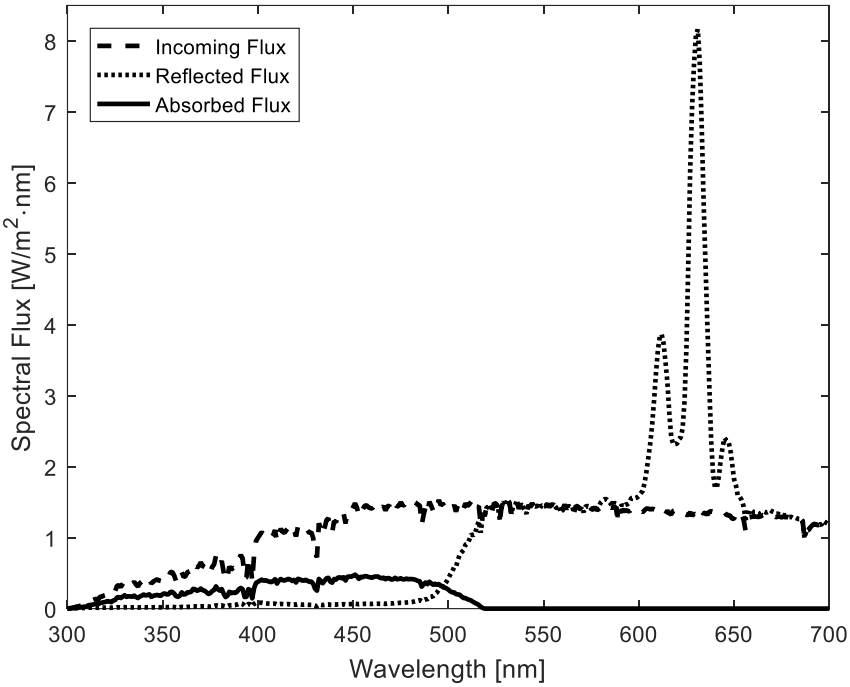

Figure 4.8. Spectral heat flux and reflectance of the coating ϕ=40º, n_d=195 and h=12.

4.3.2. Crop Estimation

Normalized light density function, $D(x,y)$ for systems with and without fluorescent coating (shown in Figures 4.3 and 4.1a, respectively) is estimated by Monte Carlo ray tracing method and the results are presented in Figure 4.9. It can be observed that scattering in the coating, diffuse reflectance at the back of reflector, isotropic nature of fluorescence emission and doubling path length of the light results a more uniform light distribution than regular light distribution with optical fibers.

Total crop per m^2 of vertical farm is estimated using Equation 4.10 for different number of shelves and latitudes as shown in Figure 4.10 by implementing estimated $D(x,y)$ and ρ_{eff}. As it could be seen from the Figure 4.10, using fluorescent particles in coating increases total crop in all three latitudes investigated.

As N_s increases, excessive light is distributed to other shelves, reducing excess PAR_{eff}, beyond optimum its point. Further increasing the number of shelves, PAR_{eff} drops so that increasing number of shelves and lettuces do not compensate slowing growth, and the

resulting total crop decreases as shown in Figure 4.10. Optimum number of shelves and corresponding crops are listed in Table 1, where optimum number of shelves increases by decreasing latitude as expected. It can also be observed from Table 1 that the total crop increases up to 31.0% using fluorescent reflectors. Both light distribution, $D(x,y)$, and effective reflectance, ρ_{eff}, have distinct effects in the increasing efficiency.

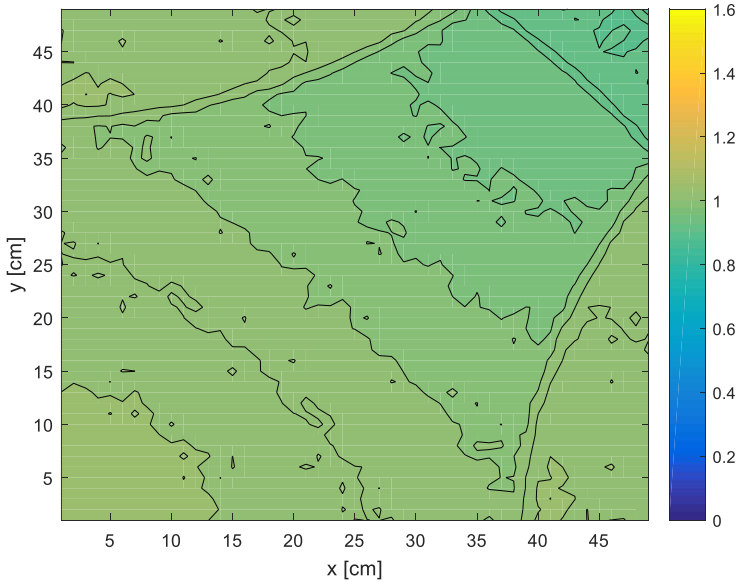

(a)

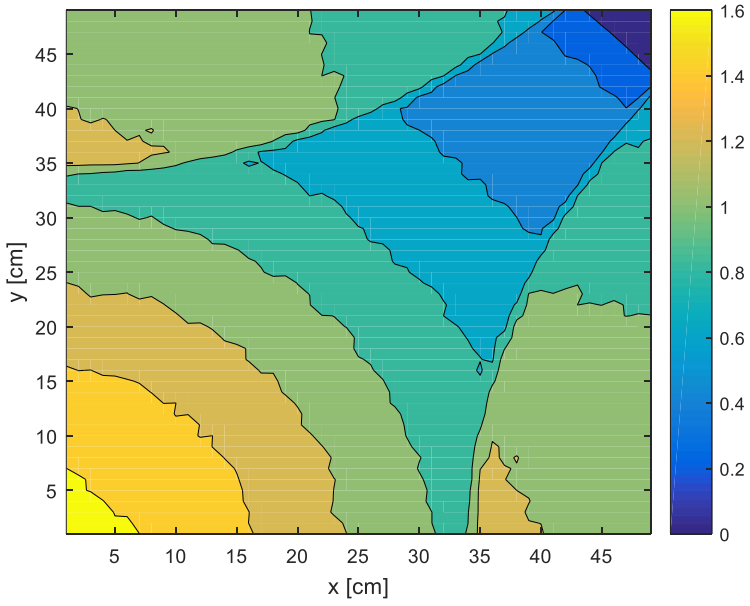

(b)

Figure 4.9. Normalized light density function $D(x,y)$ for (a) proposed vertical farm (Figure 4.3) and (b) baseline vertical farm (Figure 4.1).

In order to estimate only the effect of light distribution within the overall efficiency increase, normalized light density function of fluorescent coating presented in Figure 4.9a is used with ρ_{eff} =1 to eliminate gain provided by spectral alteration due to fluorescence. Efficiency increase of 21.4%, 21.1%, and 16.4% are estimated for ϕ=20º, ϕ=40º and ϕ=60º, respectively. Therefore, the remaining increase can be attributed to spectral alteration due to fluorescence, which is 10.1%, 8.2% and 7% for latitudes ϕ=20º, ϕ=40º and ϕ=60º, respectively.

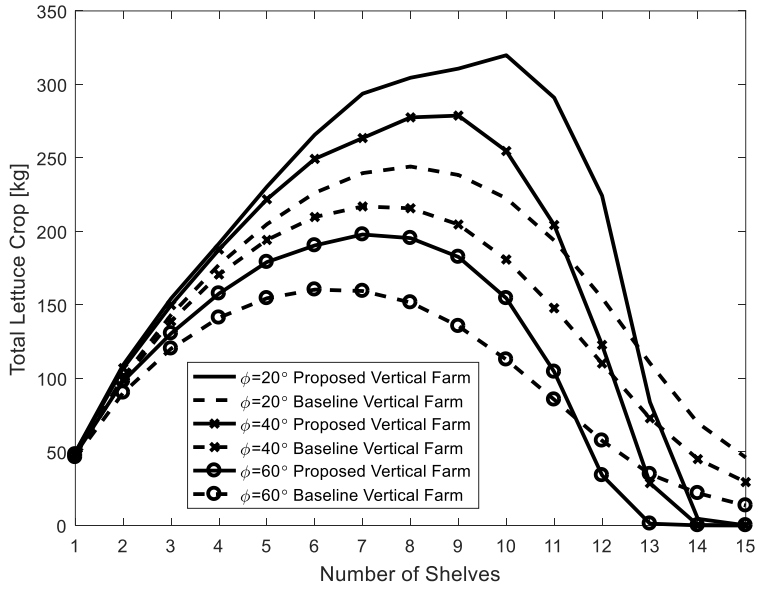

Figure 4.10. Total yearly lettuce crop per greenhouse unit for different number of shelves and latitudes, with and without fluorescent reflector.

Table 4.1. Yearly optimum lettuce crop in kg of a vertical greenhouse unit and corresponding optimum shelf numbers.

	Proposed Design		Base Design		
Latitude	Optimum N_s	Crop [kg]	Optimum N_s	Crop [kg]	Crop Increase %
20º	10	326	8	244	33.6
40º	9	284	7	217	31.1
60º	7	200	6	160	24.5

PAR changes timely as it is mentioned earlier, and it might be worthwhile to change shelf numbers monthly to improve monthly production. An additional study is conducted to investigate the benefits of using monthly optimum shelf number instead of permanent ones to find feasibility of changing shelf number monthly. Corresponding shelf numbers and crop results are tabulated at Table 4.2 and Figure 4.11 respectively.

Table 4.2. Monthly optimum shelf number for corresponding latitude.

	Optimum Shelf Number for Each Month											
Latitude	1	2	3	4	5	6	7	8	9	10	11	12
20º	10	10	10	10	10	10	10	10	10	10	9	10
40º	7	8	9	10	9	9	9	10	9	8	8	6
60º	3	5	7	8	9	8	9	8	8	6	3	2

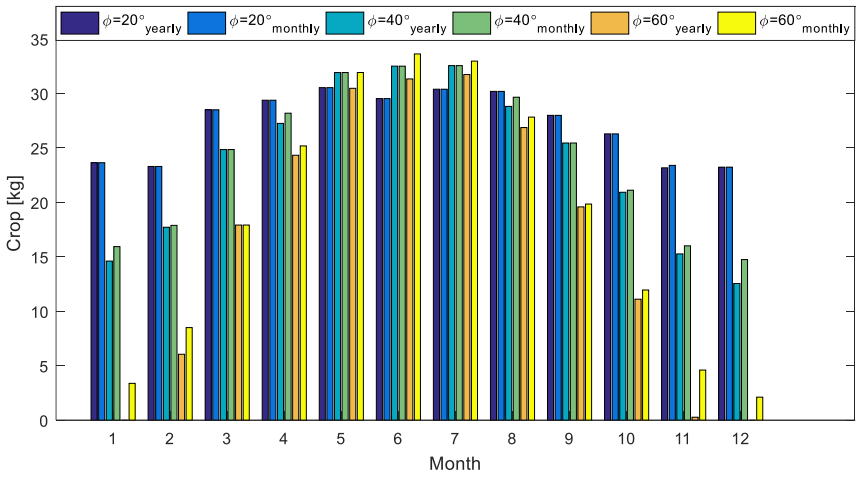

Figure 4.11. Total lettuce crop in kg of a vertical greenhouse unit with optimum shelf numbers optimized monthly and yearly.

Yearly crops per unit, increase to 326 kg, 291 kg and 220 kg for low, mid and high latitudes respectively which corresponds to 0.1%, 2.3% and 10.1% further increase, by monthly changing the number of shelves used. Results show that changing shelf number for low latitudes create insignificant effect on crop, similarly at mid latitudes, increase is small. However, lowering shelf number thus increasing PAR per optical fiber bundle during November-February can contribute significantly to increase in total crop, thus 37% crop increase with respect to non-fluorescent case can be achieved.

5. CONCLUSIONS AND RECOMMENDATIONS FOR FUTURE WORK

5.1. Conclusions

Inverse design of spectrally selective pigmented coatings is proposed for solar thermal systems. A unified model and simplified unified model are developed, for predicting the radiative transport properties of pigmented coatings. In these models, Lorenz-Mie theory in conjunction with extended Hartel theory is used to predict radiative properties for independent scattering with multiple scattering effects, whereas T-matrix method is used for dependent scattering for unified model, along with effective medium theory for very small pigments. While T-matrix is a precise model, it requires significant computation time; therefore, for simplified unified model, T-matrix method is not used ignoring dependent scattering effects. Once the radiative transport properties are estimated, the spectral emittance of the coating is calculated by four flux method. It is observed that the simplified unified model is capable of designing and modeling coatings adequately and can be considered as a good compromise between efficiency and accuracy.

Ideal coating behavior depends on working conditions of the system such as absorber temperature, and concentration factor. The design problem can be formulated as estimating the design parameters, for achieving the ideal coating behavior. Such a design problem can be considered as an inverse problem, where a system that exhibits a desired behavior under known conditions is predicted. Moreover, the design problem is a non-linear inverse problem due to highly non-linear dependence of coating behavior on design parameters. Therefore, the solution of the non-linear inverse design problem is achieved through optimization techniques. The optimization problem is formulated as a minimization problem of an objective function and solution by gradient based algorithms is highly dependent on initial guess due to existing multiple local extrema. Therefore, global search algorithms must be used. Simulated Annealing algorithm is used in this study that successfully locates global minimum independent of initial condition.

It was found that the net solar absorptance of coatings with lead sulfide pigments is superior to carbon and nickel pigments for medium temperature applications. While the

solar absorptance of lead sulfide pigmented coating is similar to that of carbon pigments, it has significantly lower total emittance. Therefore, the net heat flux for absorber with lead sulfide pigmented coatings is larger. However, as lead sulfide is unstable at high temperatures and nickel has lower absorptance, carbon pigment is used for high temperature applications where it shows better performance with respect to medium temperature. The optimal pigment radius, coating thickness and volume fraction is dependent on prescribed absorber temperature and concentration factor. Therefore, it was shown that pigmented coatings must be designed considering the operating conditions of the system.

Based on this study, it can be concluded that inverse design is a useful tool that can be applied for solution of design problems in different energy systems. The design method presented in this study is flexible and by modifying the objective function, different constraints and considerations can be easily incorporated to the design problem.

Effect of fluorescent and scattering pigmented greenhouse coatings to net photosynthesis of soybean is investigated at different latitudes. Monte Carlo method is used to solve radiative transfer equation in an absorbing, emitting and scattering fluorescent medium and transmittance of the coating under direct and diffuse sunlight is estimated at selected latitudes. Estimated transmitted intensity from the coating is used to calculate net photosynthesis based on data from previous experimental and theoretical studies that relates photosynthetically active radiation and net photosynthesis.

Results show that embedding fluorescent particles does not increase effective transmissivity of the greenhouse coating. However, it can contribute to growth in low latitudes where excessive photosynthetically active irradiation stresses the plant by decreasing the transmissivity. Due to its high reflectance, using coatings with scattering particles such as TiO_2 have similar effect. Moreover, the results also showed that embedding TiO_2 as scattering particles to a coating yields to a higher growth performance, by reducing transmissivity more effectively than embedding fluorescent particle $K_2SiF_6:Mn^{4+}$.

While similar optimal net photosynthesis values at different latitudes are predicted for both scattering and fluorescent coatings, as TiO_2 particles are cheaper and more stable than $K_2SiF_6:Mn^{4+}$, using TiO_2 scatterer appears to be a more feasible choice. However, for higher latitudes, reducing effective energy does not increase soybean's net photosynthesis and using particles in greenhouse coatings should be avoided. Further analysis is required to include the effect of changing haze so that a more accurate representation can be considered. Therefore, there is a need for more experimental data relating greenhouse coating's haze with the growth.

A novel lightning system, with a parabolic through concentrating collector, a light distribution system comprised of splitters, optical fibers and fluorescent reflectors, is proposed for vertical greenhouses. Sunlight is collected by a parabolic trough collector, and is transmitted into greenhouse shelves by splitters and optical fibers. Finally, the output of optical fibers is directed to a reflector that has a coating comprised of fluorescent ($K_2SiF_6:Mn^{4+}$) doped BK7 glass to alter solar spectrum to increase photosynthetic efficiency. Effects of fluorescent ($K_2SiF_6:Mn^{4+}$) pigmented coating and number of shelves on crop weight of lettuce are investigated at different latitudes. Monte Carlo method is used to solve radiative transfer equation in an absorbing, emitting, and scattering fluorescent medium and reflectance of the coating under fiber illumination is estimated. Estimated reflected PAR from the coating is used to calculate the lettuce growth based on data from previous experimental and theoretical studies that relate photosynthetically active radiation and lettuce mass.

Results show that embedding fluorescent coating particles increase crop growth up to 35% depending on latitude. Decreasing latitude increases optimum number of shelves; therefore, proper calculations should be carried out considering the latitude while constructing a vertical greenhouse to find optimum shelves.

5.2. Recommendations on Future Work

In this study, it is shown that using fluorescent pigments increases net photosynthesis thus growth in greenhouses. The growth is by shading effect in traditional greenhouses and by increasing effective PAR in vertical farms. In traditional greenhouses,

half of the emitted radiation by the fluorescent pigments is reflected back to space due to isotropic emission nature of fluorescent pigments. This behavior can be altered by implementing nano antennas next to fluorescent particles. Introducing nano-sized dipole antennas next to the fluorescent pigments can control emission direction as studies by [102, 103]. Embedding antenna in the coating can be a solution to minimize reflected fluorescent emission; however, proper material for antenna should be selected to minimize absorption of excitation irradiation.

Changing shape of emitting surface, effects the emission direction as suggested by [104], therefore; a forward emitting fluorescent pigment could be manufactured to minimize the loss arises from reflected fluorescent emission by altering geometry of fluorescent pigments. Resulting filter design that is embedded either by antenna or re-shaped fluorescent can have an effective PAR transmission over unity.

Correlation of PAR vs. net photosynthesis and/or crop growth are available in the literature for various plants. Although there are studies that shows plants grow better in diffuse rather than direct light, any correlation between haze vs crop growth in the literature is not available up to author's knowledge. The study that is presented in 3rd chapter shows that using scatterer and fluorescent pigments increase haze at different ratios, however; lack of correlation data that relates haze to crop growth prevents quantitative evaluation of haze effect on plant growth. Therefore, a study that relates PAR and haze to crop growth will fill the gap in the literature and enable the researchers to investigate the effect of haze on growth quantitatively.

REFERENCES

1. REN21, *Renewables 2017: global status report*, Vol. 72, 2017.

2. EIA, Today in Energy - Daily Prices - Prices - U.S. Energy Information Administration (EIA), 2017, https://www.eia.gov/todayinenergy/prices.php, accessed at December 2017.

3. TÜİK, *Bitkisel Üretim İstatistikleri*, 2017.

4. Despommier, D., "Farming up the city: The rise of urban vertical farms", *Trends in Biotechnology*, Vol. 31, No. 7, pp. 388–389, 2013.

5. Ajansı, T. C. D. A. K., *Seracılık (Örtüaltı Bitki Yetiştiriciliği) Sektör Raporu*, 2015.

6. Kalogirou, S. A., "Solar thermal collectors and applications," *Progress in Energy and Combustion Science*, Vol. 30, No. 3, pp. 231–295, 2004.

7. Kennedy, C., "Review of mid-to high-temperature solar selective absorber materials", *NREL Technical Report*, No. 520-31267, pp. 1–58, 2002.

8. Duffie, J. A. and W. A. Beckman, *Solar Engineering of Thermal Processes*. John Wiley & Sons, Inc., Hoboken, NJ, USA, April 2013.

9. Peterson, R. E. and J. W. Ramsey, "Thin film coatings in solar−thermal power systems", *Journal of Vacuum Science and Technology*, Vol. 12, No. 1, p. 174, 1975.

10. Orel, B., I. Radoczy, and Z. Crnjak Orel, "Organic soot pigmented paint for solar panels: Formulation, optical properties and industrial application", *Solar and Wind Technology*, Vol. 3, No. 1, pp. 45–52, 1986.

11. Klanjšek Gunde, M., J. Kožar Logar, Z. Crnjak Orel, and B. Orel, “Optimum thickness determination to maximise the spectral selectivity of black pigmented coatings for solar collectors”, *Thin Solid Films*, Vol. 277, No. 1–2, pp. 185–191, 1996.

12. Crnjak Orel, Z. C. and M. Klanjšek Gunde, “Spectrally selective paint coatings: Preparation and characterization”, *Solar Energy Materials and Solar Cells*, Vol. 68, No. 3–4, pp. 337–353, 2001.

13. Granqvist, C. G., “Spectrally selective coatings for energy efficiency and solar applications”, *Physica Scripta*, Vol. 32, No. 4, pp. 401–407, 1985.

14. Niklasson, G., “Modeling the optical properties of nanoparticles”, *SPIE Newsroom*, 2006.

15. Vargas, W. E. and G. A. Niklasson, “Applicability conditions of the Kubelka–Munk theory”, *Applied Optics*, Vol. 36, No. 22, p. 5580, 1997.

16. Vargas, W. E. and G. A. Niklasson, “Generalized method for evaluating scattering parameters used in radiative transfer models”, *Journal of the Optical Society of America A*, Vol. 14, No. 9, p. 2243, 1997.

17. Maheu, B. and G. Gouesbet, “Four-flux models to solve the scattering transfer equation: special cases”, *Applied optics*, Vol. 25, No. 7, p. 1122, 1986.

18. Vargas, W. E., “Generalized four-flux radiative transfer model”, *Applied Optics*, Vol. 37, No. 13, p. 2615, 1998.

19. Siegel, R., J. R. Howell, and M. P. Mengüç, *Thermal radiation heat transfer*, CRC Press, Boca Raton, FL, USA, 2015.

20. Vargas, W. E., “Optical properties of pigmented coatings taking into account particle interactions”, *Journal of Quantitative Spectroscopy and Radiative Transfer*, Vol. 78, No. 2, pp. 187–195, 2003.

21. Vargas, W. ., E. . Lushiku, G. . Niklasson, and T. M. . Nilsson, “Light scattering coatings: Theory and solar applications”, *Solar Energy Materials and Solar Cells*, Vol. 54, No. 1–4, pp. 343–350, 1998.

22. Vargas, W. E. and G. A. Niklasson, “Reflectance of pigmented polymer coatings: comparisons between measurements and radiative transfer calculations”, *Applied Optics*, Vol. 40, pp. 85–94, 2001.

23. Vargas, W. E., “Optimization of the diffuse reflectance of pigmented coatings taking into account multiple scattering”, *Journal of Applied Physics*, Vol. 88, No. 7, p. 4079, 2000.

24. Baneshi, M., S. Maruyama, H. Nakai, and A. Komiya, “A new approach to optimizing pigmented coatings considering both thermal and aesthetic effects”, *Journal of Quantitative Spectroscopy and Radiative Transfer*, Vol. 110, No. 3, pp. 192–204, 2009.

25. Baneshi, M., S. Maruyama, and A. Komiya, “Comparison between aesthetic and thermal performances of copper oxide and titanium dioxide nano-particulate coatings”, *Journal of Quantitative Spectroscopy and Radiative Transfer*, Vol. 112, No. 7, pp. 1197–1204, 2011.

26. Gonome, H., M. Baneshi, J. Okajima, A. Komiya, and S. Maruyama, “Controlling the radiative properties of cool black-color coatings pigmented with CuO submicron particles”, *Journal of Quantitative Spectroscopy and Radiative Transfer*, Vol. 132, pp. 90–98, 2014.

27. Yalcin, R. A. and H. Ertürk, “Optimization of Pigmented Coatings for Concentrating Solar Thermal Applications”, *Volume 4: Energy Systems Analysis, Thermodynamics and Sustainability; Combustion Science and Engineering; Nanoengineering for Energy, Parts A and B*, pp. 1703–1713, 2011.

28. Zhao, S. and E. Wäckelgård, “Optimization of solar absorbing three-layer coatings”, *Solar Energy Materials and Solar Cells*, Vol. 90, No. 3, pp. 243–261, 2006.

29. Etherden, N., T. Tesfamichael, G. A. Niklasson, and E. Wäckelgard, “A theoretical feasibility study of pigments for thickness-sensitive spectrally selective paints”, *Journal of Physics D: Applied Physics*, Vol. 37, No. 7, pp. 1115–1122, 2004.

30. Gonome, H., J. Okajima, A. Komiya, and S. Maruyama, “Experimental evaluation of optimization method for developing ultraviolet barrier coatings”, *Journal of Quantitative Spectroscopy and Radiative Transfer*, Vol. 133, pp. 454–463, 2014.

31. Lamnatou, C. and D. Chemisana, “Solar radiation manipulations and their role in greenhouse claddings : Fresnel lenses, NIR- and UV-blocking materials”, *Renewable and Sustainable Energy Reviews*, Vol. 18, pp. 271–287, 2013.

32. Pearson, S., A. E. Wheldon, and P. Hadley, “Radiation Transmission and Fluorescence of Nine Greenhouse Cladding Materials”, *Journal of Agricultural Engineering Research*, Vol. 62, No. 1, pp. 61–69, 1995.

33. Corrado, C., S. W. Leow, M. Osborn, I. Carbone, K. Hellier, M. Short, G. Alers, S. A. Carter, C. Corrado, S. W. Leow, M. Osborn, I. Carbone, K. Hellier, M. Short, G. Alers, and S. A. Carter, “Power generation study of luminescent solar concentrator greenhouse”, *Journal of Renewable and Sustainable Energy*, Vol. 8, No. 4, p. 43502, 2016.

34. Hemming, S., E. A. Van Os, J. Hemming, and J. A. Dieleman, “The effect of new developed fluorescent greenhouse films on the growth of Fragaria x ananassa ‘Elsanta’”, *European Journal of Horticultural Science*, Vol. 71, No. 4, pp. 145–154, 2006.

35. Hemming, S., E. van Os, A. Dieleman, J. Hemming, G. J. Swinkels, J. Breuer, and J. Slangen, “Possibilities of increasing production and quality of strawberry fruits and several flowers by new blue fluorescent greenhouse films.”, *Acta Horticulturae*, No. 691, pp. 225–232, 2005.

36. Novoplansky, A., T. Sachs, D. Cohen, R. Bar, J. Bodenheimer, and R. Reisfeld, “Increasing plant productivity by changing the solar spectrum”, *Solar Energy Materials*, Vol. 21, No. 1, pp. 17–23, 1990.

37. El-Bashir, S. M., F. F. Al-Harbi, H. Elburaih, F. Al-Faifi, and I. S. Yahia, “Red photoluminescent PMMA nanohybrid films for modifying the spectral distribution of solar radiation inside greenhouses”, *Renewable Energy*, Vol. 85, pp. 928–938, 2016.

38. El-Bashir, S. M., I. S. Yahia, F. Al-Harbi, H. Elburaih, F. Al-Faifi, and N. A. Aldosari, “Improving photostability and efficiency of polymeric luminescent solar concentrators by PMMA/MgO nanohybrid coatings”, *International Journal of Green Energy*, Vol. 14, No. 3, pp. 270–278, 2017.

39. Wakchaure, G. C. and P. S. Minhas, “Effect of reduced PAR on growth and photosynthetic efficiency of soybean genotypes”, *Journal of Agrometeorology*, Vol. 19, No. 1, pp. 1–9, 2017.

40. Fu, W., P. Li, and Y. Wu, “Scientia Horticulturae Effects of different light intensities on chlorophyll fluorescence characteristics and yield in lettuce”, *Scientia Horticulturae*, Vol. 135, pp. 45–51, 2012.

41. Aikman, D., “Potential Increase in Photosynthetic Efficiency from the Redistribution of Solar Radiation in a Crop”, *Journal of Experimental Botany*, Vol. 40, No. 8, pp. 855–864, 1989.

42. Pieters, J. G. and J. M. Deltour, “Modelling solar energy input in greenhouses”, *Solar Energy*, Vol. 67, No. 1–3, pp. 119–130, 1999.

43. Kang, D. Y., E. Wu, and D. M. Wang, “Modeling white light-emitting diodes with phosphor layers”, *Applied Physics Letters*, Vol. 89, No. 23, 2006.

44. Liu, Q., C. Zhu, and N. Ramanujam, “Experimental validation of Monte Carlo modeling of fluorescence in tissues in the UV-visible spectrum”, *Journal of Biomedical Optics*, Vol. 8, No. 2, pp. 223–36, 2003.

45. Mycek, M. A. and B. W. Pogue, *Handbook of Biomedical Fluorescence*, CRC Press, April 2003.

46. Ishida, K., I. Mitsuishi, Y. Hattori, and S. Nunoue, “A revised Kubelka-Munk theory for spectral simulation of phosphor-based white light-emitting diodes”, *Applied Physics Letters*, Vol. 93, No. 24, pp. 1–4, 2008.

47. Ertürk, H. and J. R. Howell, “Monte Carlo Methods for Radiative Transfer,” in *Handbook of Thermal Science and Engineering*, F. A. Kulacki, Ed. Springer International Publishing, Cham, pp. 1–43, 2007.

48. Wilson, B. C. and G. Adam, “A Monte Carlo model for the absorption and flux distributions of light in tissue”, *Medical Physics*, Vol. 10, No. 6, pp. 824–830, 1983.

49. Keijzer, M., S. L. Jacques, S. A. Prahl, and A. J. Welch, “Light distributions in artery tissue: Monte Carlo simulations for finite-diameter laser beams”, *Lasers in Surgery and Medicine*, Vol. 9, No. 2, pp. 148–154, 1989.

50. Jacques, S. L. and L. Wang, “Monte Carlo Modeling of Light Transport in Tissues,” *Optical-Thermal Response of Laser-Irradiated Tissue*, Vol. 47, pp. 73–100, 1995.

51. Neuman, M., S. Edvardsson, and P. Edström, “Solving the radiative transfer equation with a mathematical particle method”, *Optics Letters*, Vol. 40, No. 18, p. 4325, 2015.

52. Liaparinos, P. F., “Light wavelength effects in submicrometer phosphor materials using Mie scattering and Monte Carlo simulation.”, *Medical physics*, Vol. 40, No. 10, p. 101911, 2013.

53. Hsiao, S. L., N. C. Hu, and C. C. Wu, “Reducing the required amount of phosphor in warm white-light-emitting diodes by enhancing the scattering effect of wavelength conversion layer: A simulation study”, *Applied Physics Express*, Vol. 6, No. 3, 2013.

54. Hammam, M., M. K. El-Mansy, S. M. El-Bashir, and M. G. El-Shaarawy, “Performance evaluation of thin-film solar concentrators for greenhouse applications”, *Desalination*, Vol. 209, No. 1–3, pp. 244–250, 2007.

55. Shakespeare, T. and J. Shakespeare, “A fluorescent extension to the Kubelka-Munk model”, *Color Research and Application*, Vol. 28, No. 1, pp. 4–14, 2003.

56. Ghisi, E. and J. A. Tinker, “Evaluating the potential for energy savings on lighting by integrating fibre optics in buildings”, *Building and Environment*, Vol. 41, No. 12, pp. 1611–1621, 2006.

57. Ullah, I. and S. Shin, “Highly concentrated optical fiber-based daylighting systems for multi-floor office buildings”, *Energy and Buildings*, Vol. 72, pp. 246–261, 2014.

58. Junfeng, Qiao Zhaoyu, Z., “Fiber-guided sunlight cultivation system for three-dimensional greenhouse,” *Light, Energy and the Environment*, 2014.

59. Howell, J. R., K. Daun, H. Erturk, M. Gamba, and M. H. Sarvari, “The use of inverse methods for the design and control of radiant sources”, *JSME International Journal Series B*, Vol. 46, No. 4, pp. 470–478, 2003.

60. Daun, K., H. Erturk, and J. R. Howell, “Inverse design methods for high-temperature systems”, *Arabian Journal for Science and Engineering*, Vol. 27, No. 2, pp. 3–48, 2002.

61. Yalcin, R. A. and H. Erturk, “Inverse design of spectrally selective thickness sensitive pigmented coatings for solar thermal applications”, *Journal of Solar Energy Engineering*, 2018.

62. Yalcin, R. A. and H. Erturk, “Improving photosynthetic efficiency using greenhouse coatings with scattering and fluorescent pigments”, *Manuscript submitted for publication*, 2017.

63. Yalcin, R. A. and H. Erturk, “Improving concentrated optical fiber lighting with fluorescence reflectors for vertical farming” , *Manuscript submitted for publication*, 2017.

64. Modest, M. F., *Radiative Heat Transfer*, Academic Press, Oxford, UK, 2013.

65. Mackowski, D. W. and M. I. Mishchenko, “A multiple sphere T-matrix Fortran code for use on parallel computer clusters”, *Journal of Quantitative Spectroscopy and Radiative Transfer*, Vol. 112, No. 13, pp. 2182–2192, 2011.

66. ASTM, “ASTM G173 - Standard tables for reference solar spectral ırradiances: direct normal and hemispherical on 37 tilted surface”, *American Society for Testing and Materials*, Vol. 3, pp. 1–21, 2008.

67. Tesfamichael, T., A. Hoel, E. Wäkelgård, G. A. Niklasson, M. K. Gunde, and Z. C. Orel, “Optical characterization and modeling of black pigments used in thickness-sensitive solar-selective absorbing paints”, *Solar Energy*, Vol. 69, pp. 35–43, 2000.

68. Sadovnikov, S. I., N. S. Kozhevnikova, and A. A. Rempel, “Stability and recrystallization of PbS nanoparticles”, *Inorganic Materials*, Vol. 47, No. 8, pp. 837–843, 2011.

69. Kirkpatrick, S., C. D. Gelatt, and M. P. Vecchi, “Optimization by Simulated Annealing”, *Science*, Vol. 220, No. 4598, pp. 671–680, 1983.

70. Porter, J., M. Larsen, J. Barnes, and J. Howell, “Metaheuristic optimization of a discrete array of radiant heaters”, *Journal of Heat Transfer*, Vol. 128, No. 10, pp. 1031–1040, 2006.

71. Bertsimas, D. and J. Tsitsiklis, “Simulated Annealing”, *Statistical Science*, Vol. 8, No. 1, pp. 10–15, 1993.

72. Laaksonen, K., S. Y. Li, S. R. Puisto, N. K. J. Rostedt, T. Ala-Nissila, C. G. Granqvist, R. M. Nieminen, and G. A. Niklasson, “Nanoparticles of TiO_2 and VO_2 in dielectric media: Conditions for low optical scattering, and comparison between effective medium and four-flux theories”, *Solar Energy Materials and Solar Cells*, Vol. 130, pp. 132–137, 2014.

73. McCree, K. J., “Test of current definitions of photosynthetically active radiation against leaf photosynthesis data”, *Agricultural Meteorology*, Vol. 10, pp. 443–453, 1972.

74. Myers, D. R. and C. A. Gueymard, “Description and availability of the SMARTS spectral model for photovoltaic applications”, *Nrel*, pp. 1–12, 2004.

75. K.P. Bhagat, S.K. Bal, Y. Singh, S. Potekar, Saha S., P. Ratanakumar, G.C. Wakchaure, P. S. M., "Effect of reduced PAR on growth and photosynthetic efficiency of soybean genotypes", *Journal of Agrometeorology*, Vol. 19, No. 1, pp. 1–9, 2017.

76. Pust, P., V. Weiler, C. Hecht, A. Tücks, A. S. Wochnik, A. Henß, D. Wiechert, C. Scheu, P. J. Schmidt, and W. Schnick, "Narrow-band red-emitting $Sr[LiAl_3N_4]:Eu^{2+}$ as a next-generation LED-phosphor material", *Nature Materials*, Vol. 13, No. 9, pp. 891–896, 2014.

77. Siegel, R., J. R. Howell, and M. P. Mengüç, Thermal radiation heat transfer, CRC Press, Boca Raton, FL, USA, 2015.

78. Elman, J. F., J. Greener, C. M. Herzinger, and B. Johs, "Characterization of biaxially-stretched plastic films by generalized ellipsometry", *Thin Solid Films*, Vol. 313–314, pp. 814–818, 1998.

79. Siefke, T., S. Kroker, K. Pfeiffer, O. Puffky, K. Dietrich, D. Franta, I. Ohidal, A. Szeghalmi, E. B. Kley, and A. Tinnermann, "Materials pushing the application limits of wire grid polarizers further into the deep ultraviolet spectral range", *Advanced Optical Materials*, Vol. 4, No. 11, pp. 1780–1786, 2016.

80. Pust, P., V. Weiler, C. Hecht, A. Tücks, A. S. Wochnik, A.-K. Henß, D. Wiechert, C. Scheu, P. J. Schmidt, and W. Schnick, "Narrow-band red-emitting $Sr[LiAl_3N_4]:Eu^{2+}$ as a next-generation LED-phosphor material", *Nature Materials*, Vol. 13, No. 9, pp. 891–896, 2014.

81. Sijbom, H. F., J. J. Joos, L. I. D. J. Martin, K. Eeckhout, D. Poelman, and P. F. Smet, "Luminescent Behavior of the $K_2SiF_6:Mn^{4+}$ Red Phosphor at High Fluxes and at the Microscopic Level", *ECS Journal of Solid State Science and Technology*, Vol. 5, No. 1, pp. 3040–3048, 2016.

82. Yeo, B., Y. Cho, and Y. Huh, “Synthesis and photoluminescence properties of a red-emitting phosphor, $K_2SiF_6:Mn^{4+}$, for use in three-band white LED applications”, *Optical Materials*, Vol. 51, pp. 50–55, 2016.

83. Oh, J. H., H. Kang, Y. J. Eo, H. K. Park, and Y. R. Do, “Ultrahigh color quality warm-white LEDs”, *Journal of Materials Chemistry C: Materials for optical and electronic devices*, Vol. 3, pp. 607–615, 2014.

84. Liao, C., R. Cao, Z. Ma, Y. Li, G. Dong, K. N. Sharafudeen, and J. Qiu, “Synthesis of $K_2SiF_6:Mn^{4+}$ Phosphor from SiO2 Powders via Redox Reaction in $HF/KMnO_4$ Solution and Their Application in Warm-White LED”, *Journal of the American Ceramic Society*, Vol. 96, No. 11, pp. 3552–3556, 2013.

85. Howell, J. R. and M. Perlmutter, “Monte Carlo Solution of Thermal Transfer Through Radiant Media Between Gray Walls”, *Journal of Heat Transfer*, Vol. 86, No. 1, p. 116, 1964.

86. Liu, Q., C. Zhu, and N. Ramanujam, “Experimental validation of Monte Carlo modeling of fluorescence in tissues in the UV-visible spectrum”, *Journal of Biomedical Optics*, Vol. 8, No. 2, p. 223, 2003.

87. Vargas, W. E., P. Greenwood, J. E. Otterstedt, and G. A. Niklasson, “Light scattering in pigmented coatings: Experiments and Theory”, *Solar Energy*, Vol. 68, pp. 553–561, 2000.

88. American Society for Testing and Materials, A., “Standard test method for haze and luminous transmittance of transparent plastics. ASTM D1003 - 00 ”, *Annual Book of ASTM*. Philadelphia, PA, 2000.

89. Yang, L., M. Chen, Z. Lv, S. Wang, X. Liu, and S. Liu, “Preparation of a YAG:Ce phosphor glass by screen-printing technology and its application in LED packaging.”, *Optics letters*, Vol. 38, No. 13, pp. 2240–3, 2013.

90. Liang, D., L. Fraser Monteiro, M. Ribau Teixeira, M. . Fraser Monteiro, and M. Collares-Pereira, “Fiber-optic solar energy transmission and concentration”, *Solar Energy Materials and Solar Cells*, Vol. 54, No. 1–4, pp. 323–331, 1998.

91. Jaramillo, O. A., J. A. del Río, and G. Huelsz, “A thermal study of optical fibres transmitting concentrated solar energy”, *Journal of Physics D: Applied Physics*, Vol. 32, No. 9, pp. 1000–1005, 1999.

92. Fu, W., P. Li, and Y. Wu, “Effects of different light intensities on chlorophyll fluorescence characteristics and yield in lettuce”, *Scientia Horticulturae*, Vol. 135, pp. 45–51, 2012.

93. Duffie, J. A. and W. A. Beckman, *Solar Engineering of Thermal Processes*, Wiley, Hoboken, NJ, USA, 2013.

94. Pearson, S., A. E. Wheldon, and P. Hadley, “Radiation transmission anf fluorescence of nine greenhouse cladding materials,” *Agricultural Engineering*, Vol. 62, pp. 61–70, 1995.

95. Brik, M. G. and A. M. Srivastava, “Ab Initio Studies of the Structural, Electronic, and Optical Properties of K2SiF6 Single Crystals at Ambient and Elevated Hydrostatic Pressure”, *Journal of The Electrochemical Society*, Vol. 159, No. 6, p. 212, 2012.

96. Refractiveindex.info, *Optical Constants of Glass - BK7 Optical Glass*, 2017, https://refractiveindex.info/?shelf=3d&book=glass&page=BK7, accessed at December 2017 .

97. Dodge, M. J., “Refractive properties of magnesium fluoride”, *Applied Optics*, Vol. 23, No. 12, p. 1980, 1984.

98. Oh, J. H., H. Kang, Y. J. Eo, H. K. Park, and Y. R. Do, “Ultrahigh color quality warm-white LEDs”, *Journal of Materials Chemistry C: Materials for optical and electronic devices*, Vol. 3, pp. 607–615, 2014.

99. Murphy, J. E., F. Garcia-Santamaria, A. A. Setlur, and S. Sista, “PFS, $K_2SiF_6:Mn^{4+}$: the red-line emitting LED phosphor behind GE’s TriGain Technology^{TM} platform”, *SID Symposium Digest of Technical Papers*, Vol. 46, No. 1, pp. 927–930, 2015.

100. Nakamura, T., Z. Yuan, and S. Adachi, “Micronization of red-emitting $K_2SiF_6:Mn^{4+}$ phosphor by pulsed laser irradiation in liquid”, *Applied Surface Science*, Vol. 320, pp. 514–518, 2014.

101. De Boer, D. K. G., D. J. Broer, M. G. Debije, W. Keur, A. Meijerink, C. R. Ronda, and P. P. C. Verbunt, “Progress in phosphors and filters for luminescent solar concentrators”, *Opt. Express*, Vol. 20, pp. 395-405, 2012.

102. Kosako, T., Y. Kadoya, and H. F. Hofmann, “Directional control of light by a nano-optical Yagi-Uda antenna”, *Nature Photonics*, Vol. 4, pp. 312–315, 2010.

103. Taminiau, T. H., F. D. Stefani, F. B. Segerink, and N. F. Van Hulst, “Optical antennas direct single-molecule emission”, *Nature Photonics*, Vol. 2, No. 4, pp. 234–237, 2008.

104. Greffet, J. J., R. Carminati, K. Joulain, J. P. Mulet, S. Mainguy, and Y. Chen, “Coherent emission of light by thermal sources”, *Nature*, Vol. 416, No. 6876, pp. 61–64, 2002.

APPENDIX A: FLOW CHART OF MONTE CARLO METHOD

Flow chart of the code to solve broadband radiative transfer equation in fluorescent medium is presented in Figure A.2. Details of execution of the Monte Carlo method is presented in Figure A.3. Nomenclature for the flow chart is given in Figure A.1.

r	Position vector
s	Direction vector
λ	Wavelength
λ’	New wavelength after flourescence
A(λ)	1D energy array of absorbed photons at λ
R(r,s,λ,λ’)	4D energy array of reflected photons from λ to λ’ at r and s
e	Photon bundle’s energy
e_{in}	Energy input which is 1 for a bundle
N_p	Number of photons
L_{min}	Minimum length
L_{wall}	Length to wall
L_{ext}.	Length to extinction
QY	Quantum yield
rnd	Random number
alive	Integer that is 1 is for alive, 0 is for dead photon bundle

Figure A.1. Nomenclature for the flow chart.

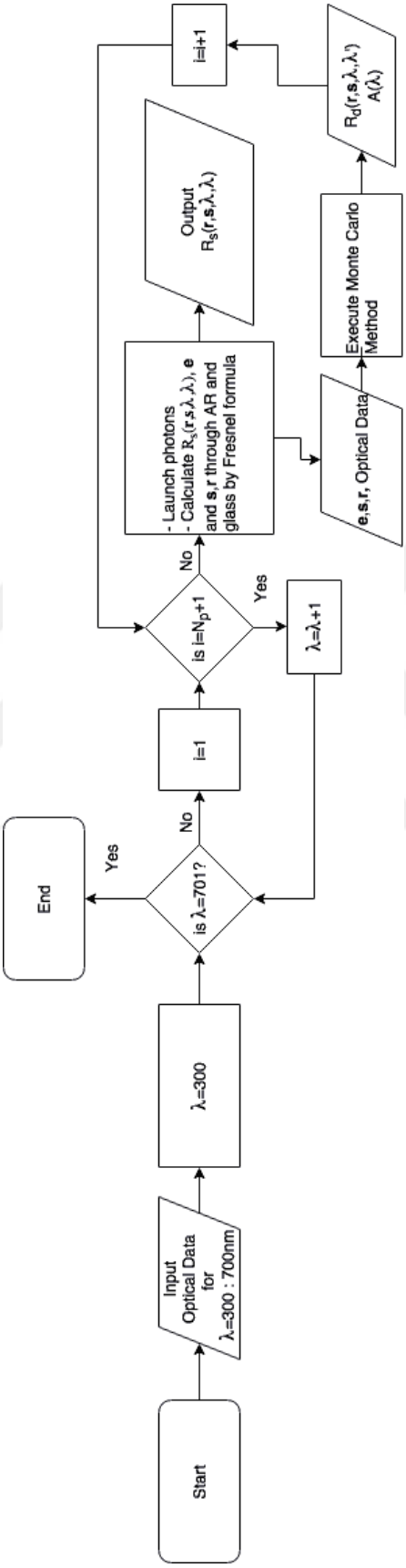

Figure A.2. Flow chart of the code to solve broadband radiative transfer equation in fluorescent medium.

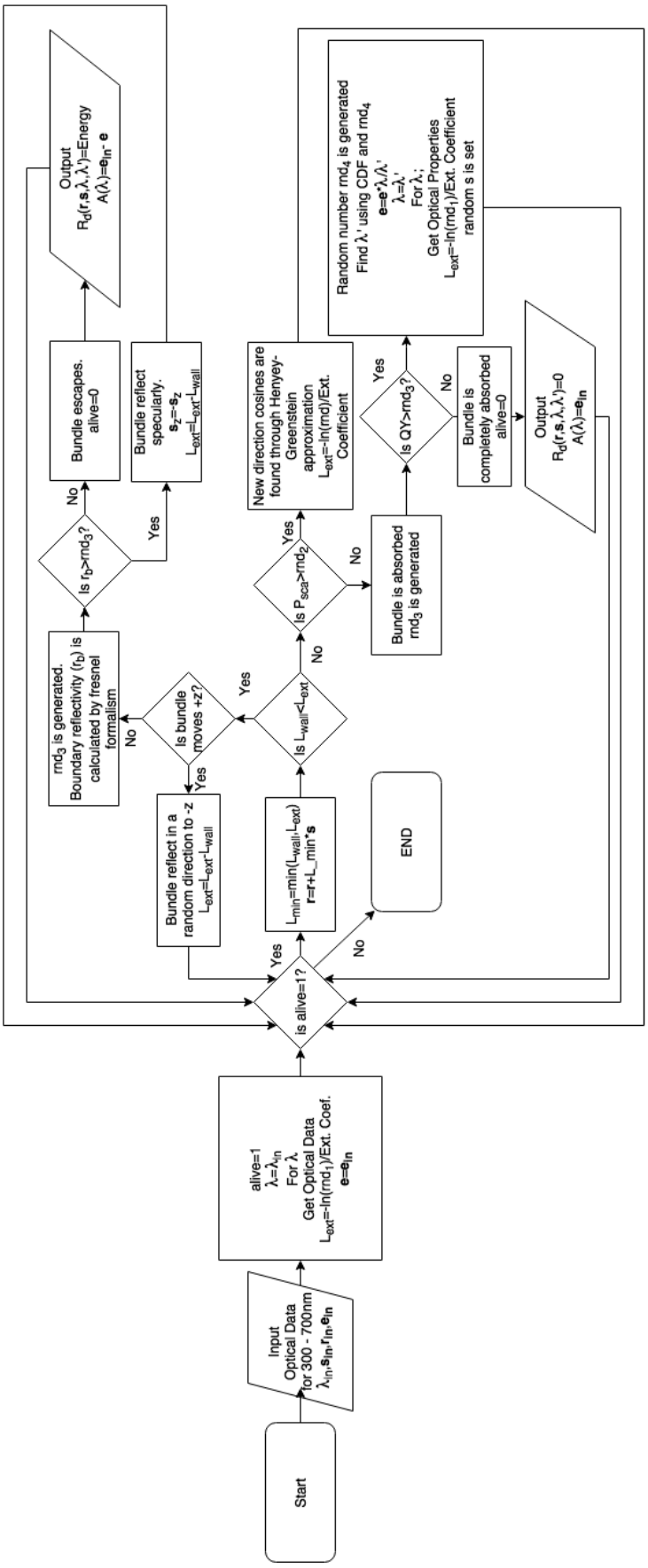

Figure A.3. Details of execution of the Monte Carlo method.